



Michigan Technological University
Create the Future Digital Commons @ Michigan Tech

Dissertations, Master's Theses and Master's
Reports - Open

Dissertations, Master's Theses and Master's
Reports

2012

Slope stability analysis of the Pacaya Volcano, Guatemala, using limit equilibrium and finite element method

Patrick. Manzoni
Michigan Technological University

Follow this and additional works at: <https://digitalcommons.mtu.edu/etds>



Part of the [Geology Commons](#)

Copyright 2012 Patrick. Manzoni

Recommended Citation

Manzoni, Patrick., "Slope stability analysis of the Pacaya Volcano, Guatemala, using limit equilibrium and finite element method ", Master's Thesis, Michigan Technological University, 2012.
<https://doi.org/10.37099/mtu.dc.etds/332>

Follow this and additional works at: <https://digitalcommons.mtu.edu/etds>



Part of the [Geology Commons](#)

SLOPE STABILITY ANALYSIS OF THE PACAYA VOLCANO, GUATEMALA,
USING LIMIT EQUILIBRIUM AND FINITE ELEMENT METHOD

By

Patrick Manzoni

A THESIS

Submitted in partial fulfillment of the requirements for the degree of

MASTER OF SCIENCE

(Geology)

MICHIGAN TECHNOLOGICAL UNIVERSITY

2012

© 2012 Patrick Manzoni

This thesis, "Slope Stability Analysis of the Pacaya Volcano, Guatemala, using Limit Equilibrium and Finite Element Method," is hereby approved in partial fulfillment of the requirements for the Degree of MASTER OF SCIENCE IN GEOLOGY

Department of Geological and Mining Engineering and Sciences

Signatures:

Thesis Co-Advisor

Dr. Thomas Oommen

Thesis Co-Advisor

Dr. Alessandro Tibaldi

Committee Member

Dr. John Gierke

Department Chair

Dr. Wayne D. Pennington

Date

DEDICATION

To My Family

TABLE OF CONTENTS

List of figures	viii
List of tables	xiv
Acknowledgments	xvi
Abstract	xvii
Chapter 1: INTRODUCTION	1
1.1 AIMS AND OBJECTIVES	1
1.2 GEOLOGICAL SETTING OF GUATEMALA	2
1.3 STUDY AREA	3
Chapter 2: LITERATURE REVIEW	6
2.1 landslide in volcanic setting	6
2.1.1 FREQUENCY	6
2.1.2 SOURCE AND MORPHOLOGIC CHARACTERISTICS	7
2.1.3 DEPOSIT MORPHOLOGY	8
2.1.4 CLASSIFICATION OF LATERAL COLLAPSE	9
2.2 DESTABILIZING FACTORS ON VOLCANO LANDSLIDE	9
2.2.1 OVERVIEW	9
2.2.2 DESTABILIZING LAYERS	10
2.2.3 MAGMA INTRUSION	10
2.2.4 SEISMIC LOAD	11
2.2.5 HYDROTHERMAL ALTERATION	11
2.2.6 LATERAL EDIFICE GROWTH	12
2.3 GEOTECHNICAL CLASSIFICATION OF VOLCANO	14
2.3.1 ROCK MASS CLASSIFICATION	15
2.3.2 MODELING DATA	19
2.4 STABILITY MODELING	21
2.4.1 ROC DATA	21

2.4.2 SLIDE	21
2.4.3 PHASE.....	22
Chapter 3: GEOLOGY AND TECTONIC SETTING.....	23
3.1 REGIONAL GEOLOGY OF PACAYA	23
3.1.1 PHASE I.....	24
3.1.2 PHASE II	24
3.1.3 PHASE III.....	25
3.2 structural setting.....	25
Chapter 4: METHODOLOGY	28
4.1 INTRODUCTION	28
4.2 GEOMORPHOLOGY	28
4.2.1 GEOLOGICAL SYSTEM INFORMATION	28
4.2.2 TOPOGRAPHICAL PROFILES.....	29
4.2.3 GEOMORPHOLOGY EVOLUTION	31
4.3 GEOTECHNICAL SURVEY.....	34
4.3.1 ROCK MASS DESCRIPTION.....	35
4.3.2 ROCK MASS STRENGTH.....	38
4.4 LITHOTECHNICAL UNITS	45
4.5 COMPUTING DISCONTINUITY ORIENTATION.....	48
4.6 SEISMIC SURVEY AND ANALYSIS	50
4.7 STRUCTURAL IMPLICATION AND RELATIONSHIP WITH SEISMIC DATA AND VENTS LOCATION	55
4.8 LABORATORY TESTING.....	58
4.8.1 PREPARING CORES	58
4.8.2 UNIAXIAL COMPRESSIVE STRESS	61
4.8.3 BULK VOLUME AND DENSITY.....	63
Chapter 5: GEOTECHNICAL PROPERTIES	65
5.1 INTRODUCTION	65
5.2 ROCK MASS PROPERTIES	65

5.2.1 PETROLOGIC AND MINERALOGIC PROPERTIES	65
5.2.2 ROCK MASS RATING (RMR).....	66
5.2.3 GEOLOGICAL STRENGTH INDEX (GSI)	66
5.2.4 DISCONTINUITY	66
5.2.5 BULK VOLUME AND DENSITY VALUE	69
5.2.6 SCHMIDT HAMMER VALUE (JCS).....	70
5.2.7 UNIAXIAL COMPRESSIVE STRENGTH (UCS)	72
5.2.8 UNIAXIAL COMPRESSIVE STRENGTH (UCS) ULTIMATE.....	74
5.3 LITHOTECHNICAL UNITS	77
5.3.1 HOEK AND BROWN STRENGTH PARAMETERS AND ELASTIC PROPERTIES	79
5.3.2 MOHR-COULOMB STRENGTH PARAMETERS.....	80
5.3.3 SUMMARY.....	80
Chapter 6: MODELING	82
6.1 INTRODUCTION	82
6.2 MODELING DEFINITION.....	82
6.2.1 SLOPE PROFILES.....	82
6.2.2 MATERIAL AND WATER PROPERTIES	84
6.3.3 IN SITU STRESS RATIO (K)	84
6.2.4 INTERNAL STRUCTURES.....	85
6.2.5 SCENARIO ANALYZED.....	88
6.2.6 ANALYSIS METHOD.....	89
6.3 LIMIT EQUILIBRIUM METHOD (LEM).....	92
6.3.1 SENSITIVITY ANALYSIS	92
6.3.2 LEM RESULTS.....	97
6.4 numerical modeling: finite element method (fem)	102
6.4.1 STRESS	103
6.4.2 STAGE OF ANALYSIS AND FAILURE SURFACE	103
6.4.3 FEM RESULTS.....	118

6.5 SCEARIO FOCUSED (MAGMA OVERPRESSURE)	122
6.5.1 CASES ANALYZED AND RESULTS	123
Chapter 7: CONCLUSION	126
Reference	127
Appendix	133
APPENDIX A: ROSE DIAGRAM (DIP DIRECTION) OF PRINCIPAL DISCONTINUITIES	133
APPENDIX B: PROJECTION ON EQUAL SCHMIDT’S STEREOGRAMS OF POLES TO PLANES OF DISCONTINUITIES	136
APPENDIX C: GEOTECHNICAL SURVEY ON SITES INVESTIGATED IN THE FIELD	137
APPENDIX D: LIST OF UNIAXIAL COMPRESSIVE TEST PERFORMED IN THE LABORATORY	147
APPENDIX E: COPYRIGHT PERMISSIONS	162

LIST OF FIGURES

<i>Number</i>	<i>Page</i>
Figure 1.1: Central American volcanic arc and tectonics plates near the study area. Red triangle indicates the location of Pacaya Volcano (OtoMatias et al. 2009).	2
Figure 1.2: Location of Pacaya volcano south of Guatemala City. The study area is bordered by a red square.	4
Figure 1.3: Zoom in of the Pacaya location indicated by red square in previous figure. Map modified from Gomez et al. 2010.....	5
Figure 2.1: A horseshoe shaped amphitheater. Morphologic characteristic of landslide deposit and lava flow distribution influenced by collapse. Tibaldi A., 2001.....	7
Figure 2.2: Cross-section of volcano landslide compared with non-volcanic one. Shaded portion represents volume of the material removed by the from slip surface. Siebert (1999).	8
Figure 2.3: Factors affecting volcano stability and promoting volcanic collapse. McGuire (1996)	10
Figure 2.4: Orientation of sector collapses in relation to direction of maximum stress and dyke systems (Moriya, 1980).....	11
Figure 2.5: Structural features, which may be associated with gravitational spreading or gravitational sliding (McGuire, 1996)	13
Figure 2.6: Experimental result by Walter et al., 2006 for two cones of different age spreading differently. A rift zone forms in direction E-W, parallel to the boundary of both cones. Image modified from Walter et al., 2006.	14
Figure 2.7: Procedure and measurements for calculation of RQD (after Deere, 1989).....	16
Figure 2.8: Geological Strength Index (GSI), introduced by Hoek and Marinos (2000).	18

Figure 3.1: Geological map of Guatemala. from “Instituto Geografico Nacional” (IGN) of Guatemala, 1974.	24
Figure 3.2: Regional tectonics and deformation pattern of Pacaya zone. Tectonic Plates involved and deformation rate. Orientation of the main faults (Carr, 1976) The red triangle indicates the location of Pacaya volcano in Guatemala. Mapa Geologico de Guatemala Escala 1:250000; IGN/Bonis, 1993 modified. (Rudiger Escobar Wolf, 2010).	26
Figure 4.1: Cross section of the Pacaya volcano slope. Section AA’ and BB’.	30
Figure 4.2: Vents distribution since 1961 and recent lava flow. Modified map from Gomez et al. (2010).....	32
Figure 4.3: New vents distribution on southwest flank of Pacaya Volcano. 1) “Vent 5” located on downhill southwest flank. 2) Small cone along “Vent 7” fissure.	33
Figure 4.4: Sites of geomechanical survey executed. Based map modified from Gomez et al. (2010).....	34
Figure 4.5: Lava outcrop, site A120, with surfaces slightly weathered with very small joint opening.	36
Figure 4.6: Autoclastic breccia block-supported good interlocked. Red bar represents 0.5 m	37
Figure 4.7: Autoclastic breccia clast-supported with poor to medium-matrix. Red bar represents 30 cm	38
Figure 4.8: Horizontal Scanline survey undertaken along 115 site.	40
Figure 4.9: Schematic illustration of dip and dip direction of discontinuity (Wyllie & Mah 2004).....	42
Figure 4.10: Roughness profiles and corresponding JRC values (After Barton and Choubey 1977).....	44
Figure 4.11: Image processing method to classify lithotechnical units. Site A08, which is classified as BRECCIA-LAVA unit. Lava range to 42% compared to breccia of 58%.	46

Figure 4.12: Image processing method to classify lithotechnical units. Site A09, which is classified as LAVA-BRECCIA unit. Lava range to 65% instead breccia to 35%. Geometric correction was achieved on this picture.	47
Figure 4.13: Image processing method to classify lithotechnical units. Site A113, which is classified as LAVA unit. Lava range from 80% to 100%. Geometric correction was achieved on this picture.	48
Figure 4.14: Projection on equal Schmidt's stereograms of poles to planes (e.g. A115 site). All discontinuity families present in this site are plotted here, K1, K2,K3, K5 and S1.	49
Figure 4.15: Projection on equal Schmidt's stereograms of poles to planes of K1 discontinuity. The plane here represented, is the average computed of K1 discontinuity orientation with 95% of confidence, corresponding to $248^{\circ}/72^{\circ}$. The legend represents the concentration of poles in different areas.	50
Figure 4.16: Small array deployed on the southwest flank of Pacaya volcano. Red circles represent single stations, which compose the array.....	51
Figure 4.17: Computed time delay for each station with respect to station 3, centered here.....	52
Figure 4.18: Semblance analysis plotted as function of slowness and azimuth. Example with best-fit azimuth indicate by white star. The plane direction correspond to 168° from north.....	53
Figure 4.19: Seismic stations shown on the modified volcanological map from Gomez et al. (2010). Section AA' perpendicular to this magmatic trend is represented here.	55
Figure 4.20: Rosette plot of K1 joint strike representing the most reliable direction of this fracture, which is between $20\text{-}30^{\circ}\text{NW}$	56
Figure 4.21: The main direction of the dry fissure, vents, and fracture (K1) are NW-SE (red rectangle). Schmidt's projection of planes and rosette plot for K1	

discontinuity. Along red rectangle in sequence from NW to SE: Cerro Chino, 27 th May trough, Dry and volcanic fissure, New vents location.	57
Figure 4.22: Coring device (FOSDICK M.T) with water as cooling fluid.	58
Figure 4.23: Cutting diamond blade. The blade is manually shifted.	59
Figure 4.24: Autoclastic Breccia cores.	60
Figure 4.25: Material Testing System (MTS 810).	62
Figure 4.26: Volume determination by the displacement of a dry medium, which is employed to compute the bulk density (P. A. Webb, 2001)	64
Figure 5.1: Lava sample n° 1 tested under uniaxial compressive strength. Maximum compressional strength equal to 34.00 MPa.	72
Figure 5.2: Lava cores tested under uniaxial compressive strength.	73
Figure 5.3: Geological Strength Index (GSI), introduced by Hoek and Marinos (2000) ..	78
Figure 6.1: AA' section representing the slope surface investigated. Topographic surfaces come from 1954-2001-2006 DEMs.	83
Figure 6.2: BB' section representing the slope surface investigated. Topographic surfaces come from 1954-2001-2006 DEMs. Comparing profiles coming from different DEM, 1954 to 2006, a latest geomorphologic evolution of the surface of Pacaya volcano is derived.	83
Figure 6.3: Section AA'. a) first model; b) second model; c) third model; d) fourth model.	86
Figure 6.4: Section BB'. a) first model; b) second model; c) third model; d) fourth model.	87
Figure 6.5: Section AA' (first model) with magma pressure applied corresponding to 21783 KN/m ² . Magma conduit depth from field investigation.	88
Figure 6.6: Sensitivity of the Safety Factor to variations of magma pressure component: section AA' magma load ranging from mean input \pm 21783 KN/m ² . Section BB' magma load ranging from mean input \pm 16686 KN/m ²	93

Figure 6.7: Sensitivity of the Safety Factor to variations of seismic load component: seismic load ranging from mean input ± 0.26	94
Figure 6.8: Sensitivity of the Safety Factor to variations: 1) geomechanical parameters: friction angle; cohesion; and unit weight. Mean input in base of lithotechnical unit considered.	95
Figure 6.9: Sensitivity analysis of safety factor to variations of geomechanical parameters conducted on fourth model. Section AA'	96
Figure 6.10: Sensitivity analysis of safety factor to variations of geomechanical parameters conducted on fourth model. Section BB'	96
Figure 6.11: Critical slip surface of fourth model. Section AA'	97
Figure 6.12: Critical slip surface of fourth model. Section BB'	98
Figure 6.13: Slip surface from seismic load scenario analyzed.....	99
Figure 6.14: Distribution of safety factor on fourth model (section AA'). Green zone represents worst values of safety factor under static condition.	101
Figure 6.15: Third model generated using a 2 dimensional automatic finite element mesh. Section AA'	102
Figure 6.16: Initial shear strength stage. Maximum shear strain presented. Fourth model section AA' analyzed under static condition.	104
Figure 6.17: Critical shear strength stage (strength reduction factor). Maximum shear strain presented. Fourth model section AA' analyzed under static conditions.....	105
Figure 6.18: Final shear strength stage. Maximum shear strain presented. Fourth model section AA' analyzed under static condition.	106
Figure 6.19: Final shear strength stage. Maximum shear strain presented. First model section AA' analyzed under static conditions.....	108
Figure 6.20: Initial shear strength stage. Maximum shear strain presented. Third model section AA' analyzed under static condition	110
Figure 6.21: Critical shear strength stage (strength reduction factor). Maximum shear strain presented. Third model section AA' analyzed under static conditions.....	111

Figure 6.22: Final shear strength stage. Maximum shear strain presented. Third model section AA' analyzed under static condition	112
Figure 6.23: Deformation vectors indicate strain direction and distribution. Fourth model section AA'	113
Figure 6.24: Horizontal displacement at the critical stage. It is observed opposite direction of displacement arrows in the upper slope, indicate tensile fracturing. Fourth model section AA'	114
Figure 6.25: deformation contour indicated material volume slip direction. Fourth model section AA'	115
Figure 6.26: Total displacement at the critical stage. Fourth model section AA'	116
Figure 6.27: Total displacement at the final stage. Fourth model section AA'	117
Figure 6.28: Magma overpressure component added to magmastatic one. Fourth model section AA'	123
Figure 6.29: Magma overpressure of 2.5 MPa. Joint Normal and shear stiffness equal to 10 MPa.....	124
Figure 6.30: Magma overpressure of 2.5 MPa. Joint Normal stiffness equal to 45 MPa and shear stiffness equal to 18 MPa.....	124
Figure A.1: Dip direction of K3 discontinuity.....	133
Figure A.2: Projection of all discontinuities measured on the field, representing K3.....	134
Figure A.3: Dip Direction of S1 stratigraphic discontinuity.....	134
Figure A.4: Projection of all stratigraphic contact between lava and breccia layer measured on the field, representing S1	135
Figure B.1: Projection on equal Schmidt's stereograms of poles to planes of discontinuities for each site investigated	136
Figure D.1: Autoclastic Breccia cores (1-14)	147
Figure D.2: Lava cores (1-12).....	155

LIST OF TABLES

<i>Number</i>	<i>Page</i>
Table 4.1: Terms describing discontinuity spacing. Adapted from Burns et al. 2005.....	41
Table 4.2: Terms describing discontinuity persistence from Brown, 1981.	43
Table 4.3: Terms describing discontinuity persistence from Brown, 1981.	60
Table 4.4: Terms describing discontinuity persistence from Brown, 1981.	61
Table 5.1: RMR classification for each site investigated.	67
Table 5.2: Site A117 where geotechnical survey was performed. Parameters carried out during investigation are listed below. “Pa” and “Pl” correspond to Areal persistence and linear persistence.	68
Table 5.3: Breccia samples	69
Table 5.4: Autoclastic Breccia samples	69
Table 5.5: Lava samples	69
Table 5.6: Schmidt hammer tests on field survey: uniaxial compressional strength.....	71
Table 5.7: Uniaxial compressional test performed on lava and autoclastic breccia	74
Table 5.8: Evaluation between uniaxial compressional strength from laboratory and field data. Comparable result for lava sample.	76
Table 5.9: Physical and mechanical properties of the lithotechnical units: established rock mass values of friction angle, cohesion, strength and elastic parameters from input data necessary to define the Mohr-Coulomb equivalent parameters as well	81
Table 6.1: Results of limit equilibrium analysis	100
Table 6.2: Results of Numerical Modeling Analysis. Strength Reduction Factor (SRF) correspond to Safety Factor (SF)	117
Table 6.3: Shear Strength Reduction Method. Gravity and Magma Pressure scenario analyzed. Result of Finite Element Method.....	120

Table 6.4: Shear Strength Reduction Method. Seismic and Magma + Seismic scenario analyzed. Result of Finite Element Method.....	121
Table C.1: A08 site	138
Table C.2: A09 site	139
Table C.3: A112 site	140
Table C.4: A113 site	141
Table C.5: A115 site	142
Table C.6: A118 site	143
Table C.7: A119 site	144
Table C.8: A120 site	145
Table C.9: A122 site	146

ACKNOWLEDGMENT

I'm especially thankful to my advisor, Thomas Oommen, who supported and guided me in the development of this research.

I would like to thank Alessandro Tibaldi, William I. Rose, B. van Wyk de Vries, who gave me the possibility to be involved in this international project (INVOGE).

I'm really grateful to all the students I've shared the Guatemala field trip with, especially to Lauren who worked with me in the field survey.

Thanks to Rudy for sharing with me his knowledge and experience about Pacaya volcano.. Special thanks to Stanley J. Vitton for allowing me to use his laboratory for completing this research task.

Finally, a singular thanks to INVOGE, MICHIGAN Tech's NSF PIRE project # 0530109, and Michigan Tech's Department of Geological and Mining Engineering and Sciences for providing me the adequate financial support for this project.

ABSTRACT

The Pacaya volcanic complex is part of the Central American volcanic arc, which is associated with the subduction of the Cocos tectonic plate under the Caribbean plate. Located 30 km south of Guatemala City, Pacaya is situated on the southern rim of the Amatitlan Caldera. It is the largest post-caldera volcano, and has been one of Central America's most active volcanoes over the last 500 years. Between 400 and 2000 years B.P, the Pacaya volcano had experienced a huge collapse, which resulted in the formation of horseshoe-shaped scarp that is still visible. In the recent years, several smaller collapses have been associated with the activity of the volcano (in 1961 and 2010) affecting its northwestern flanks, which are likely to be induced by the local and regional stress changes. The similar orientation of dry and volcanic fissures and the distribution of new vents would likely explain the reactivation of the pre-existing stress configuration responsible for the old-collapse.

This paper presents the first stability analysis of the Pacaya volcanic flank. The inputs for the geological and geotechnical models were defined based on the stratigraphical, lithological, structural data, and material properties obtained from field survey and lab tests. According to the mechanical characteristics, three lithotechnical units were defined: Lava, Lava-Breccia and Breccia-Lava. The Hoek and Brown's failure criterion was applied for each lithotechnical unit and the rock mass friction angle, apparent cohesion, and strength and deformation characteristics were computed in a specified stress range. Further, the stability of the volcano was evaluated by two-dimensional analysis performed by Limit Equilibrium (LEM, ROCSCIENCE) and Finite Element Method (FEM, PHASE 2 7.0). The stability analysis mainly focused on the modern Pacaya volcano built inside the collapse amphitheatre of "Old Pacaya".

The volcanic instability was assessed based on the variability of safety factor using deterministic, sensitivity, and probabilistic analysis considering the gravitational instability and the effects of external forces such as magma pressure and seismicity as potential triggering mechanisms of lateral collapse. The preliminary results from the analysis provide two insights: first, the least stable sector is on the south-western flank of the volcano; second, the lowest safety factor value suggests that the edifice is stable under gravity alone, and the external triggering mechanism can represent a likely destabilizing factor.

CHAPTER 1: INTRODUCTION

Volcanic collapses have been well recognized as a common phenomenon in the literature (Voight and Elsworth 1997; Van Wyk de Vries *et al.* 2000). Debris avalanche, lateral blast and lahars may be associated to the volcanic collapse providing extreme hazard because they can move rapidly and destroy everything in their paths. There have been several instances of volcanic collapses reported along the Guatemala volcanic arc associated with Cerro Quemado, Fuego, Pacaya, Tecuamburro, and other unidentified volcanoes (Vallance *et al.* 1994). While a number of volcano collapses around the world have been investigated using different stability analysis approaches, inadequate study has been done on the stability of volcanoes along the Guatemala volcanic arc. Pacaya is a stratovolcano located at the southern edge of the Amatitlán caldera. Between 400 and 2000 years B.P, the Pacaya volcano had experienced a huge collapse, which resulted in the formation of horseshoe-shaped scarp that is still visible. In this study, we perform numerical modeling to determine the possibility of collapse and most important factors that affect the stability of the edifice at Pacaya.

1.1 AIMS AND OBJECTIVES

The aim of this research is to analyze the stability of Pacaya volcano and assess the principal destabilizing factors and mechanism that may trigger collapse. The objectives of this study include:

- 1) Analyze the geotechnical parameters of lithotechnical units and their distribution at Pacaya to develop a potential internal structure of the volcano;
- 2) Evaluate the possible destabilizing factors, such as magma pressure, seismicity, and overpressure;
- 3) Investigate the local tectonic structures, its distribution, and regional stress to understand its influence on the control of paths for magma arises.

1.2 GEOLOGICAL SETTING OF GUATEMALA

Guatemala is centrally located within an area of active convergent and transform plate motions. The tectonic processes responsible for the structural and volcanic setting of the region are still active today. Central American volcanic arc (Fig.1.1), which extends from Mexico-Guatemala border to southern Costa Rica, is a result of the subduction of Cocos plate beneath the North American-Caribbean plate with a northwest component of movement. The Caribbean plate is split from the North American plate by Motagua transform fault, which cross Guatemala's central region. The southern portion of the Guatemala is located on the Caribbean tectonic plate, and it's subject to an 8 mm/yr east-west crustal extension, which has formed a series of north-south trending grabens such as the Guatemala City Graben (Bukart and Self 1985). The Caribbean plate in this region is also split by the right-lateral strike-slip Jalpatagua fault zone, which broadly coincides with the northwest-southeast trend of volcanic arc, and moves at a relative rate of 10 mm/yr (Carr 1976; White and Harlow 1993).

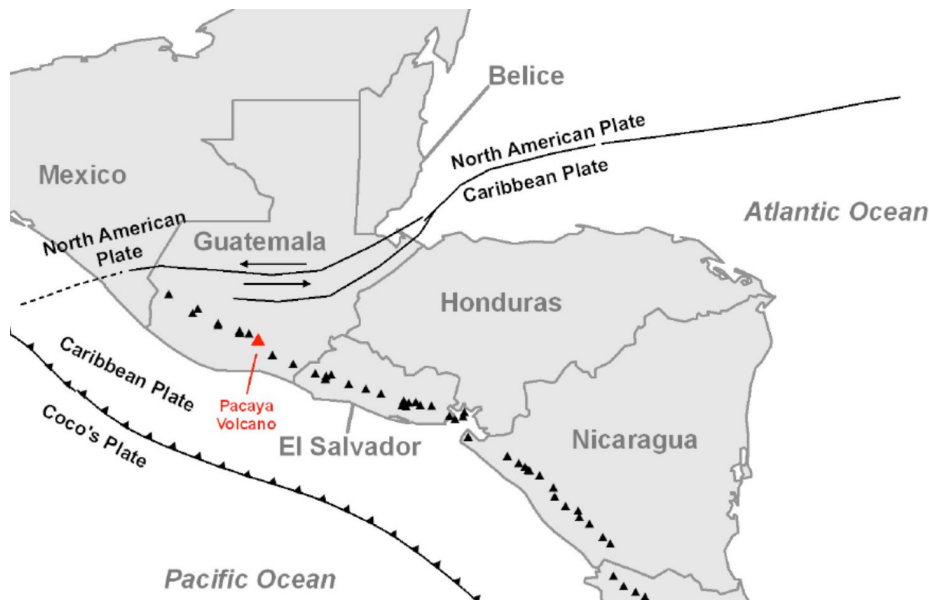


Figure 1.1: Central American volcanic arc and tectonics plates near the study area. Red triangle indicates the location of Pacaya Volcano. Figure modified from Gomez's thesis 2009.

1.3 STUDY AREA

Pacaya volcano is situated about 30 Km south of Guatemala City and is directly south of the large lake-filled Amatitlan Caldera (Fig.1.2). More than 1.5 million peoples are located at the Guatemala City urban center. A recent volcanologic report sourced from (<http://www.goto-guatemala.com>) reveals that, “The 1989 eruption produced a 4.5-kilometer-tall eruption column and enlarged the MacKenney crater. Lava flows followed in 1990-91. Strong eruptive activity in June-August 1991 destroyed part of the MacKenney cone and damaged villages to the west. Lavas have often flowed out of the collapsed south-southwest sector, traveling away from most inhabited areas”. The specific area is restricted along modern composite Pacaya volcano, which has been built inside the collapse Amphitheatre of “Old Pacaya” (Fig.1.3). The maximum elevation of this area, which reflects the volcano summit, is around 2600 m and drop down to 1100 m.

Figure 1.2: Location of Pacaya volcano south of Guatemala City. The study area is bordered by a red square



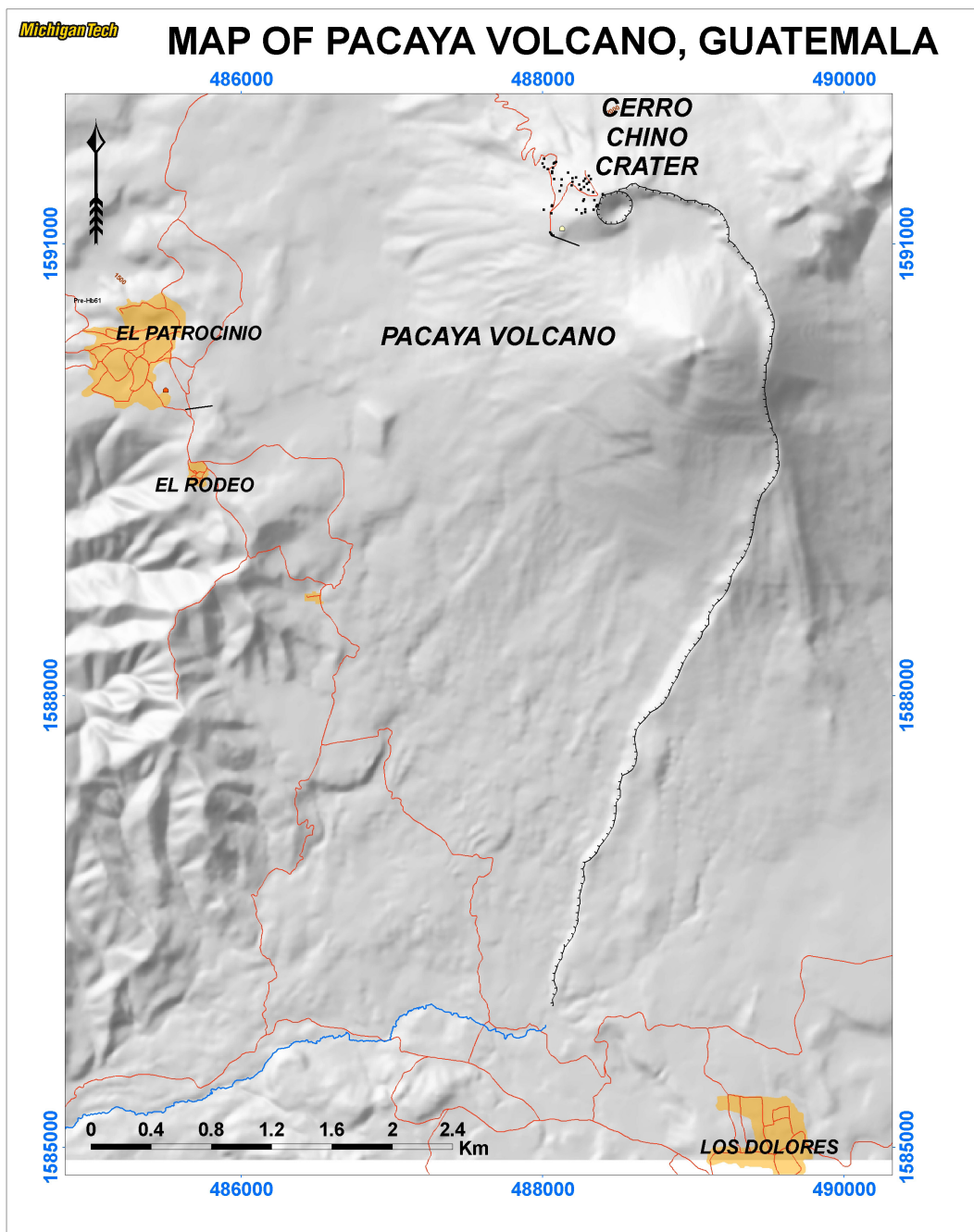


Figure 1.3: Zoom in of the Pacaya location indicated by red square in previous figure. Map modified from Gomez et al. 2010

CHAPTER 2: LITERATURE REVIEW

A literature review was completed to identify the important aspects in the evaluation of the stability of volcano. This section is subdivided into the following four sub-sections:

- i. Section 2.1 will address volcanic landslide frequency, source area and morphology;
- ii. Section 2.2 defines the factors that may affect volcano stability;
- iii. Section 2.3 argues about geotechnical classification of volcanoes underlining the importance of rock mass characterization in order to evaluate volcano stability. Introduction of data for stability modeling;
- iv. Section 2.4 introduces methods of stability analysis.

2.1 LANDSLIDE IN VOLCANIC SETTING

Landslide in a volcano environment shares multiple characteristics with the non-volcanic one. However, volcanic landslides are most dangerous because the material removed by the landslide could be the seal to the magma reservoir and its removal could trigger blast. Classification of volcanic mass movement has been improved over the years. A brief catalog of volcanic landslides is proposed in Siebert (2002), which include rockfall avalanche, debris avalanche, debris flow and sturzstrom. The most common terminology used to refer volcanic landslide is debris avalanche and debris flow, which differ from each other in terms of its water content. The water content varies from totally dry to enough amounts of water for generating the flow (water-saturated). The reader should note that in this study the term volcanic landslide is used to refer to all volcanic mass movements.

2.1.1 FREQUENCY

It was thought that this type of phenomena occurred once or twice in a life cycle of a volcano. This assumption, made on deficiency of landslide deposits documented, has been reviewed. Recent studies demonstrate that repetitive landslide can occur on a volcano. Large-scale of edifice collapse has occurred from 6-12 times at Myoko volcano in Japan (Kawachy and Hayatsu 1994), Colima in Mexico (Komorowski et al. 1997), etc. The great majority of volcanoes in the world have suffered lateral collapses interleaved

by growth phases (e.g. 75% volcanoes of the Andes) as response of fast evolution of the volcano.

2.1.2 SOURCE AND MORPHOLOGIC CHARACTERISTICS

Although discrepancies may occur, typically volcanic collapses present an ordinary geometry of deep slip surface with sub-vertical upper section and a lower flat section. Based on the structural evidences, the volcanic collapses could be subdivided into “flank collapse”, which doesn’t involve magmatic conduit, from “Sector collapse” which affects magmatic conduit in failure slip surface.

Typically, volcanic collapse leads to a horseshoe shaped amphitheater (Fig.2.1)

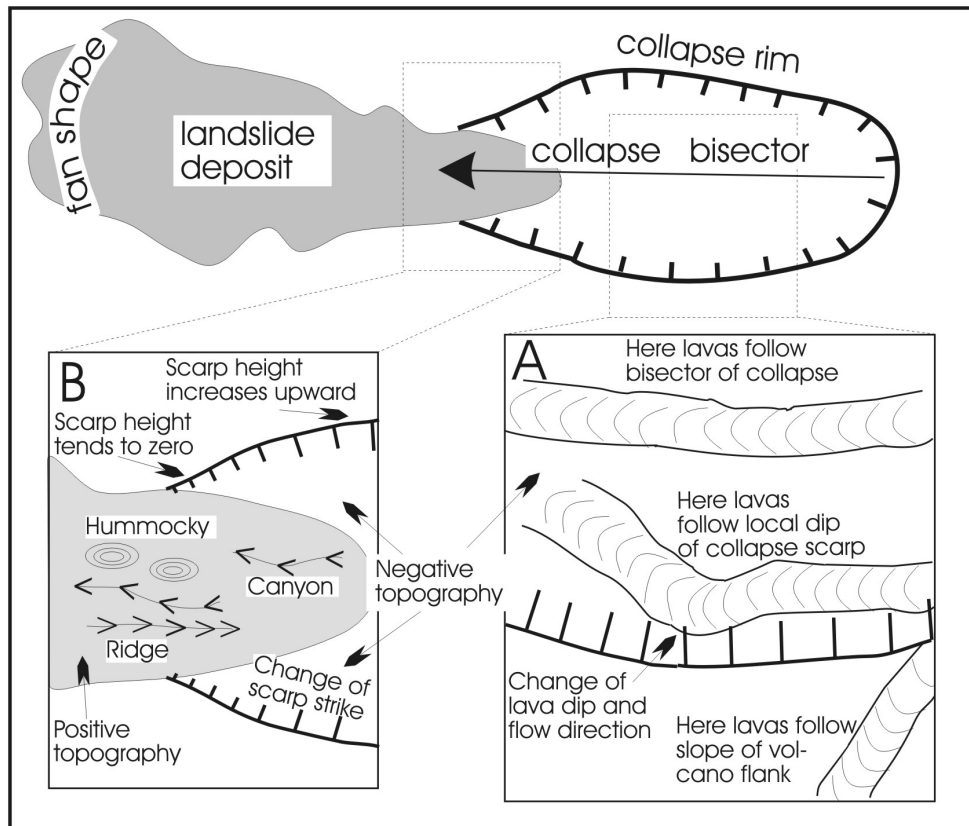


Figure 2.1: A horseshoe shaped amphitheater. Morphologic characteristic of landslide deposit and lava flow distribution influenced by collapse. Tibaldi 2001.

The morphology, structures, and dimensions of the collapse may vary from Km to tens of Km. Examples of longitudinal sections of lateral collapse, compared with non-volcanic one, demonstrate the large volume involved, which emphasizes the hazard linked to a volcanic collapse (fig.2.2).

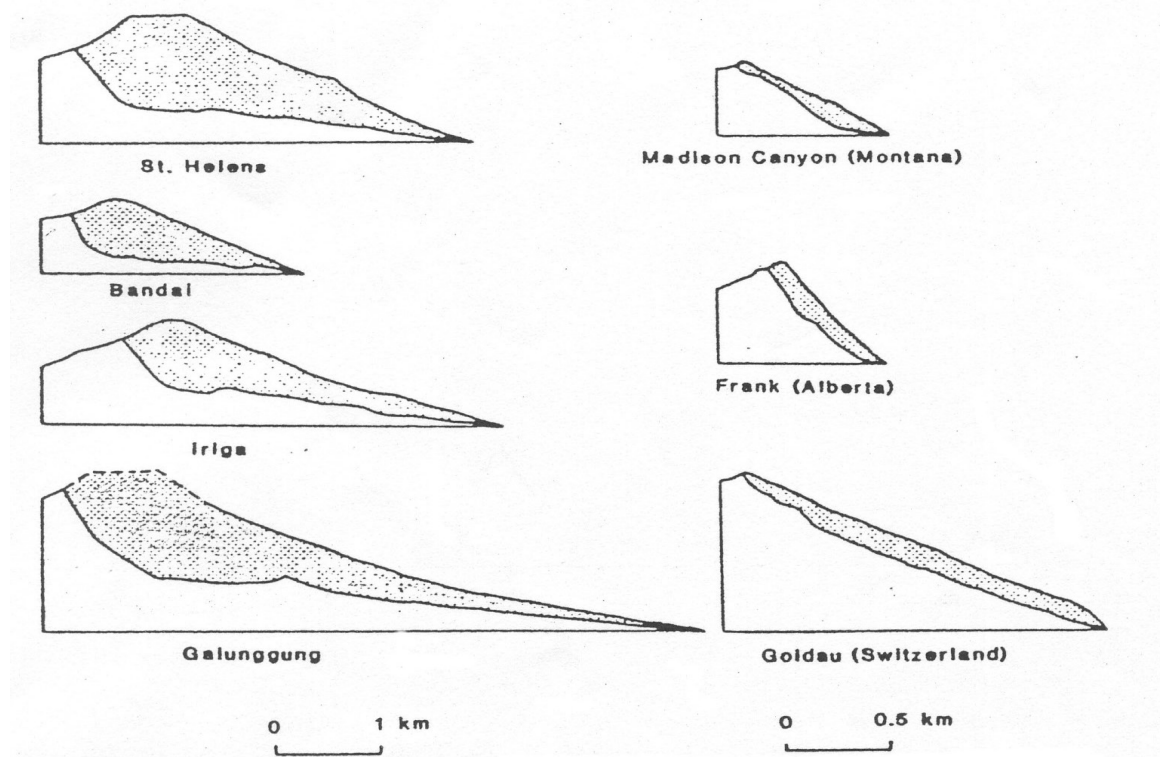


Figure 2.2: Cross-section of volcano landslide compared with non-volcanic one. Shaded portion represents volume of the material removed by the from slip surface. Figure modified from Siebert 1999.

2.1.3 DEPOSIT MORPHOLOGY

Although quite similar, deposits from volcanic landslide differ from those non-volcanic because of large volume involved. A hummocky terrain with hills and depressions usually characterizes the morphology surface of debris avalanche deposit. This morphology signature, produced by collapse of large-sector of volcanic edifice under water-undersaturated conditions, is characterized by two depositional facies, “block and matrix” (McGuire 1996; Siebert 2002).

2.1.4 CLASSIFICATION OF LATERAL COLLAPSE

Several case studies of volcanoes demonstrate the characteristics of volcano landslide deposit, landforms of volcano affected by collapse, and type of associated eruption behavior. A comprehensive classification of lateral collapses is given below. Although collapse can be related with complex and multiple causes, gravity plays an ultimate role in every volcanic landslide.

- Bezymianni type: associated with magmatic-phreatomagmatic eruptions (e.g. Mt. St. Helens) (Siebert 1984; Siebert 1987);
- Bandai type: associated with phreatic eruptions (Siebert 1984; Siebert 1987);
- Unzen/Onkate type: associated with gravity only, and no eruption (Francis and Self 1987).

2.2 DESTABILIZING FACTORS ON VOLCANO LANDSLIDE

The instability of volcanoes is attributed to a wide number of factors, acting individually or simultaneously. Although research has improved our knowledge about the physical mechanism responsible for the instability, information about causes, acting time, and behavior are not well understood. Thus, sudden volcanic landslides may occur.

2.2.1 OVERVIEW

The high relief and steep slopes of many volcanoes promote failure, as Francis and Wells (1988) noticed of Central Andes volcanoes. Structural factors as high relief, steep slope, interbedded competent with incompetent layers as pyroclastic or breccia deposit, asymmetrical edifices, incremental displacement due to dykes intrusion, seismicity, basement uplift and subsidence, hydrothermal weathering, weak material properties of volcano, debuttreassing, climatic effects, etc., may destabilize volcano flank (fig.2.3). A better explanation of most of these factors is explained in the following sessions.

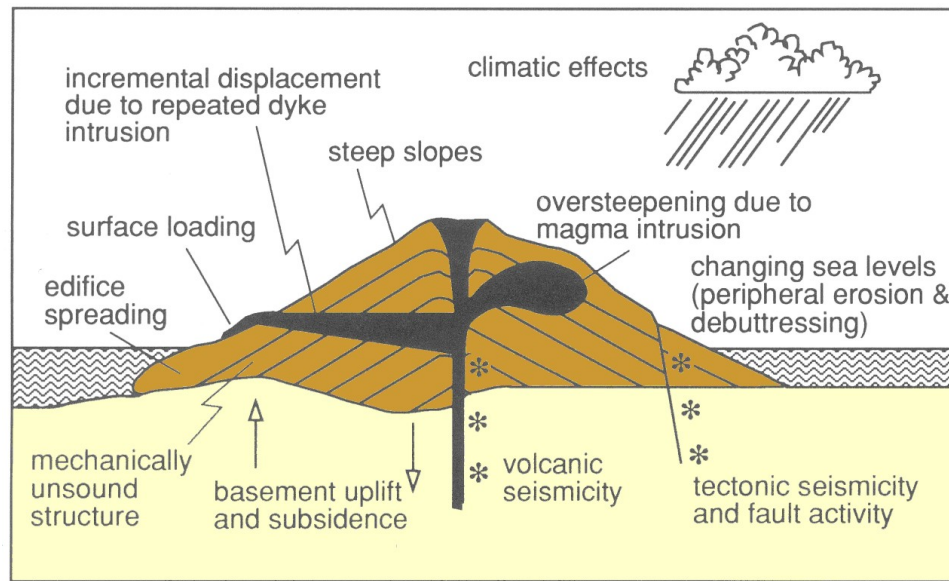


Figure 2.3: Factors affecting volcano stability and promoting volcanic collapse. McGuire (1996)

2.2.2 DESTABILIZING LAYERS

Stability modeling indicates that volcano slopes formed by common strength properties are very stable, suggesting that the presence of a weak “destabilizing layer” is required to reduce the strength of the volcanic edifice (Hürlimann et al. 1999). Pyroclastic rocks have been proposed as weak material affecting volcano stability (Siebert 1984). Besides pyroclastic layers, breccia and tuff layer may also affect the stability. At Pacaya, pyroclastic and tuff layers occasionally exist, but they will not be considered in the modeling. We recognized only one tuff layer and two pyroclastic layers, which are neglected because of inconsistent thickness in our scale modeling.

2.2.3 MAGMA INTRUSION

Particular attention was addressed in Siebert (1984), in his global review of structural destabilizing factors, on dyke parallel emplacement. Linear source of rising magma and volcanic rift has been documented as the major cause of edifice destabilization and failure. A multiple intrusion of dykes along preferential path for long period would generate an axial rift zone, which may result in a less stable sector susceptible to failure. Otherwise dyke emplacement along linear paths produce increasing pressure acting all along volcano edifices, which may reduce resistance and favor perpendicular collapse to the rift zone (Fig.2.4). Details about distribution of vents

(which would well represent the intersection of dykes at the surface) will be addressed in Section 4.2.3.1 and global consideration argued in Section 4.7.

Moreover, sub-horizontal dykes (sill) have been proposed as destabilizing factor. Steepening of slope and displacement due to magma intrusion are causes of likely collapses.

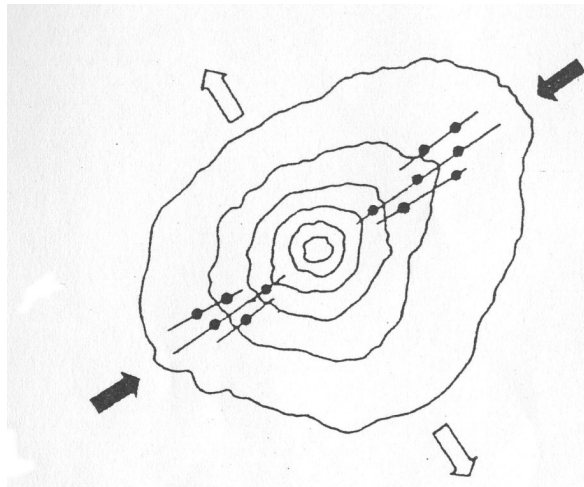


Figure 2.4: Orientation of sector collapses in relation to direction of maximum stress and dyke systems. Figure modified from Moriya 1980.

2.2.4 SEISMIC LOAD

Seismicity has been recognized as an important factor in destabilizing volcanic slopes. Earthquakes explain most of volcanic collapses related to a complex tectonic situation for volcanoes located within subduction margin (West coast of United States of America; Colima Volcanic Complex, Mexico; Mount Taranaki, New Zealand) (Voight and Elsworth 1997). The earthquake event leads to reduction in volcanic strength, lowering of friction, and horizontal movements that destabilizes the volcano. Pacaya is situated in complex tectonic setting (Section 3.2), in which seismic load must be considered.

2.2.5 HYDROTHERMAL ALTERATION

Hydrothermal alteration is a process, existing in multitude of volcanoes, where intrusive bodies interact with groundwater producing highly acidic hot fluids which promote rock dissolution and clay mineral formation along geologic structures and lithologic boundaries (López and Williams 1993; Watters *et al.* 2000). This process

results in supplanting strong material with weak clay mineral layers, which are positioned along flank slope and may contribute to create potential sliding surfaces. Otherwise, not all types of hydrothermal alteration result in lowered rock mass strengths. Silicification, can be an example, which increase generally the rock strength producing a stronger and more elastic rock mass (Watters *et al.* 2000). Usual consequence of hydrothermal alteration, accepted from scientist community, is in reducing material strength. This process might act long after last volcanic growing phase. Thus, hydrothermal alteration must be considered as one of the persistent factors acting in a volcano environment. Additionally, elevated pore pressure affects the rock mass strength, whereas, lowering it would increase the susceptibility to failure. Day (1996) argued that instability results not so much by lowering friction coefficient, but instead from increased permeability that elevates pore-fluid pressure. Saturation of volcano edifice portions by hydrothermal water accompanying magma intrusion can lead to elevated fluid pressure and weakening of the edifice. In this study hydrothermal alteration at Pacaya is not assessed, even though, a first analysis using Shear Strength Reduction (SSR) method was applied. This interesting tool produces a progressive reduction of material properties until final properties, which lead to trigger failure, are reached. The main utility of SSR method is to analyze the significance of reduction in input strength parameters potentially caused by hydrothermal weathering especially in environments such as volcanoes. Further study focused on rocks mass alteration may implement this investigation. This method will be discussed in Section 2.4.3 and 6.4.

2.2.6 LATERAL EDIFICE GROWTH

Recent studies have introduced different modalities of volcano failures during lateral expansion. Two contrasting mechanism involves (McGuire 1996):

- A. Gravitational spreading along basal thrust due to volcanic growth;
- B. Gravitational sliding due to over steepening, peripheral erosion, basement tilting or a combination of these factors;

These mechanisms of lateral growing may promote volcano collapse under gravity control, which is the dominant factor acting here (Fig.2.5).

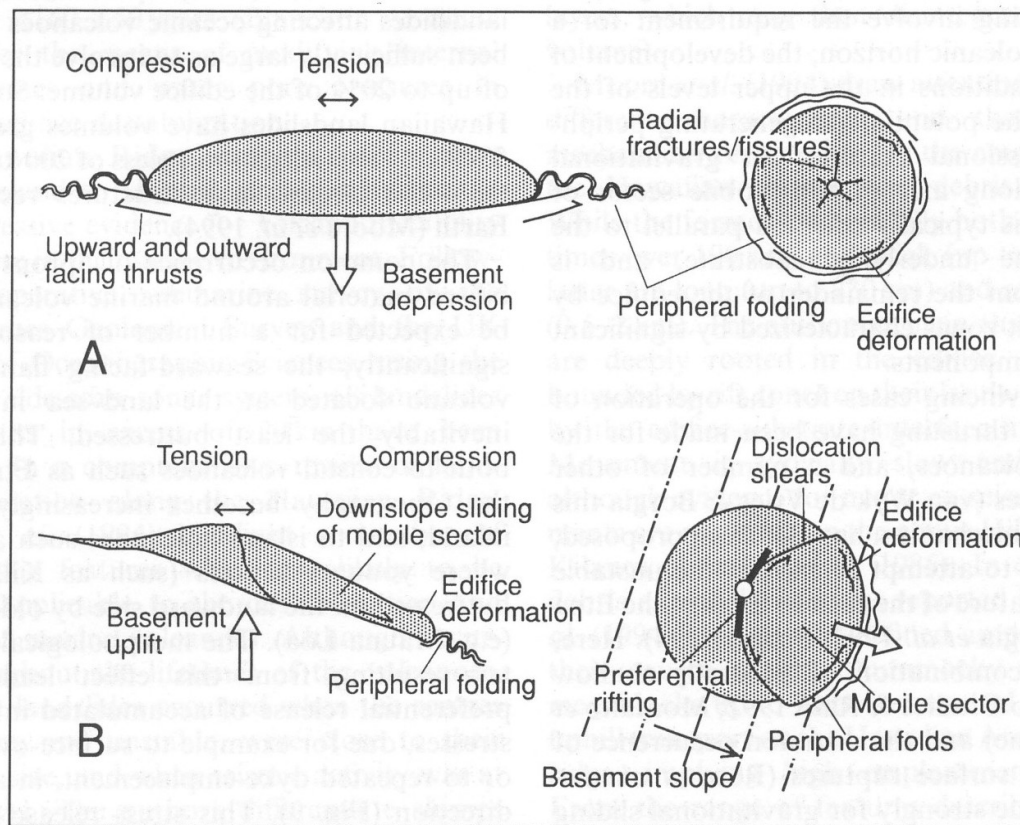


Figure 2.5: Structural features, which may be associated with gravitational spreading or gravitational sliding (McGuire 1996).

Thomas R. Walter's studies (e.g. ReÅLunion Island, Canary Islands) propose that the major processes that control the structural evolution of the volcano edifice are: volcanic rift zones and the gravitational spreading associated with flank instability. The overlapping and merging of individual volcanoes each other, may affect the spreading process and the activity of the rift zone. A possible mechanism of recent spreading applicable at Pacaya is the overlapping of McKenny cone on its southwest flank. Fig.2.6 demonstrates overlapping of cones of different ages, which would possibly represent the growing of McKenny cone on southwest flank of Pacaya.

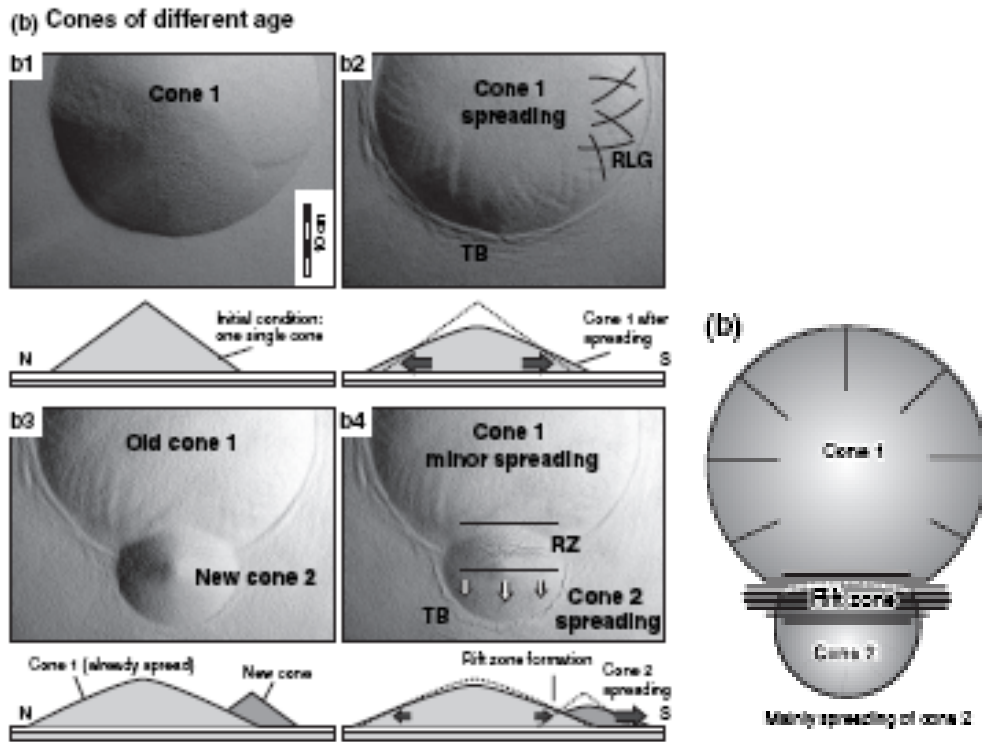


Figure 2.6: Experimental result by Walter et al., 2006 for two cones of different age spreading differently. A rift zone forms in direction E-W, parallel to the boundary of both cones. Image modified from Walter et al. 2006.

2.3 GEOTECHNICAL CLASSIFICATION OF VOLCANO

The geotechnical classification of volcanoes has been improved along the years. Recent studies in a volcanic environment highlighted the complexity to establish a comprehensive classification of volcanic rocks. Here a list of different classifications from Potro et al. (2008) is presented: Genetic classification, which considers different fragmental process; classification based upon the mineralogical composition; geological and morphological classification that reflect type of eruption, transportation, deposition process. Recently, volcanic rocks have been grouped into geotechnical units according to the degree of alteration and strength (Apuani et al. 2005), although this classification is site-specific and thus uncertainties must be counted by extrapolation all along the volcano.

2.3.1 ROCK MASS CLASSIFICATION

During preliminary investigation, when few details are available about the rock strength and hydrologic characteristic, rock mass classification can be a good compromise to quantify the rock mass properties. Rock mass classification provides initial estimate of strength and deformational properties of rocks. In preliminary analysis of the site investigated at least two classification systems are required in order to not neglect some parameters respect to the others. For this study, the Rock Quality Designation (RQD), basic Rock Mass Rating (RMR), and modified Geological Strength Index (GSI) were assessed.

2.3.1.1 ROCK QUALITY DESIGNATION INDEX (RQD)

Deer et al. 1967 developed the Rock Quality Designation Index (RQD). It provides a quantitative estimation of rock mass quality using drill core logs. The RQD is described as the percentage of intact core pieces longer than 100 mm in the total length of core (Fig.2.7). The absence of appropriated coring tool during our investigations performed at Pacaya avoids the straight measure of RQD. We overcame this problematic following Palmström (1982), which suggested that the value of RQD might be evaluated by number of discontinuity per unit volume. The equation is represented here:

$$RQD = 115 - 3.3 \times Jv$$

Where Jv is the sum of number of Joints per unit length for all joint. RQD value may vary among, 0-100. Although this approach was widely used in North America, RQD has significance as components of RMR classification covered later in this chapter.

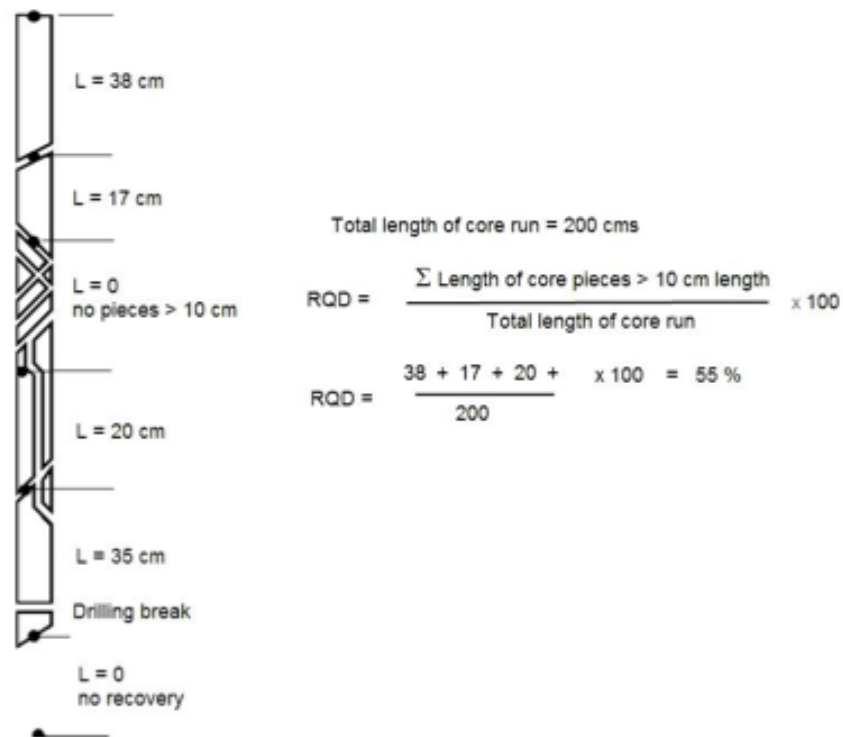


Figure 2.7: Procedure and measurements for calculation of RQD (after Deere 1989).

2.3.1.2 ROCK MASS RATING SYSTEM

Rock Mass Rating or Geotechnical classification was introduced in Bieniaswki (1976). RMR has been refined over the years, revising ratings assigned to different parameters. The 1989 version is the accepted classification (Bieniaswki 1989), in which six parameters are required:

1. Orientations of discontinuities;
2. Spacing between discontinuities;
3. Conditions of discontinuities;
4. Uniaxial compressive strength of rock material;
5. Rock Quality Designation (RQD);
6. Groundwater conditions;

In order to apply the above classification, the rock mass is partitioned into a number of structural regions. And each of these regions are classified individually. The boundary of these regions is chosen according to structural features as fault or lithology variations. RMR ratings varies from 0 – 100.

2.3.1.3 GEOLOGICAL STRENGTH INDEX (GSI)

Hoek *et al.* (1992), Hoek (1994) and Hoek *et al.* (1995) developed the GSI to overcome some of the limitations that had been recognized when using the RMR scheme for rock mass strength criteria. Poor quality rock mass has encountered many difficulties to be evaluated using RMR classification. The strength of a jointed rock mass invariably depends upon the properties of the intact rock block and also upon the grade of interlocking between them. The interlocking is controlled by the geometrical shape of the intact rock and the condition of the surfaces that separate them. Alteration, roughness and undulation surface control the strength of the rock mass. This system is presented in Fig.2.8, for blocky rock mass. The GSI table can be used with confidence when spacing of discontinuities is small compared with the structure.





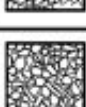

<p>GEOLOGICAL STRENGTH INDEX FOR JOINTED ROCKS (Hoek and Marinos, 2000)</p> <p>From the lithology, structure and surface conditions of the discontinuities, estimate the average value of GSI. Do not try to be too precise. Quoting a range from 33 to 37 is more realistic than stating that $GSI = 35$. Note that the table does not apply to structurally controlled failures. Where weak planar structural planes are present in an unfavourable orientation with respect to the excavation face, these will dominate the rock mass behaviour. The shear strength of surfaces in rocks that are prone to deterioration as a result of changes in moisture content will be reduced if water is present. When working with rocks in the fair to very poor categories, a shift to the right may be made for wet conditions. Water pressure is dealt with by effective stress analysis.</p>		<p>SURFACE CONDITIONS</p> <p>VERY GOOD Very rough, fresh unweathered surfaces</p> <p>GOOD Rough, slightly weathered, iron stained surfaces</p> <p>FAIR Smooth, moderately weathered and altered surfaces</p> <p>POOR Slackensided, highly weathered surfaces with compact coatings or fillings or angular fragments</p> <p>VERY POOR Slackensided, highly weathered surfaces with soft clay coatings or fillings</p>				
<p>STRUCTURE</p>		<p>DECREASING SURFACE QUALITY →</p>				
<p>DECREASING INTERLOCKING OF ROCK PIECES</p> <p>↓</p>	 <p>INTACT OR MASSIVE - intact rock specimens or massive in situ rock with few widely spaced discontinuities</p>	90			N/A	N/A
	 <p>BLOCKY - well interlocked undisturbed rock mass consisting of cubical blocks formed by three intersecting discontinuity sets</p>	80	70			
	 <p>VERY BLOCKY - interlocked, partially disturbed mass with multi-faceted angular blocks formed by 4 or more joint sets</p>		60			
	 <p>BLOCKY/DISTURBED/SEAMY - folded with angular blocks formed by many intersecting discontinuity sets. Persistence of bedding planes or schistosity</p>		50	40		
	 <p>DISINTEGRATED - poorly interlocked, heavily broken rock mass with mixture of angular and rounded rock pieces</p>			30	20	
	 <p>LAMINATED/SHEARED - Lack of blockiness due to close spacing of weak schistosity or shear planes</p>				10	
		N/A	N/A			

Figure 2.8: Geological Strength Index (GSI), introduced by Marinos and Hoek (2001).

2.3.2 MODELING DATA

The slope analysis stability requires rock mass data to be described by one of the two strength criteria proposed here. The Hoek-Brown criterion is an empirical failure criterion, developed to define the strength of rock in terms of major and minor principal stresses, whereas, the Mohr-Coulomb criterion is the most common failure criterion used in geotechnical engineering. It is required by the most of geotechnical analysis method and programs. The Mohr-Coulomb criterion defines a linear relationship between shear and normal stresses at failure.

2.3.2.1 HOEK-BROWN CRITERION

The Hoek-Brown criterion was developed in 1980, but further changes have been forced to meet the needs to amplify its applications to problems that were not considered in the original criterion developed. In 2002, the most important revision was implemented, necessary for the implementation of the criterion in numerical models, and to define the approach for estimating equivalent Mohr Coulomb parameters (Hoek 2000; Carranza-Torres and Corkum 2002). In this section, we propose this recent version of Hoek-Brown criterion, which has been found to offer the most reliable set of inputs for analysis in current use in rock engineering. The generalized Hoek-Brown failure criterion is described by:

$$\sigma_1 = \sigma_3 + \sigma_{ci} \times \left(mb \times \frac{\sigma_3}{\sigma_{ci}} + s \right)^a$$

where σ_{ci} is the uniaxial compressive strength of the intact rock pieces, mb is the value of the Hoek-Brown constant m for the rock mass, s and a are constants which depend upon the rock mass characteristics, and σ_1 and σ_3 are the maximum and minimum effective principal stresses at failure. The value mb is calculated from a reduced value mi , the material constant of intact rock, by incorporating the GSI and a disturbance factor D :

$$mb = mi \times \exp \left(\frac{GSI - 100}{28 - 14D} \right)$$

D varies from 0 for undisturbed in situ rocks and to 1 for very disturbed rock mass. Wyllie & Mah (2004) have presented guidelines on the categorization of D in mining situations where blast damage and stress relaxation may disturb the rock mass.

Hence, after computing the value of mb we are able to calculate s and a :

$$s = \exp \left(\frac{GSI - 100}{9 - 3D} \right)$$

$$a = \frac{1}{2} + \frac{1}{6} (e^{-GSI/15} - e^{-20/3})$$

For comparative reasons strength material properties may be presented through Mohr-Coulomb criterion.

2.3.2.2 MOHR-COULOMB CRITERION

The Mohr-Coulomb is the most common failure criterion in geotechnical engineering and describes a linear relationship between shear and normal stresses at failure. The generalized Mohr-Coulomb criterion is described by succeeding equation:

$$\tau = c + \sigma' \times \tan \varphi$$

Where τ is the shear strength, σ' is the effective normal stress and c and φ are respectable cohesion and friction angle. We computed the equivalent Mohr-Coulomb parameters corresponding to the Hoek-Brown failure envelope because many geotechnical analysis programs require Mohr-Coulomb parameters as input (cohesion and friction angle), although actual strength envelopes are often non-linear. Cohesion and friction angle are applied and incorporated into numerical models and limit equilibrium programs.

2.4 STABILITY MODELING

Rocscience is one of the most common softwares used in geotechnical engineering. Rocscience has been improved over the years, with updating and insertions as numerical modeling analysis. A comprehensive explanation of different analysis systems included in rocscience is described here

2.4.1 ROCDATA

RocData helps to analyze the rock and soil strength data, and to determine the strength envelopes and other physical parameters. In other words, for a given set of inputs (m_i , σ_{ci} , GSI, and D), *RocData* computes the parameters of the Generalized Hoek-Brown failure criterion, (m_b , s and a) and other related variables. A useful built-in charts and tables, provided in RocData, helps the estimation of input properties. RocData plots the failure envelope corresponding to the strength criteria and strength parameters currently in use. Failure envelopes are presented in both principal stress and shear-normal stress. A further important functionality of RocData is the ability to obtain the equivalent Mohr-Coulomb parameters for the associated non-linear failure envelope.

2.4.2 SLIDE

Slide is a 2D slope stability package used to analyze the stability or probability of failure, of various failure surfaces (both circular and non-circular) in soil or rock slopes. *Slide* is easy to use, and yet provides the ability to model complex surfaces and slope conditions (Hoek 2000). It also provides the ability to incorporate groundwater and external loading conditions into the model in variety of ways (Hoek 2000). *Slide* utilizes the vertical slice Limit Equilibrium Method (LEM) (e.g. Janbu, Spencer, Bishop etc) to analyze the stability of slip surfaces. Rigid-plastic behavior of all slices on the wedge is assumption on which LEM works. The program provides the capability to evaluate either individual slip surfaces or to search for critical slip surface for a given slope profile. It also provides the option to analyze the slope using safety factor (deterministic) or in terms of the probability of failure. In the LEM the assumption is that all the forces considered act through the center of each slice and the failure model is represented as translational slip

2.4.3 PHASE

Phase 2 is a powerful 2D elasto-plastic finite element stress analysis program, which enables to model a system that evolves in time, where progressive failure and deformation can be step by step monitored. *Phase2* incorporates a 2-dimensional finite element mesh generator. The automatic finite element mesh generator utilizes triangular and quadrilateral finite elements to generate the mesh. In order to perform the 2-dimensional numerical modeling, elastic-plastic behavior is assumed. One of the important features of Phase 2 is the finite element slope stability using the Shear Strength Reduction (SSR) method, which is used to determine the safety factor of a slope through computing critical strength reduction factor of a slope. The method reduces the shear strength of the material to a point where the model is unstable. And further, the point at which the model becomes unstable is taken as the factor of safety of the slope. Some advantages of this approach are:

1. No need to define failure surface or search for a failure surface with minimum factor of safety;
2. All the equations of equilibrium are satisfied;
3. Axial force, strain, moment, and displacement can be computed;
4. The progressive failure of the model can be visualized.

Importing directly a Slide file into Phase 2 program removed the complexity of defining finite-element model. Material models, boundary condition, in situ-stress states and meshing were automatically defined.

CHAPTER 3: GEOLOGY AND TECTONIC SETTING

3.1 REGIONAL GEOLOGY OF PACAYA

The eruptive history of Pacaya complex can be subdivided into three separate eruptive phases, and each one is characterized by individual petrographic and chemical signature (Eggers 1971). A geologic map of Guatemala proposed from “Instituto Geografico Nacional” IGN of Guatemala, 1974 (field work and compilation by Eggers), describes this eruptive evolution.

- I. Growth of a small ancestral strato-volcano associated with andesitic volcanism;
- II. Voluminous eruptions of dacitic pumice and domes;
- III. Eruption, which is still active today, characterized of olivine basalts eruption and growth and collapse of basaltic composite cones and cinder cones.

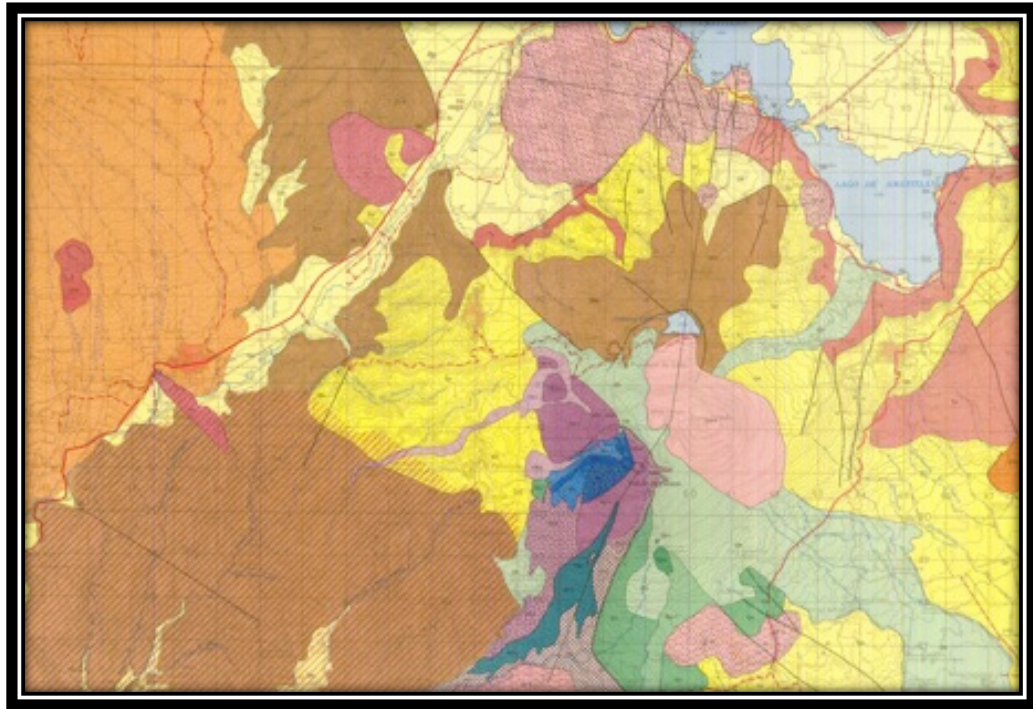


Figure 3.1: Geological map of Guatemala modified from “Instituto Geografico Nacional” (IGN) of Guatemala, 1974.

3.1.1 PHASE I

Growing of ancestral volcano that covered the area now called Calderas. A few outcrops are still exposed today in the north of Calderas zone, which underline the andesitic chemical composition, “Q_{ac}” (Fig.3.1). The growth of ancestral volcano concluded in the collapse of volcano forming a small caldera. The caldera is partially filled by a small lake, Laguna Caderas.

3.1.2 PHASE II

Volcanism began with large eruption of dacitic pumice and culminated with eruption of rhyodacite, dacite and andesite domes, e.g. “Cerro Grande, Cerro Chiquito”. “Q_p, Q_{r-d}, Q_{a-d}” are volcanic deposits depicted in the geological map (Fig.3.1)

3.1.3 PHASE III

This recent eruptive stage began shortly after Cerro Grande activity was over, and its volcanism is divided into three subphases (Egger 1971):

- 1) Initial volcanism;
- 2) Historic volcanism (collapse-1961);
- 3) Modern volcanism (1961-1970).

Growth of the Initial elongate volcano along a north-south trend, which resembles a multiple vents associated with Caldera somma, constructed of numerous basalt flows and minor pyroclastics. The growing phase ended with the southwest flank collapse, which produced a horseshoe-shaped scarp. Lava flows, which form the initial cone, are well exposed along the scarp. The volcanic material is classified in the succeeding unit “Q_{ic}, Q_b, Q_{pc}, Q_{pcf}” The historic subphase was characterized by vents activity aligned along the scarp. Two of these vents occasionally erupted basalt flows, tephra and pyroclastic, which form Pacaya and Cerro Chino. Pacaya volcano was a simple, asymmetrical, nested composite cone (Eggers 1971). The material erupted from these vents filled the area surrounded the old scarp. Significant note, which must be considered for further geotechnical assessment, is that these lava flows are typically blocky “aa type”. The volcanic units represented here are respectively “H_{p-c}, H_b”. After a quiescent period of 18 years, Pacaya erupted in 1961. In the June of 1962, a large sector of southwest flank collapsed creating a pit crater. Small basalt flows have been erupted, during Strombolean activity, confined to the crater area where a small lava-tephra volcano (McKenny cone) has grown to fill and overflow it. Subsequently, McKenny cone became a permanent feature of Pacaya volcano now totally indistinguishable to form a recent morphology. Volcanic units, “M_{c-h}, M_{b1-3}” presented in Fig.11.

3.2 STRUCTURAL SETTING

The Pacaya volcanic complex includes the Pacaya composite cone, Cerro Grande and Cerro Chiquito, and Cerro Chino (Eggers 1971). The Pacaya complex is part of the Central America volcanic arc, which is associated with subduction of the Cocos plate under the Caribbean plate. The southern portion of the Guatemala is located on the Caribbean tectonic plate, and it's subject to an 8 mm/yr east-west crustal extension, which has formed a series of north-south trending grabens (Bukart and Self 1985). The Caribbean plate in this region is also split by the right-lateral strike-slip Jalpatagua fault zone, which broadly coincides with the northwest-southeast trend of volcanic arc, and moves at a relative rate of 10 mm/yr (Carr 1976; White and Harlow 1993).

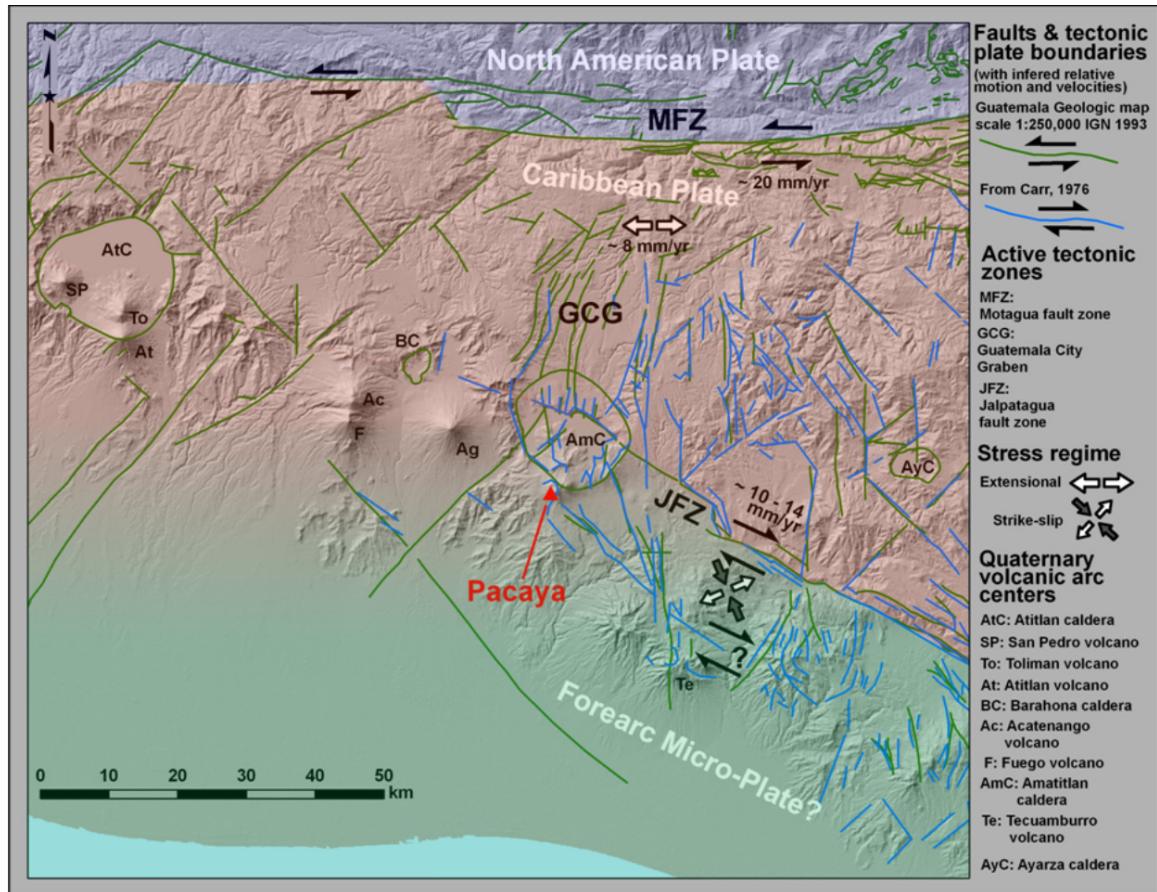


Figure 3.2: Regional tectonics and deformation pattern of Pacaya zone. Tectonic Plates involved and deformation rate. Orientation of the main faults (Carr 1976) The red triangle indicates the location of Pacaya volcano in Guatemala. Mapa Geologica de Guatemala Escala 1:250000; IGN/Bonis 1993 modified. (Rudiger Escobar Wolf 2010).

Pacaya is located near the Guatemala City (as shown in Fig.3.2) at the intersection of Guatemala City Graben extension zone and the Jalpatagua fault zone, in correspondence with the southern rim of Amatitlan Caldera (Wunderman and Rose 1984). The exact location and width of the Jalpatagua fault and its possible interaction with the Pacaya volcano is not well understood. The available geo-structural maps for the area (Fig.3.2, IGN/Eggers 1969; Eggers 1969; Eggers 1972; Carr 1976; IGN/Bonis 1993) represent a system of faults that run parallel to the principal Jalpatagua fault zone, which projected could intersect Pacaya volcano to northwest. Previous studies indicate that this near tectonic stress might facilitate magma ascent at Pacaya (Conway 1995).

CHAPTER 4: METHODOLOGY

4.1 INTRODUCTION

The methodology of this study includes four stages, which are determinant to analyze the stability of the slope. Geomorphology of Pacaya volcano using GIS consented to create accurate topographic profiles, which are the first step in building models. Geotechnical surveys are the principal needs in order to describe a preliminary strength of rock mass, which subsequently compares with the mechanical properties measured in the laboratory. Structural investigations describe the main features belonging to Pacaya volcano. Discontinuity orientations, vents, and fissures, represent a possible scenario of local stress acting through the edifice. Seismic analysis constrain an interpretation of magma sources location and inferable pathway to magma rising.

4.2 GEOMORPHOLOGY

4.2.1 GEOLOGICAL SYSTEM INFORMATION

GIS is a group of spatially referenced computer based mapping programs that allow integration and visualization of spatial data. Due to its ability to produce geographically referenced maps, ArcGIS was selected to produce maps of the study region. Pre-existing geographically referenced high-resolution map (0.5-2 m pixel size) of the field area was imported into GIS in order to obtain Digital Elevation Models (DEM), which has been involved to create topographic profiles. Areal photographs from 2000, 2005 and 2006 ortho-rectified and geo-referenced have been used as cartographic base to build the volcanological map (Gomez et al. 2010). The current map was implemented with new datasets, global positioning system (GPS) waypoints. The GPS waypoints indicate field survey where geotechnical investigations have been performed. Rock mass description, sampling site, seismic stations, new vents location are included in the geographically referenced map (as shown in Fig.4.19).

4.2.2 TOPOGRAPHICAL PROFILES

In order to perform the stability analysis of a volcano using RocScience software, it is necessary to have the topographic profiles of the slope investigated. The profiles were constructed by drawing a run-line digitally onto a DEM. The run-line represents the path of the topographic profile. A more recent available 2006 DEM was employed to achieve good approximation of real topographic surface of Pacaya volcano. Although 1954 and 2011 DEM, were able to demonstrate a recent geomorphologic evolution in topographic surface. In function of different approach to evaluate the stability of this slope, two topographic profiles were acquired, section A-A' and B-B' (Fig.4.1).

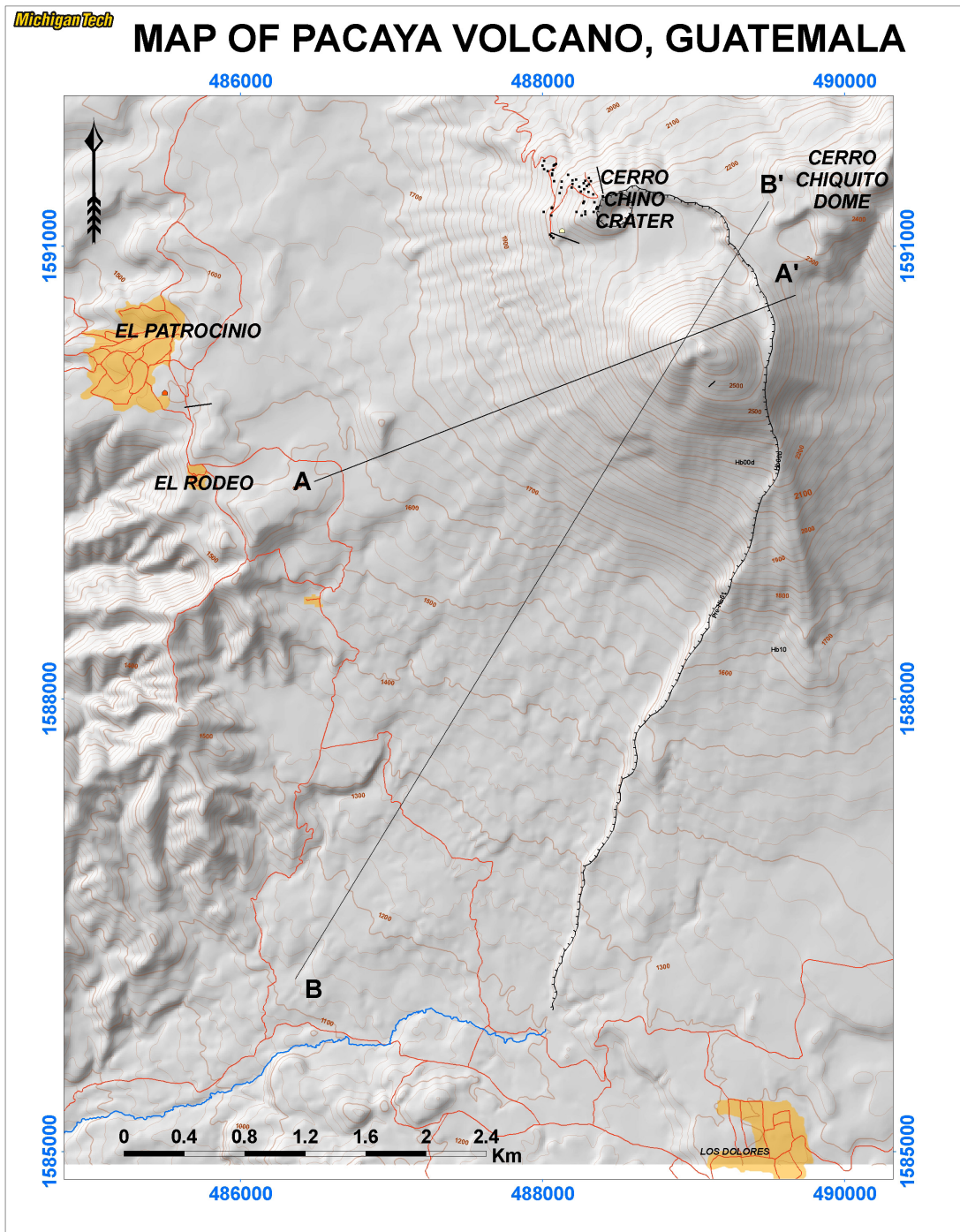


Figure 4.1: Cross section of the Pacaya volcano slope. Section AA' and BB'. Modified version of the volcanological map from Gomez et al. (2010).

4.2.3 GEOMORPHOLOGY EVOLUTION

4.2.3.1 RECENT DISTRIBUTION OF VOLCANIC LAVA FLOWS AND VENTS

Recent activity at Pacaya volcano (from May to June 2010), has experienced change in the distribution of lava flows and vents location. In the 27th May 2010, the activity migrated along south-southeast flank of volcano where a new vent produced a large lava flow (Fig.4.2). Otherwise, the eruption at the central vent (McKenny cone) created a trough on the northwest flank of the volcano aligned with the new lava flow. Surveys conducted during our fieldwork at Pacaya, January 2011, revealed the presence of seven new vents localized outside the old scarp, exactly in the same southeast flank. All the previous vents formed during the activity since 1961 were located inside the Old Pacaya collapse scarp and most of them were clustered near the Meckenney cone central vent (Fig.4.2). The distribution of the new vents marks a possible significant change in the activity at Pacaya, as it is located outside the “Old Pacaya collapse scarp”. The idea here is that the location of the new vents would represent the direction of least resistance for magma movement (Fig.4.3). Morphology analyses on spatial pattern cones located to SE slope outside the old collapse demonstrate ellipses shape with maximum axes elongated toward NW. Each vent is merged to another along linear volcanic fissures forming a sequence “cone-fissure-cone”. This linear trend, North-West – South-East, of least resistance for magma movement join together with important volcanic features as 2010 May 27th trough due to magma pressure during the eruption and relative withdraw (north-west slope); central vent (Mackenny cone); dry and volcanic fissures on the top of south-east slope of volcano and finally with historic Cerro Chino vent (as shown in Fig.4.19).

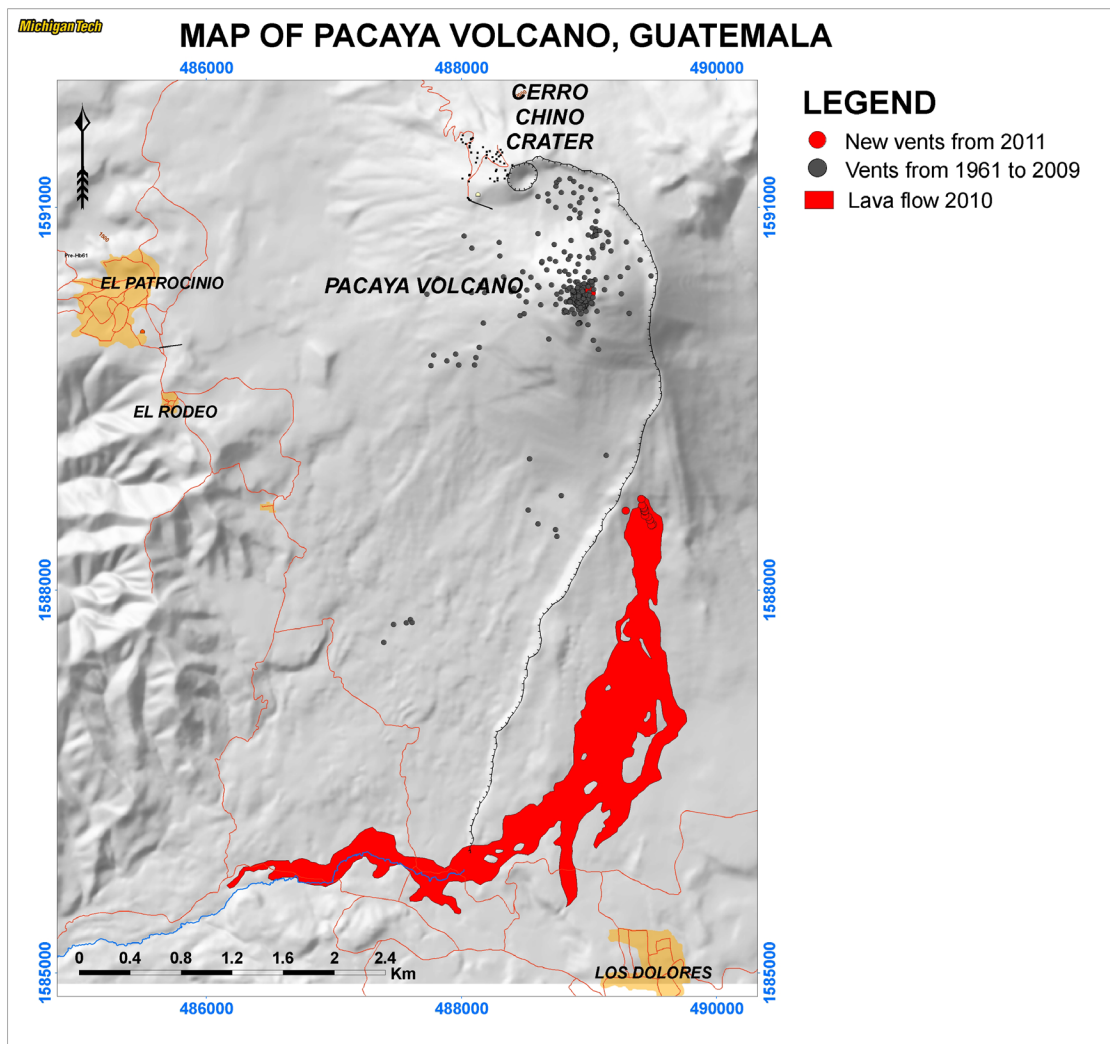


Figure 4.2: Vents distribution since 1961 and recent lava flow. Modified map from Gomez et al. (2010).



Figure 4.3: New vents distribution on southwest flank of Pacaya Volcano. 1) “Vent 5” located on downhill southwest flank. 2) Small cone along “Vent 7” fissure. 3) “Vent 6” elliptical cone morphology. 4) “Vent 7” as linear volcanic fissure NW-SE orientated.

4.2.3.2 HISTORIC GEOMORPHOLOGY EVOLUTION REVIEW

Recent significant features, which forced a change in geomorphology of Pacaya volcano, are two small collapses since 1961 to 2010. The first connected with growing of McKenny cone inside the small pit crater, which became a permanent feature of Pacaya volcano now totally indistinguishable to form a recent morphology. Otherwise, the last activity discussed above, in 2010 May 27th produced a trough still visible at present. All these features are aligned in a north-northwest orientation.

4.3 GEOTECHNICAL SURVEY

During the preliminary stages of project, when the information about rock mass, its stress and hydrologic characteristics are sparse, the use of a rock mass classification is a practical solution. The estimation of strength and deformation characteristic of a rock mass is required for any form of analysis used to assess slope. Single discontinuity has received much attention in geotechnical literature and major concern is attributed to their orientation with the purpose to have a better understanding of the structural setting of the area analyzed. In order to characterize the rock mass properties (lithological and mechanical), fracturing and weakness zones, a geomechanical survey was carried out along Pacaya volcano. The survey was mainly focused along the old collapse sector where detailed geotechnical examinations were performed on 10 sites (fig.4.4). The survey sites cover the majority of the scarp from south to north with exclusion of few inaccessible zones.

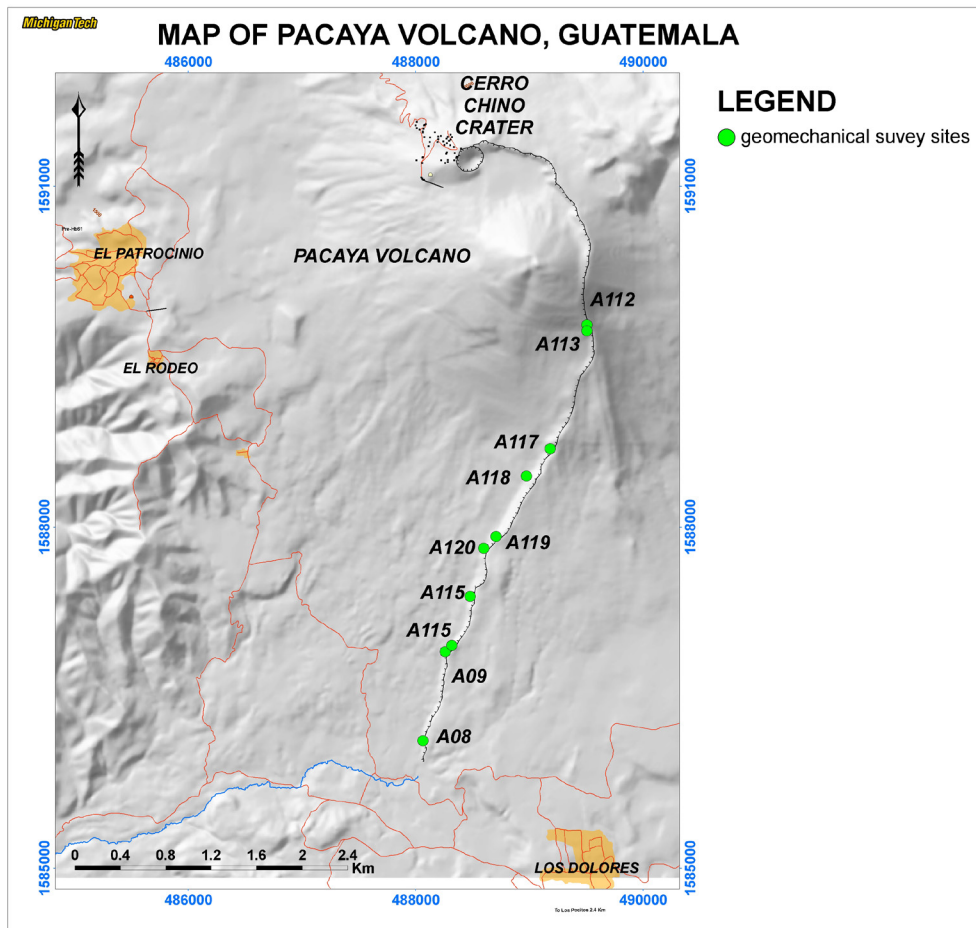


Figure 4.4: Sites of geomechanical survey executed. Based map modified from Gomez et al. (2010).

4.3.1 ROCK MASS DESCRIPTION

Previous studies carried out on Pacaya volcano considered only lithological and petrological perspective, neglecting geotechnical characteristics of the rock masses. In this study, the first geotechnical evaluation of the rock mass has been achieved. Rock mass and discontinuity description was undertaken over a total of 10 sites. The distribution of these sites is illustrated in Fig.15. Two main geotechnical classes were identified at Pacaya: lava and autoclastic breccia. Pyroclastic and tuff layers were incidentally recognized along the scarp, but their sparcity (one single layer for each) together with their small thickness, forced to neglect them from our investigation. Besides these layers are located along the old scarp of historic volcano, which could not be realistic of the recent construction of Pacaya volcano. In this study I assume that the Lava and breccia are prominently distributed over a wide area of the Pacaya volcano. Contemporary lava flows and breccia validate this assumption. Lava and autoclastic breccia materials are classified into mono-lithological geotechnical class even though the slope of a stratovolcano as Pacaya comprises layered polyolithologic sequences. In order to account for this limitation, a lithotechnical unit classification using a percentage of distribution of corresponding lava and autoclastic breccia classes were determined.

4.3.1.1 LAVA ROCK

Lavas represent the strongest geotechnical class, regardless of mineralogical composition. Lavas are intensely fractured rock mass with two main family of vertical discontinuity perpendicular to each other (Fig.4.5). Although 5 joints have been determined in 10 field surveys performed. Some lava joints are filled with weak soil giving the rock mass a lower quality rating (RMR Section 5.2.2). Lavas are further distinguished as fresh and weathered, where the alteration reduced the strength of rock. As a result of the wide aperture of some discontinuities, e.g. A117 site, the infill often drains freely, causing discontinuities to be normally dry. However, where outcrops are under vegetative shelter, infill is seen to be damp. Free water is not associated with this rock mass. A global view of rock characteristics for each site is illustrated in the Table 5.1.

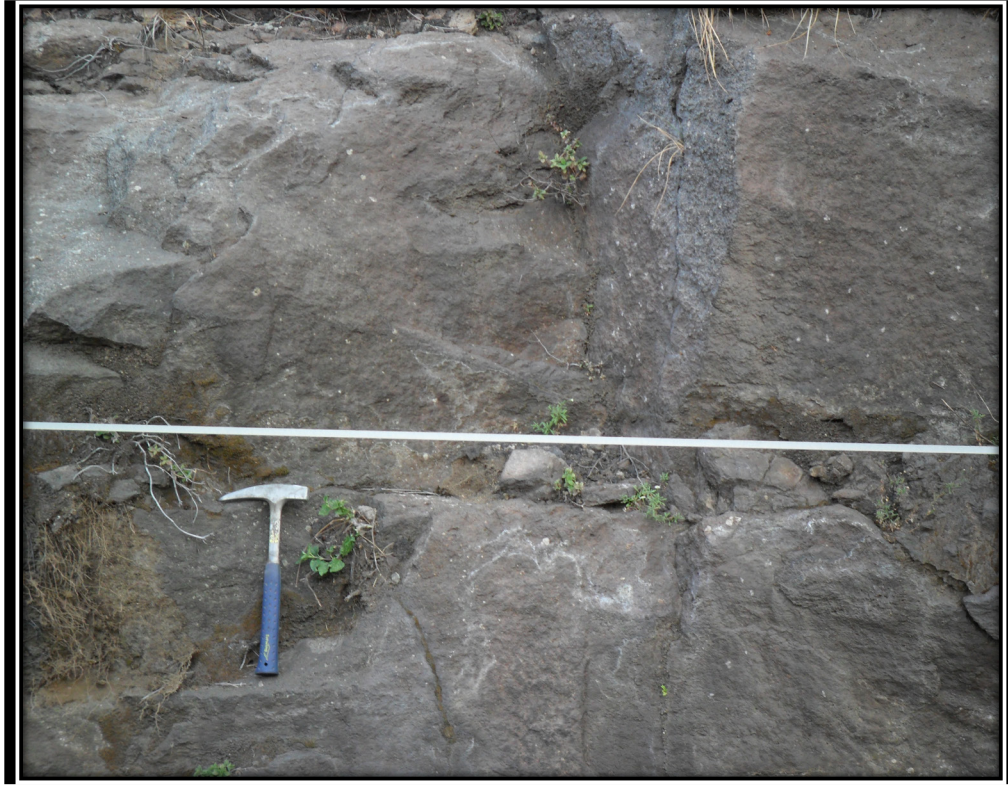


Figure 4.5: Lava outcrop, site A120, with surfaces slightly weathered with very small joint opening.

4.3.1.2 AUTOCLASTIC BRECCIA ROCK

Autoclastic breccias are produced due to the fragmentation of lava flow during cooling, which form the carapace and base of "aa" flows. Autoclastic breccias form layers of vesicular, rigid, discreetly dense, angular and sub-angular clasts can be fused together or else remain separate (Petro et al. 2007). Autoclastic breccia unit is composed of block-supported, matrix-poor, and good interlocked, and a small clast-supported with poor to medium-matrix classes (Fig.4.6 and Fig.4.7). Their formation depends on composition, temperature and strain rates, which control the rheology of the autoclastic breccias layers. Geotechnical classification of autoclastic breccia has large uncertainty because of the problem in obtaining rock mass properties representative of the global mechanical behavior of this unit. Therefore, interpreting the mechanical behavior of breccia is still an open research question (Apuani et al. 2005; Hoek 1994; Petro et al. 2007).



Figure 4.6: Autoclastic breccia block-supported good interlocked. Red bar represents 0.5 m



Figure 4.7: Autoclastic breccia clast-supported with poor to medium-matrix.
Red bar represents 30 cm

4.3.2 ROCK MASS STRENGTH

“Several different factors control the strength of rock mass leading to several classifications. The rock mechanics characterizations of 10 sites have been conducted following the International Society for Rocks Mechanics procedure (I.S.R.M. 1981) and the Geological Strength Index (GSI)” (Hoek et al. 2002). RMR classification was used to evaluate the lava rocks deposits. Whereas, for the disintegrate rocks or highly weathered rocks or poorly interlocked rocks are present it is impossible to obtain the parameters needed for the application of RMR classification. Therefore, the Geological Strength Index (GSI parameter) introduced by Hoek and Brown (1980) seems to be the better tool for characterization. It is found on visual impression of rock structures, in terms of blockiness, geological complexity, and surface conditions (roughness and weathering). In-situ accurate analyses were performed focusing on lava layer as well autoclastic breccia layer.

4.3.2.1 SCHMIDT HAMMER

The Schmidt hammer is used to obtain quick and approximate measurement of compressive strength of rock. Large number of test can be carried out in a relatively short time (Selby 1993). The working principle is based on rebound of the piston against the plane of the rock surface. The rebound number is noted and can be used to obtain the compression in MPa can be obtained. When the Schmidt Hammer is pressed against a surface, the piston is released onto the plunger. “The energy produced represents the resistance to impact (i.e. the hardness) of the surface. This enables the piston to rebound. The distance travelled by the piston after it rebounds is called the rebound value ‘R’” (Goudie 2006). The measurements were executed on plane surface to avoid false values due to irregularity (discontinuity and rock surface) of surface that limit the contact between piston tip and surface. Yet, it remains a wide variation in the procedures employed by different researchers particularly in determining the number of impacts used to obtain ‘R’ values is observed. Matthews and Shakesby (1984) “recommended 15 rebound values for each sample, with 5 values that deviate most from the mean being discarded”. At each site 20 number of impact rebound measurements were performed discarding the most deviating values. The N type Schmidt hammer was employed in this study. It provides data on different rock types from very strong to weak with compressive strengths (c) values from 20 to 250MPa (Goudie 2006). “The L type hammer has an impact three times lower than the N type. It is only appropriate for weak rocks and those with thin weathering crusts” (Goudie 2006).

4.3.2.2 DISCONTINUITY

Discontinuities within a rock mass concentrate stresses, influence groundwater movement, act as potential failure plane, and in general weaken the rock mass (Selby 1993; Wyllie and Mah 2004). Therefore, in order to acquire even a partial understanding of the rock mass, the discontinuities must first be addressed. Rocks mechanics data of 150 lava-joints were measured at 10 sites. This dataset was used to identify the number of joint sets their representative orientation, set spacing, type of movement, dilation, degree of alteration, roughness, and presence of infill, as well as the geometry of each joint (Appendix C). Further, these parameters were used to compute the Rock Mass Rating (RMR) using the Beniaowski (1989) criteria.

4.3.2.2.1 SCANLINE SURVEYS

A more in-detail description of the discontinuity at the outcrops scale has been established through a scanline approach (Fig.4.8). This method consists of attaching a tape along the outcrop and measuring the parameters, described above in Section 4.3.1.3, for each discontinuity that cross this line. Few vertical and horizontal scanline have been performed at each site.



Figure 4.8: Horizontal Scanline survey undertaken along 115 site.

4.3.2.2.2 DISCONTINUITY SPACING

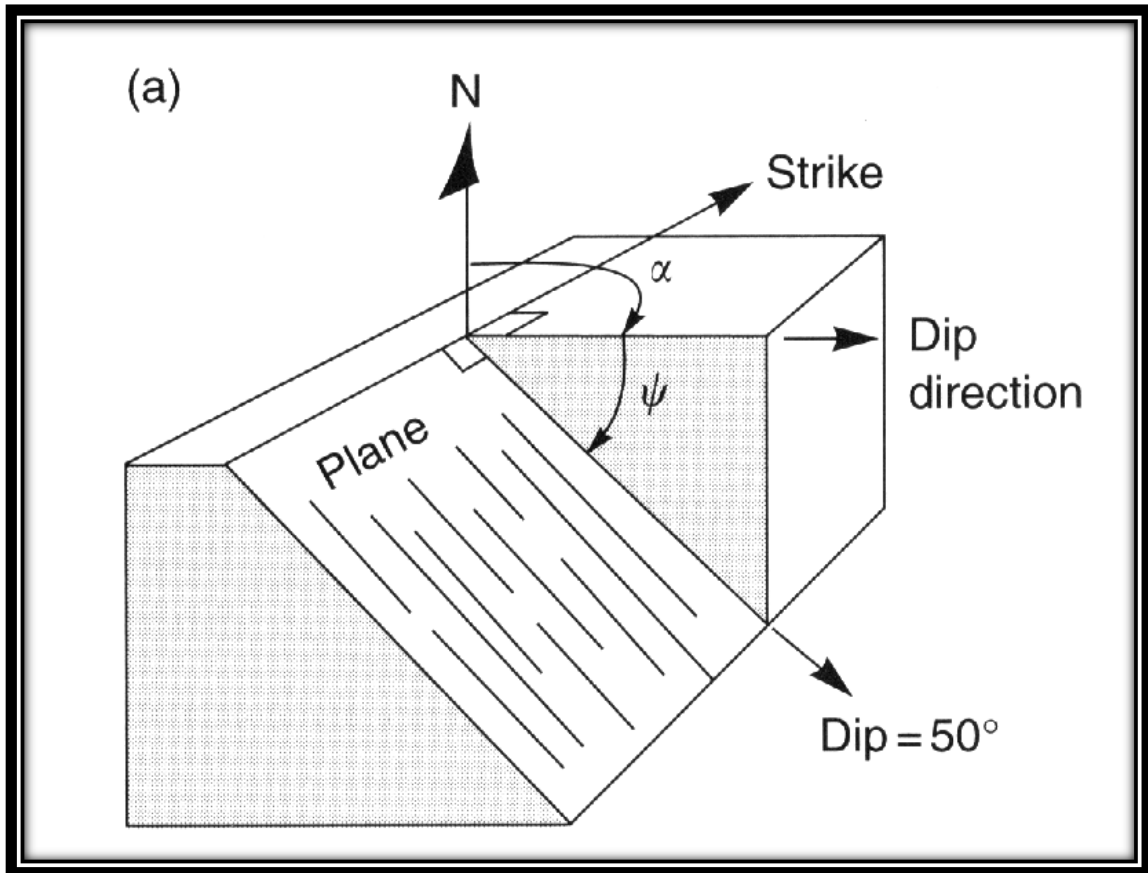
The perpendicular space between adjacent discontinuities of the same family refers to the discontinuity spacing. The spacing determines the volume of blocks mass, which influences a potential rock falls. Different approaches have been used in order to obtain spacing of discontinuity. In the scanline method the tape must be aligned perpendicular to the discontinuity investigated. The distance between adjacent discontinuities of the same family, i.e. same orientation, is measured along the tape.

Table 4.1: Terms describing discontinuity spacing. Adapted from Burns et al. 2005.

TERM	SPACING
Extremely widely spaced	> 6 m
Very widely spaced	2 – 6 m
Widely spaced	2 m – 600 mm
Moderately widely spaced	600 – 200 mm
Closely spaced	200 – 60 mm
Very closely spaced	60 – 20 mm
Extremely closely spaced	< 20 mm

4.3.2.2.3 DISCONTINUITY ORIENTATION

The orientation of discontinuities with respect to slopes is the primary geological factor influencing slope stability (although other properties such as persistence and spacing are significant) (Wyllie and Mah 2004). Discontinuity dip and dip direction were measured in the field using a geological compass. Discontinuity dip is the maximum inclination of the discontinuity measured to the horizontal in degrees. The dip direction of a discontinuity is defined as the “direction of the horizontal trace of the line of dip measured clockwise from north” (Wyllie and Mah 2004) (Fig.4.9). All discontinuity orientations presented in this study are in the form of dip/dip direction (for example 30/089).



4.3.2.2.5 DISCONTINUITY PERSISTENCE

This parameter is one of the most important information to carry out during geotechnical survey but yet the most difficult to determine. The persistence describes the discontinuity extension or the dimension of a discontinuity along plane. The persistence can be quantified measuring the trace length of a discontinuity to its termination along outcrop. Different terminations are classified in relation of their ending. “Ta” represents the discontinuity that terminate outside the outcrop, “Td” represent a discontinuity against to another one, and “Tr” indicates the discontinuity, which ends against rock.

Table 4.2: Terms describing discontinuity persistence from Brown 1981.

TERM	PERSISTENCE
Very low persistence	< 1 m
Low persistence	1 – 3 m
Medium persistence	3 – 10 m
High persistence	10 – 20 m
Very high persistence	> 20 m

4.3.2.2.6 DISCONTINUITY ROUGHNESS AND UNDULATION

The discontinuity geometry is described through two factors, as roughness and undulation, which affect the mechanical and hydraulic properties. In order to assess the roughness, Burton introduced the Joint Roughness Coefficient (JRC), which is evaluated by comparing the discontinuity profile with 10 profiles as references (Fig.4.10). The procedure to measure the undulation and roughness consists to recognize the discontinuity profile. A shape tracer, consisting of a row of pins held together in a single layer, which is free to move in response to undulations on the discontinuity surface, was used to measure the surface roughness of discontinuities. The shape tracer was pressed against the surface and the resulting profiles sketched and compared against roughness grades.

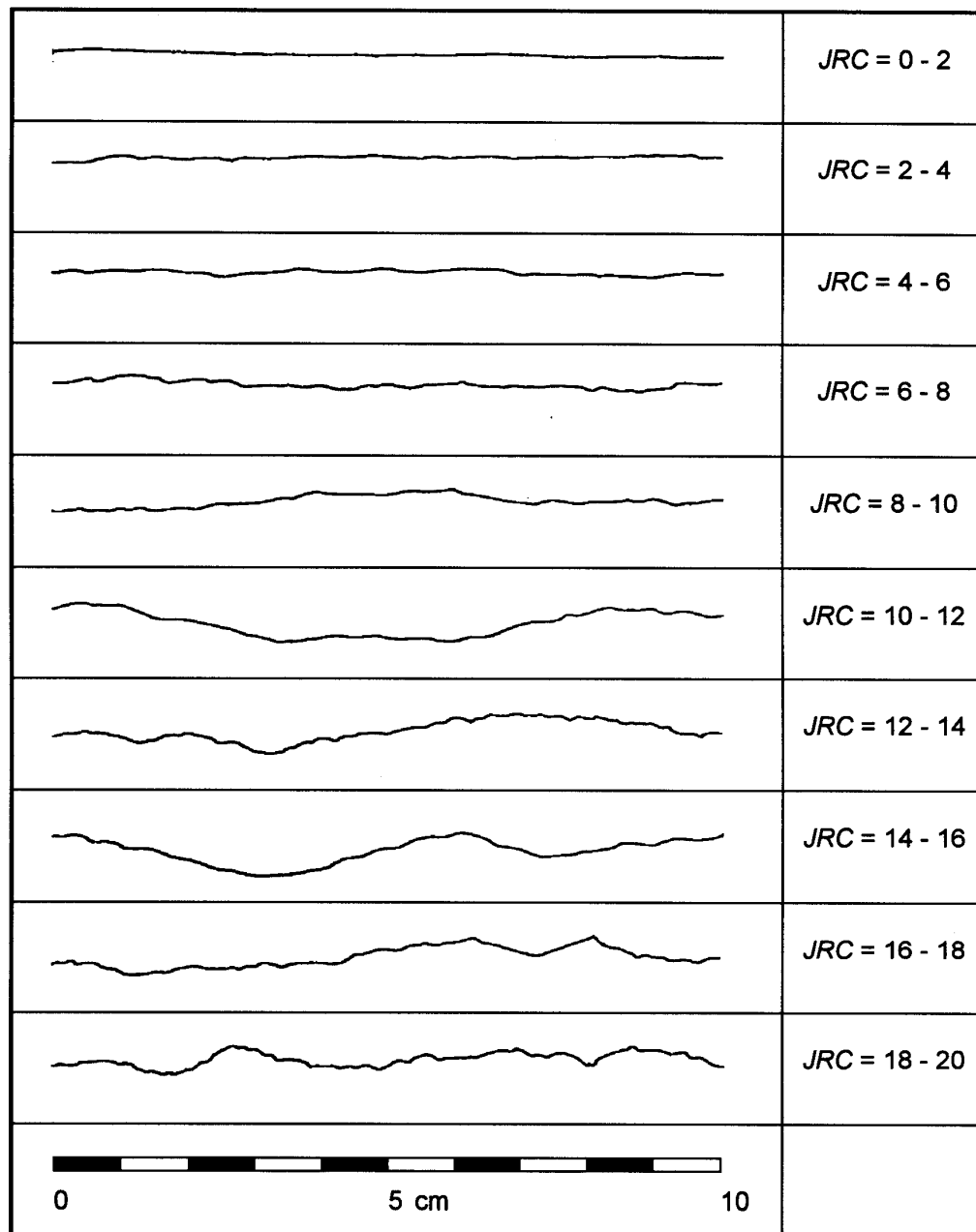


Figure 4.10: Roughness profiles and corresponding JRC values (After Barton and Choubey 1977).

4.3.2.3 SAMPLING

Rock samples were collected for laboratory analysis. During the geotechnical survey two samples as fallen block have been collected from site A08 and A09. These samples represent lava and autoclastic breccia layer. Following the ISRM recommendation, we carried out bulk density, bulk volume, and uniaxial compressive strength tests on the collected samples.

4.4 LITHOTECHNICAL UNITS

Recent studies, have shown the applicability of lithotechnical characterization of volcanic units for stability analysis (Apuani T. 2004). In this study, we present the first approach to Pacaya volcano stability analysis using the lithotechnical units and geotechnical data. The rock succession at Pacaya volcano was classified into lithotechnical units based on in-situ and laboratory investigations. The in-situ investigation includes rock mechanics characterizations of 10 sites conducted following the “International Society for Rocks Mechanics procedure (I.S.R.M. 1981) and the Geological Strength Index (GSI)” (Hoek et al. 2002) was evaluated. The distinction in lithotechnical units was based on the different percentage of breccia fraction vs. lava deposits (Fig.4.11). And three main lithotechnical units were defined as follows:

1. Lava unit (L): lava layer (80-100%) with rarely thin layer of breccia;
2. Lava-Breccia unit (LB): alternation of lava (ranging from 65-80%) and breccia layers;
3. Breccia unit (B): alternation of lava (less than 50%) and breccia layers;

Variable rock masses competence between lava and breccia deposit claim comprehensive classification. RMR classification was able to evaluate only lava rock deposits. By the way where disintegrate rocks or highly weathered rocks or poorly interlocked rocks are present it is impossible to obtain the parameters for the application of RMR classification. Therefore, the GSI parameter introduced by Hoek and Brown (1980) seems to be the better tool for characterization. It is found from visual analysis of the rocks structures based on the blockiness, geological complexity, and surface conditions (roughness and weathering).



Figure 4.11: Image processing method to classify lithotechnical units. Site A08, which is classified as BRECCIA-LAVA unit. Lava range to 42% compared to breccia of 58%.

The figure above explains the visual method used in order to classify the different lithotechnical units. Subdividing the image into small equal fragments (yellow rectangles, Fig.4.11) we are able to find an approximated average of lava and breccia distribution. A visual angle from a point of view not always permits a frontal visualization of the outcrops, creating a geometric distortion of the image. In order to surmount this problem a geometric correction was computed. The thicknesses of lava and breccia layers in the upper sector of the image were increased by a factor obtained from the angular perspective. However, the homogeneous distribution of stacked lava and breccia layers for each region individually considered, in the upper sector of the image caused no great difference in ratio percentage (Fig.4.12 and Fig.4.13).

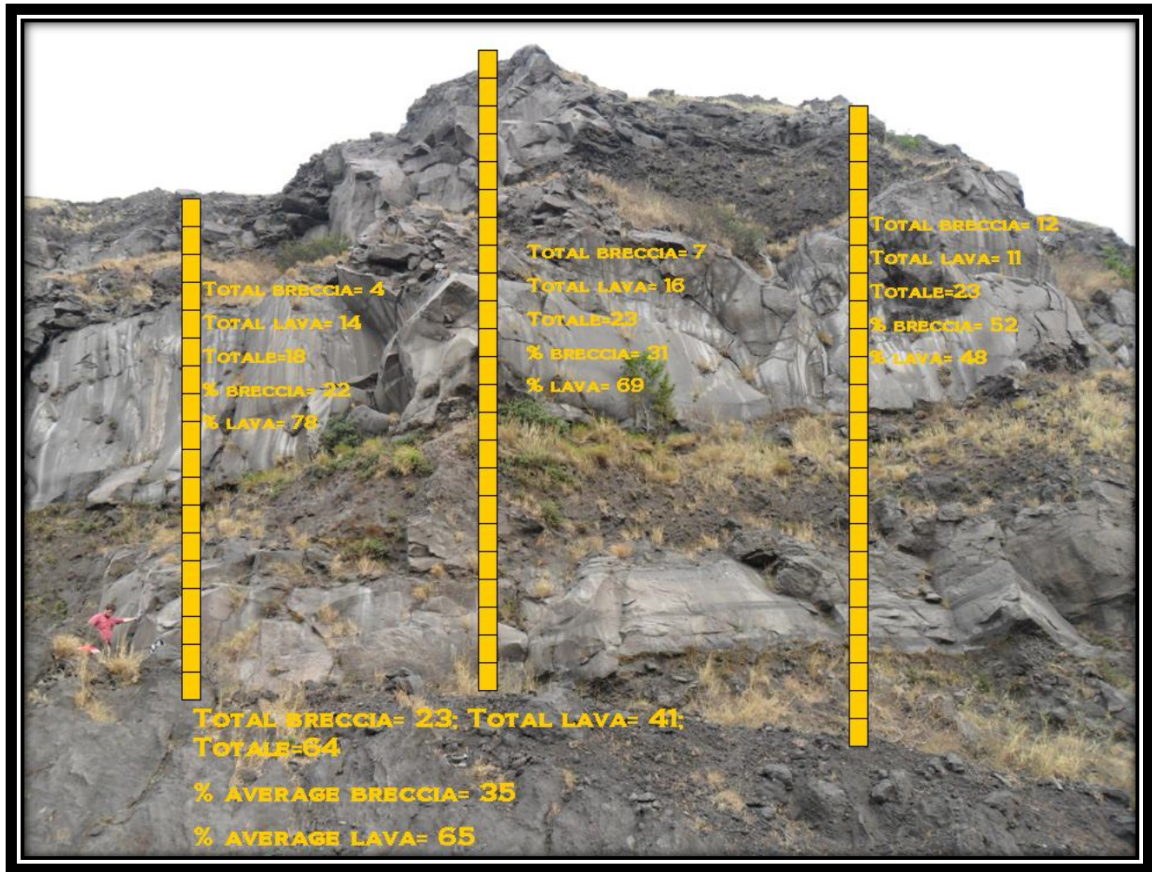


Figure 4.12: Image processing method to classify lithotechnical units. Site A09, which is classified as LAVA-BRECCIA unit. Lava range to 65% instead breccia to 35%. Geometric correction was achieved on this picture.



Figure 4.13: Image processing method to classify lithotechnical units. Site A113, which is classified as LAVA unit. Lava range from 80% to 100%. Geometric correction was achieved on this picture.

4.5 COMPUTING DISCONTINUITY ORIENTATION

Geotechnical investigations of more than 150 joints were performed along the old collapse scarp, concentrated in 10 sites. Data collected during these surveys were then analyzed to process a global behavior of rocks mass over local stress acting at Pacaya. This dataset was used to identify the number of joint sets and their representative geometries: strike, dip-direction and dip; and other parameters mentioned in Section 4.3.1.3. Discontinuities for each outcrop are plotted in Fig.4.14 as projection on equal Schmidt's stereograms of poles to planes. These plots show a characteristic cluster of

points (poles), representing discontinuity families grouped up. We identified existence of 3 to 5 set of families in each sites. Joint labeled from K1 to K5 and S1 as stratigraphic contact between lava and breccia layer. The average of dip and dip-direction, e.g. K1 in Fig.4.15, (Fisher statistic method, 95% cone of confidence), for each of them are the following:

- K1 is $248^{\circ}/72^{\circ}$;
- K2 is $17^{\circ}/64^{\circ}$;
- K3 is $317^{\circ}/74^{\circ}$;
- K4 is $180^{\circ}/74^{\circ}$
- S1 is $131^{\circ}/21^{\circ}$.

We also found gravity dependence discontinuity, called K5 with range values dispersive following the changing orientation for every outcrop.

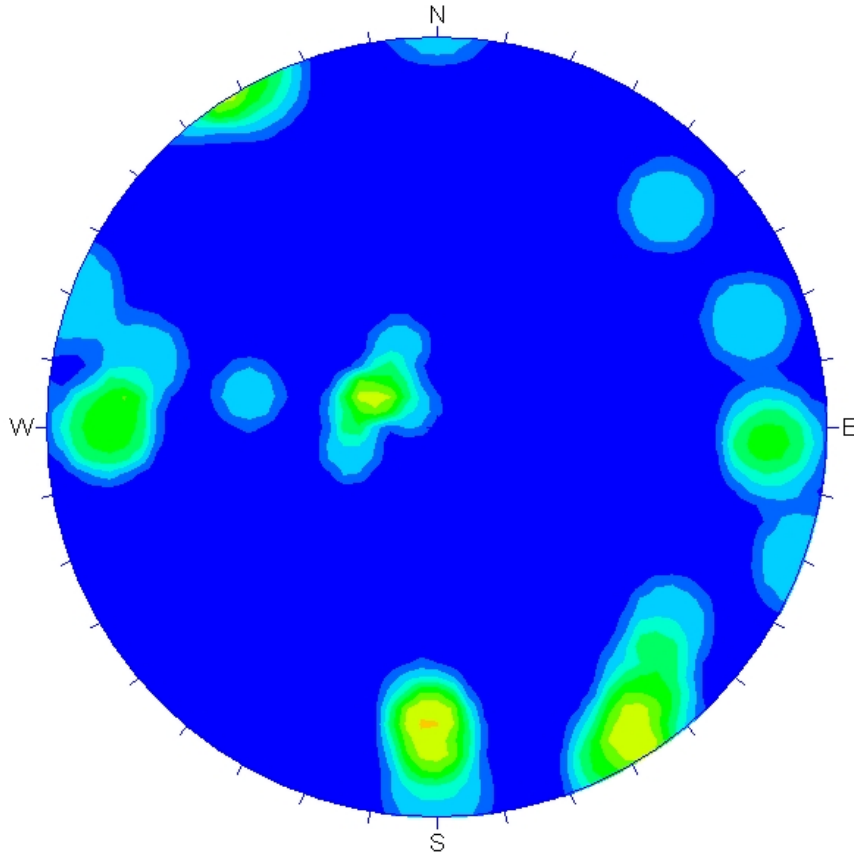


Figure 4.14: Projection on equal Schmidt's stereograms of poles to planes (e.g. A115 site). All discontinuity families present in this site are plotted here, K1, K2, K3, K5 and S1.

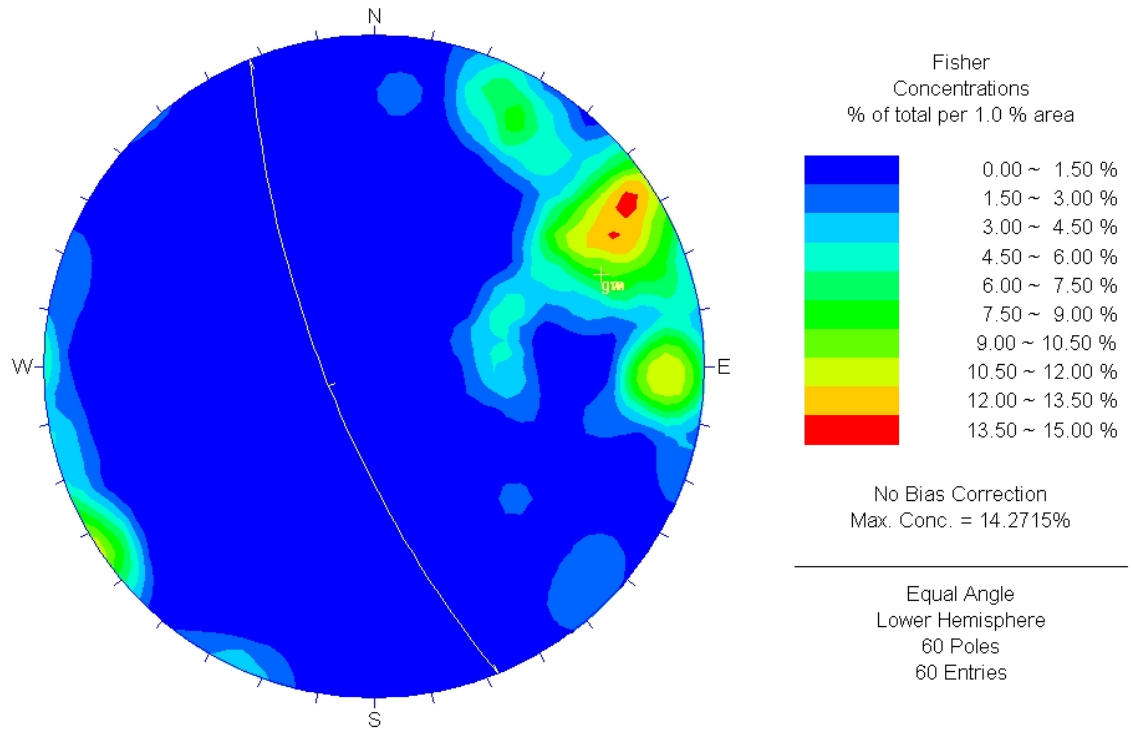


Figure 4.15: Projection on equal Schmidt's stereograms of poles to planes of K1 discontinuity. The plane here represented, is the average computed of K1 discontinuity orientation with 95% of confidence, corresponding to $248^{\circ}/72^{\circ}$. The legend represents the concentration of poles in different areas.

4.6 SEISMIC SURVEY AND ANALYSIS

During 2011 field campaign a small array was deployed on the western flank of Pacaya volcano (Fig.4.19). Vertical component channels from 12 short-period stations, red circles in Fig.4.16 were analyzed to obtain information on the tremor source and wave travelling direction.

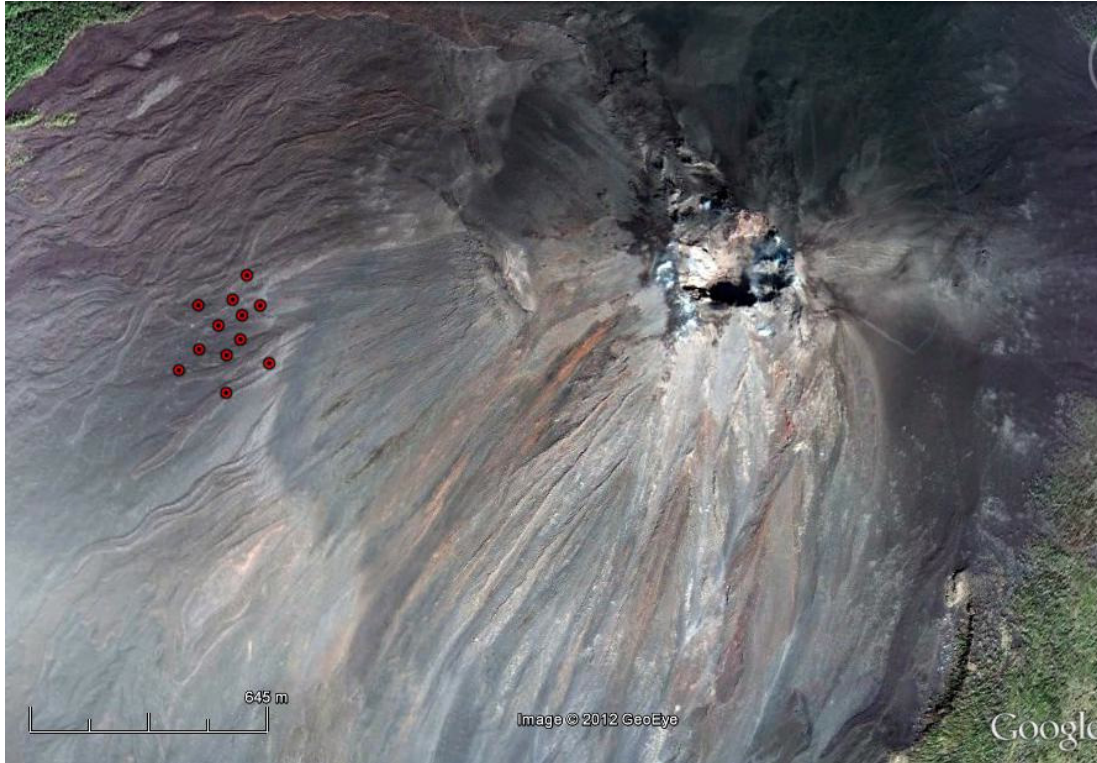


Figure 4.16: Small array deployed on the southwest flank of Pacaya volcano. Red circles represent single stations, which compose the array. Image modified from Google-earth.

The seismic processing data needed some constrictions to be satisfied. The aperture of the array should be less than 2-3 times the distance to the source in order to assume the incoming wave is planar, and wide enough to capture a significant portion of a wavelength. An aperture of 200-300 m satisfied the requests above mentioned. Semblance analysis method, which is similar tool as cross-correlation, was performed computing the semblance of the shifted traces where L is the number of samples and N is the number of stations. Maintaining path of the semblance values for each azimuth and slowness.

$$S = \frac{\sum_{j=1}^L \left(\sum_{i=1}^N A_{i,j+k(i)} \right)^2}{N \sum_{j=1}^L \sum_{i=1}^N A_{i,j+k(i)}^2},$$

Measuring the arrival time of waves and computing the time delay (Δt) for each station with respect to station 3, center in Figure 4.17, and shifting the traces at the other stations appropriately, were the primary procedures in order to proceed with semblance analysis.

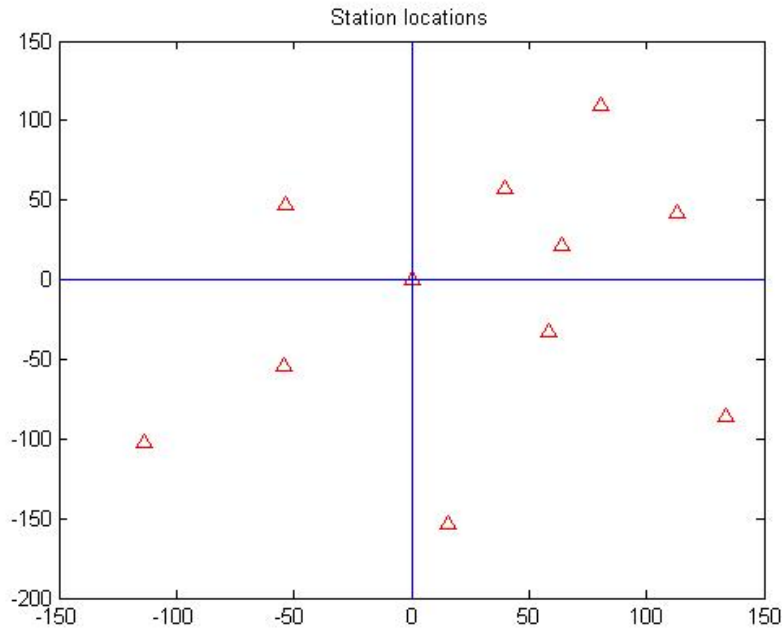


Figure 4.17: Computed time delay for each station with respect to station 3, centered here.

This method involved a grid search over plane wave orientations to determine the best fit to the data. At each step, the appropriate time delays for a wave of the given orientation were calculated and the waveforms were shifted. The similarity of the waveforms has been measured using semblance. Finally, semblance were plotted as function of slowness and azimuth in Fig.4.18. The best-fit location (largest semblance) is marked with a white star.

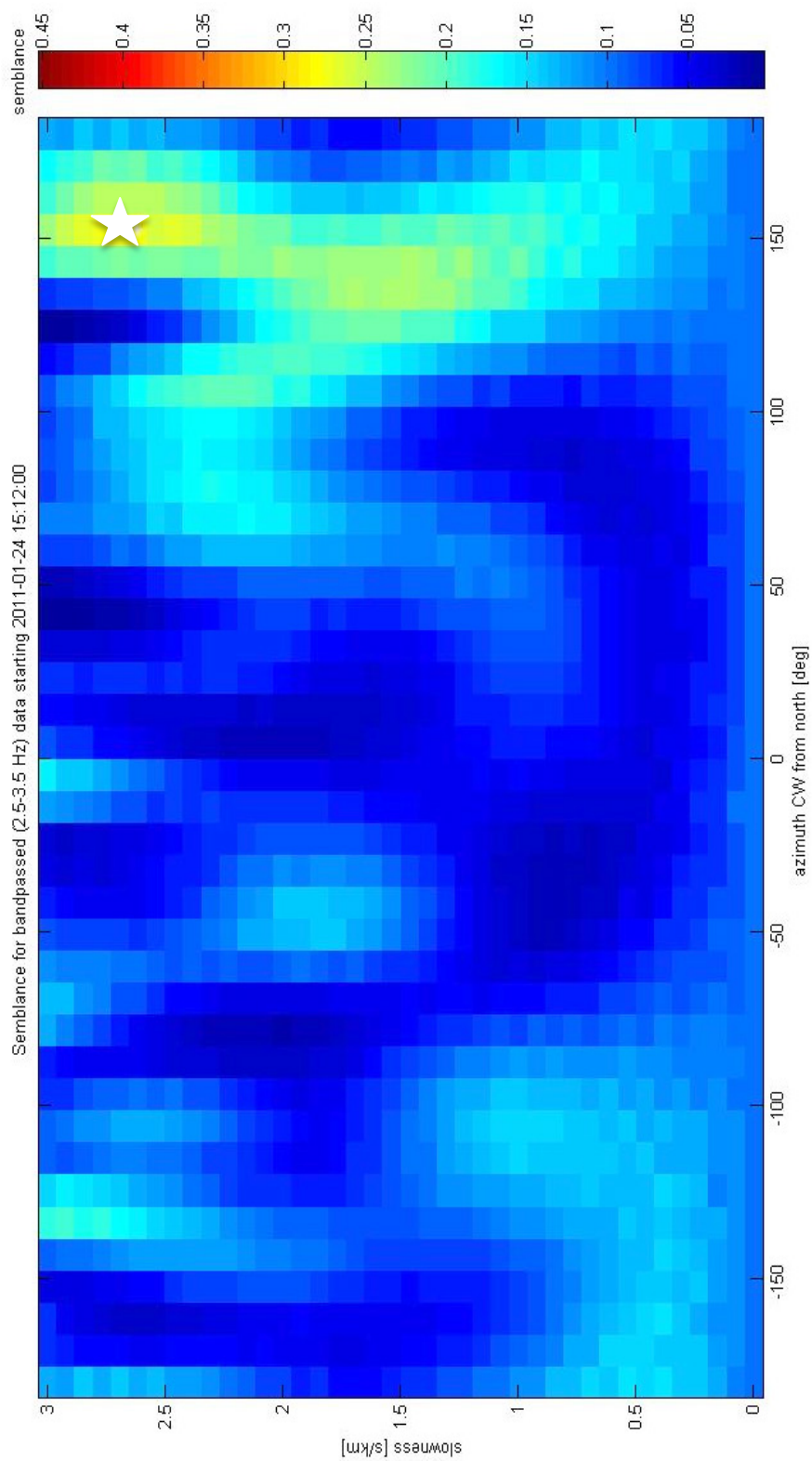


Figure 4.18: Semblance analysis plotted as function of slowness and azimuth. Example with best-fit azimuth indicate by white star. The plane direction correspond to 168 ° from north.

We determined the orientation of the plane wave. The orientation of the plane provides information about the source location and the type of wave. The direction the wave is traveling should be 180° from the direction to the source. The seismic analysis was directed on classify 3 Hz pulsating tremor recorded by all stations. In particular, we analyzed 1 min. window for each station. To compute the semblance, we used range of azimuth ($-\pi/2$ to $\pi/2$) and slowness from 0 to 0.003 s/m. Locations, as best fit of source where tremor coming out, were determined from this analysis. The sites found out corresponding old vent and new vents location. Plane wave shown as dashed-line, indicates the direction to the sources (as shown in Fig.4.19). Inferred magmatic activity preferential direction, as connection between the sources along NW-SE trend, is required to know which cross-section is the correct one to apply magma load. Magma load is applied perpendicularly at this magmatic trend.

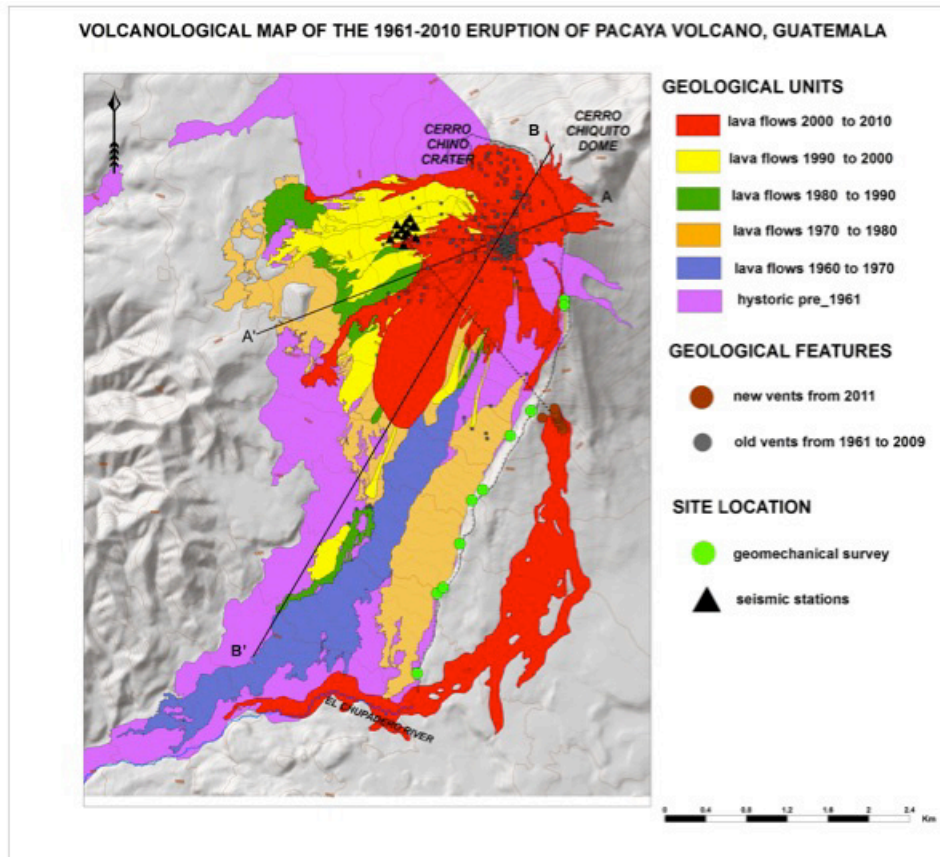


Figure 4.19: Seismic stations shown on the modified volcanological map from Gomez et al. (2010). Section AA' perpendicular to this magmatic trend is represented here.

4.7 STRUCTURAL IMPLICATION AND RELATIONSHIP WITH SEISMIC DATA AND VENTS LOCATION

Discontinuities, faults, vents, and seismic data must be considered in a comprehensive sight in order to obtain likely stress configuration acting at Pacaya. Although we found four sets of discontinuity (Section 4.5), the most important, and omnipresent joint families are just two: K1 and K3, which should be very important to infer the complicated local stresses occurring at the Pacaya volcano. The stereographic projection of the aforementioned fractures reveal orientation joint pattern, which presented interesting affinity with the recent stress configuration. In particular, the strike of the K1 fracture (Fig.4.20) falls in a particular direction coeval with other volcanic features, as linear vents forming a sequence “cone-fissure-cone” discussed in Section 4.2.3.1. These linear vents, associated with the volcano summit vent, would well

represent the magma feeding system concentrated along the NW-SE axial rift crossing the volcano. The particular change in location of vents is likely to be related to the local and regional structure and tectonics, and possibly reflects the condition of stress of the volcano edifice during the eruption.

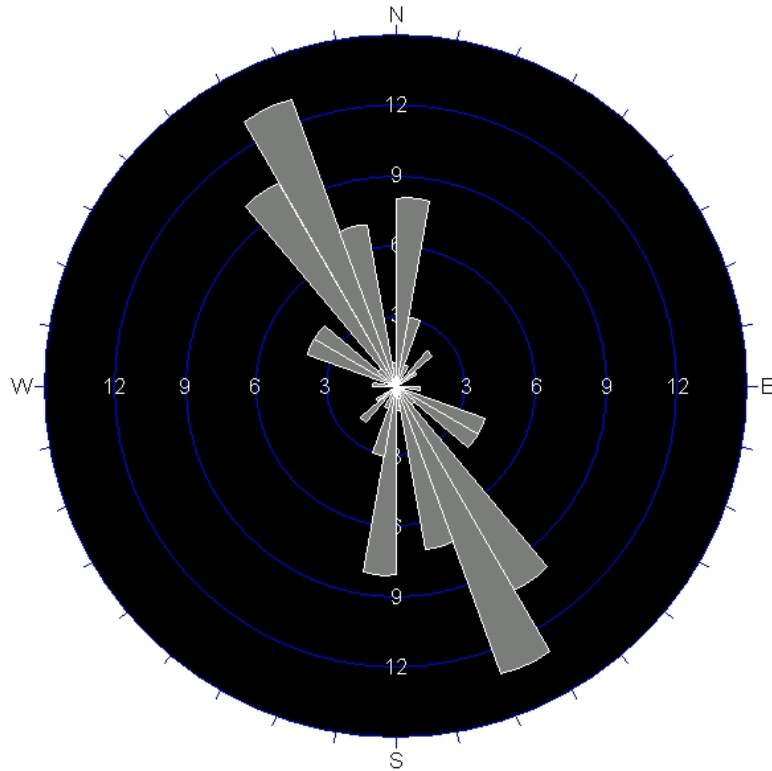


Figure 4.20: Rosette plot of K1 joint strike representing the most reliable direction of this fracture, which is between 20-30°NW.

The orientation of discontinuity (K1), dry and volcanic fissures, presence of parallel faults, and the new vents likely explain the reactivation of the pre-existing stress configuration responsible for the old-collapse at Pacaya. Moreover, the magma activity located outside of the old scarp is the evidence of how regional stresses affect recent Pacaya's vent distribution (Fig.4.2). Seismic sources suggest a possible direction of magma path from new vents location to volcano summit (old eruptive center). Combination of structural and seismic data indicates the presence of preferential magma rise in the northwest-southeast direction (red rectangle, Fig.4.21). Therefore, the flank stability analysis at Pacaya should account for the possible magma pressure that an eruption might cause in the perpendicular direction to preferential magma path. These inferences indicate that the Southwest slope would be most vulnerable for flank instability.

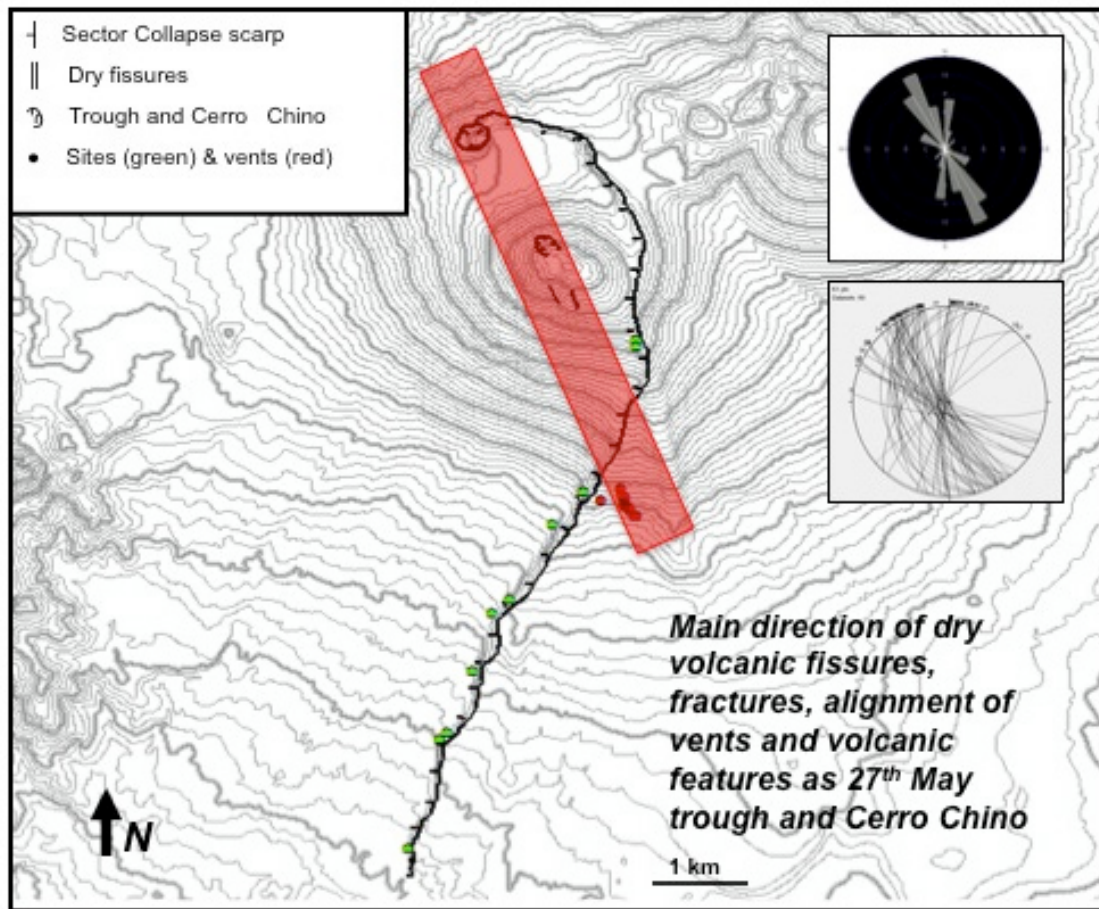


Figure 4.21: The main direction of the dry fissure, vents, and fracture (K1) are NW-SE (red rectangle). Schmidt's projection of planes and rosette plot for K1 discontinuity. Along red rectangle in sequence from NW to SE: Cerro Chino, 27th May trough, Dry and volcanic fissure, New vents location.

4.8 LABORATORY TESTING

During the field survey, two samples were collected for laboratory analysis (A08 and A09 sites). These samples represent lava and autoclastic breccia layer. Small samples of superficial breccia were collected, as well. Following the ISRM recommendation, bulk density, bulk volume, and uniaxial compressive strength tests were carried out on the collected samples.

4.8.1 PREPARING CORES

The field samples were cored for strength testing. The coring provided 12 lava and 14 autoclastic breccia samples for uniaxial compressive strength testing. The cores were of specific length-diameter ratio between 2 to 2.5 (ASTM 2000). The diameters chosen, conform to the ASTM standards and are 23 and 20 mm respectively for lava and autoclastic breccia rocks. This following section explains the procedure operated in order to obtain the sample mentioned above. The first step has been the sampling of rocks using a coring device, which is composed by different tools. A core tool connected to the cue track, which consents the vertical movement is driven manually through a cog mechanism. The final sector of core tool is coupled with an appropriate core barrel (23 or 20 mm) consisting of diamond shoe. The complete device (Fig.4.22) allows the realization of cylindrical specimens by means of a rotary motion conjugate with vertical movement, using water as cooling fluid.



Figure 4.22: Coring device (FOSDICK M.T) with water as cooling fluid.

The complexity encountered during the coring, due to the deterioration of rocks and device vibration, forced losing of some samples. The second step of the procedure consist to using the cutting diamond blade, Fig.4.23, in order to obtain cores with specific length-diameter ratio as required by ASTM 2000. The core is fixed through a vise and the blade instead, slides along a guide-way through a manually operated handle. This device use water as cooling fluid as well.



Figure 4.23: Cutting diamond blade. The blade is manually shifted.

The final result over all this procedure is a number of cores to be tested. Autoclastic breccia cores are illustrated in Fig.4.24. The degree of deterioration caused the failing of some cores during testing under compression.



Figure 4.24: Autoclastic Breccia cores.

In table 3-4 all the cores were obtained and the computed unit weight using empirical formula are shown. Otherwise, bulk density test values discussed in Section 5.2.5 are more reliable one, which are employed in computing lithotechnical parameters.

Table 4.3: Terms describing discontinuity persistence from Brown, 1981.

Samples	Mass (Kg)	Height (m)	average Diameter (m)	Volume (m3)	Unit weighth (KN/m3)
1	0.06	0.05	0.02	0.000021	26.56
2	0.06	0.05	0.02	0.000021	26.86
3	0.06	0.05	0.02	0.000022	26.86
4	0.05	0.05	0.02	0.000020	26.72
5	0.06	0.05	0.02	0.000020	26.74
6	0.06	0.05	0.02	0.000021	26.86
7	0.06	0.05	0.02	0.000020	26.78
8	0.06	0.05	0.02	0.000022	26.92
9	0.06	0.05	0.02	0.000022	26.92
10	0.06	0.05	0.02	0.000021	26.97
11	0.06	0.05	0.02	0.000022	26.87
12	0.05	0.05	0.02	0.000019	26.99

Table 4.4: Terms describing discontinuity persistence from Brown, 1981.

Samples	Mass (m)	Height (m)	average Diameter (m)	Volume (m3)	Unit weight (KN/m3)
1	0.04	0.05	0.02	0.000016	21.99
2	0.03	0.04	0.02	0.000013	22.74
3	0.04	0.05	0.02	0.000015	23.05
4	0.03	0.04	0.02	0.000013	23.02
5	0.03	0.04	0.02	0.000013	23.42
6	0.03	0.04	0.02	0.000013	22.65
7	0.03	0.04	0.02	0.000014	23.13
8	0.03	0.04	0.02	0.000013	24.07
9	0.04	0.05	0.02	0.000016	24.53
10	0.03	0.05	0.02	0.000014	21.96
11	0.03	0.04	0.02	0.000013	22.81
12	0.03	0.05	0.02	0.000014	21.95
13	0.03	0.04	0.02	0.000012	24.67
14	0.03	0.04	0.02	0.000012	23.07

4.8.2 UNIAXIAL COMPRESSIVE STRESS

In order to carry out the uniaxial compressive strength, we used the Material Testing System (MST 810). “The 810 Material Testing System, in Fig.4.25, delivers a broad array of testing capabilities for both low and high force static and dynamic testing. By selecting from a variety of force capacities, servovalve flow ratings, pump capacities, software, and accessories, the floor-standing 810 system can easily be configured to meet specific material or component testing needs”. The versatile 810 system features, sourced from (composites.engineering.txstate.edu):

- Force ranges from 25 kN (5.5 kip) to 500 kN (110 kip);
- Large range of performance;
- The ability to test different materials;
- Large test space to accommodate different size specimen;
- The capability to perform test types from tensile to high cycle fatigue, fracture mechanics, and durability of components.

The MTS device is powered by high- pressure hydraulic fluid and is force rated up to 500 KN (50 Tons). The procedure involves a constant increasing load through axial displacement (velocity of 0.2 mm/min) of the flat base rising against the core, rod load eventually against the crosshead. Crosshead mounted load cell provides force reading and the displacement transducer is integral to the actuator to determine the position measurement and for control. The procedure is maintained up to failure of the core where the maximum compression strength is obtained.



Figure 4.25: Material Testing System (MTS 810).

The uniaxial compressive strength is obtained through this formula:

$$\sigma_c = N/A$$

Where N is the maximum load (KN) experienced of cores during compressive test before breaking. In addition, A is the cross sectional area of cores (mm²).

4.8.3 BULK VOLUME AND DENSITY

The displacement technique is used in this automated volume-determining method. “The displacement technique applies to a solid object immersed in a bed of much smaller particles as well in liquid and gas” (P. A. Webb, 2001). The difference between free flowing mediums in which the samples are immersed is the capability to fill void and pores. The particles (solid) don’t occupy the pores and provide a mean by which envelope density can be measured. A brief description of this device, sourced from (<http://www.micromeritics.com>) is here presented: “The GEOPYC 1360 is the only one device, which automatically computes bulk volume and density of solid by displacement of solid medium. The medium is a narrow distribution of small, rigid spheres that have a high degree of flow ability and achieve close packing around the object under investigation. The particles are sufficiently small that during consolidation, they conform closely to the surface of the object, yet do not invade pore space. Repeatability and reproducibility are achieved by a controlled method of compaction. The sample cell in which the dry medium is placed is a precision cylinder. A plunger compresses the powder as the cell vibrates; the force of compression is selectable and, therefore, repeatable from test to test. A preliminary compaction with only the displacement medium in the cell establishes a zero-volume baseline. The object is then placed in the cylinder with the dry medium and the compaction process is repeated. The difference in the distance ‘ht’ the piston penetrates the cylinder during the test and the distance ‘h0’ it penetrates during the baseline procedure ($h = h_0 - ht$) is used to calculate the displacement volume of the medium using the formula for the volume of a cylinder of height ‘h’ ”.

$$V = \pi r^2$$

Figure 4.26 illustrates the process. We performed bulk volume for lava, autoclastic breccia and breccia samples, in order to assess density value, using the device, Geopyc 1360. We obtained the envelope volume through multiple cycles of measuring. The density was directly acquired from the device as ratio between mass and volume:

$$density = mass \div volume$$

The precision of this device is enhanced by the fact that each cycle consists into a five subsequent cycles of measuring.

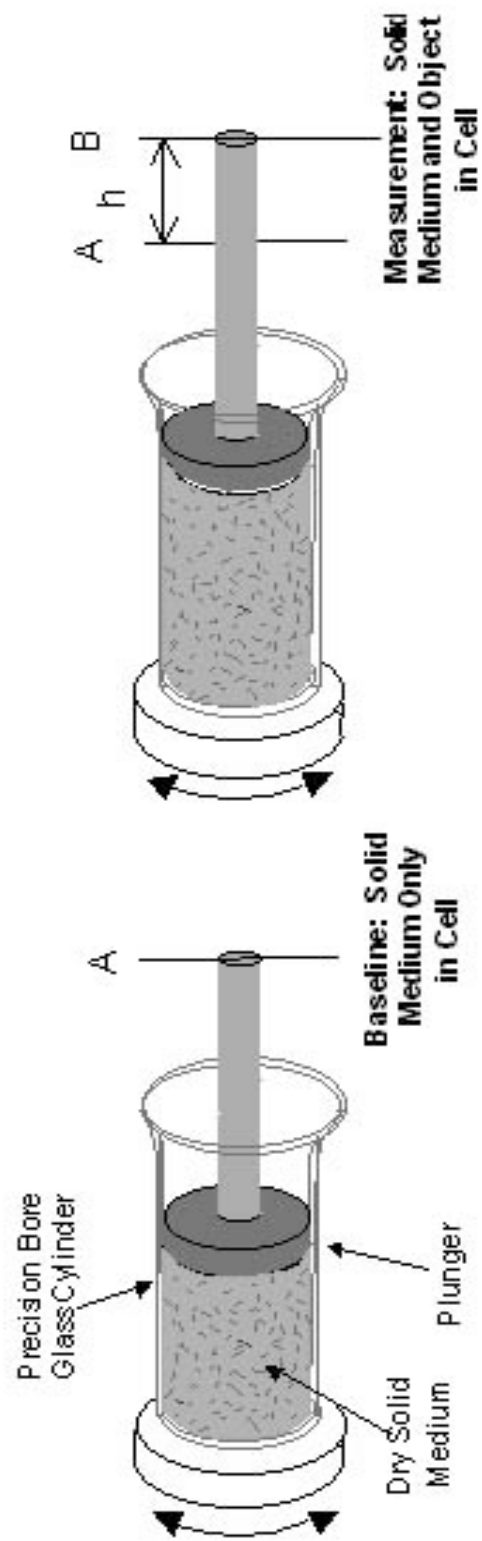


Figure 4.26: Volume determination by the displacement of a dry medium, which is employed to compute the bulk density (P. A. Webb 2001)

CHAPTER 5: GEOTECHNICAL PROPERTIES

5.1 INTRODUCTION

Geotechnical data obtained and estimated for each rock mass and lithotechnical units will be addressed in the subsequent sections. Geotechnical properties are required in order to assess the stability of Pacaya volcano. The RMR classification was implemented only for lava rocks, which are the strongest rock group. For the other lithotechnical units, a GSI classification was implemented to compute the Hoek-Brown and equivalent Mohr-Coulomb parameters using RocLab.

5.2 ROCK MASS PROPERTIES

Section 4.8.1 discussed the preparing of cores and testing procedure of the samples were collected. Following the ISRM recommendation, bulk density, bulk volume, and uniaxial compressive strength tests were done on the collected samples. The resultant properties of these samples combined with field data, according to the corresponding percentage of lava and breccia were used to define the properties of the lithotechnical units.

5.2.1 PETROLOGIC AND MINERALOGIC PROPERTIES

The basalts of this series are texturally and mineralogically uniform and have been described by Williams (1960), Eggers (1971) and Rose (1967). The texture of these basalts is porphyritic, intergranular. Large Plagioclase and Olivine phenocrysts always occur in these lavas. Clinopyroxene is usually present as phenocryst but much less abundant than Olivine. The matrix of these basalts is a dense, black to brown, semi-opaque ash of ore, clinopyroxene, and calcic andesine microphenocrysts. Olivine is rare in the matrix. Petrographically these basalts have most of the characteristic of high-alumina basalt (Kuno 1960). No major time dependent chemical or petrographic variations were detected between any of the modern lavas.

5.2.2 ROCK MASS RATING (RMR)

Rocks mechanics data of 150 lava-joints were measured at 10 sites. This dataset was used to identify the number of joint sets orientation, as well as the geometry of each joint, type of movement, set spacing, degree of alteration, amount of dilation, roughness coefficient, and the presence and type of infill. Further, these parameters were used to compute the Rock Mass Rating (RMR) using the Beniaowski (1989) criteria. The computed RMR indicates that the rock mass at the pacaya volcano range from “medium to good quality” with the range of values from 52 to 74. A lower RMR is expected for breccia unit, however the almost complete absence of distinct joints forbids their RMR computation. In table 5.1, the RMR classification for each site is described.

5.2.3 GEOLOGICAL STRENGTH INDEX (GSI)

Where disintegrate rocks or highly weathered rocks or poorly interlocked rocks are present and it is difficult or impossible to obtain the parameters needed for the application of RMR classification. Therefore, the GSI parameter introduced by Hoek and Brown (1980) is considered a better tool for characterization of weathered rocks. The GSI classification is based on visual analysis of rocks structures, for blockiness, geological complexity, and surface conditions (roughness and weathering). A GSI range evaluated for different rocks mass corresponds respectively to 55-75 for lava and 15-35 for breccia, high value up to 40 is expected to represent autoclastic breccia. GSI value for each lithotechnical unit considered will be described in Section 5.3.

5.2.4 DISCONTINUITY

Geotechnical survey conducted in each site, observing joints properties, addressed an accepted characterization of rock masses. We used to identify all parameters discussed above in section 5.2.2. Parameters measured during geotechnical survey, e.g. A117, are shown in Table 5.2.

Table 5.1: RMR classification for each site investigated.

	A08		A09		A112		A113		A115		A117		A118		A119		A120		A122	
PARAMETERS	MEASURE	RATING	MEASURE	RATING	MEASURE	RATING	MEASURE	RATING	MEASURE	RATING	MEASURE	RATING	MEASURE	RATING	MEASURE	RATING	MEASURE	RATING	MEASURE	RATING
UCS (Mpa)	45	4	80	7	57	7	55	7	59	7	55	7	62	7	78	7	48	4	80	7
RQD	97	20	100	20	100	20	19	3	65	13	100	20	27	8	100	20	78	17	100	20
Discontinuity spacing (mm)	0.6-2m	15	>2m	20	>2m	20	0.6-2m	15	0.6-2m	15	>2m	20	0.6-2m	15	0.6-2m	15	0.6-2m	15	>2m	20
Discontinuity																				
Persistence (m)	1-3 m	4	1-3 m	4	1-3 m	4	1-3 m	4	1-3 m	4	1-3 m	4	1-3 m	4	1-3 m	4	1-3 m	4	1-3 m	4
Opening (mm)	>5 mm	0	>5 mm	0	>5 mm	0	>5 mm	0	>5 mm	0	>5 mm	0	>5 mm	0	>5 mm	0	>5 mm	0	>5 mm	0
Roughness	rough	5	rough	5	slightly rough	3	rough	5	rough	5	rough	5	rough	5	rough	5	rough	5	rough	5
Infill	soft 5 mm	0	soft 5 mm	0	soft 5 mm	0	soft 5 mm	0	soft 5 mm	0	soft 5 mm	0	soft 5 mm	0	soft 5 mm	0	soft 5 mm	0	soft 5 mm	0
Weathering	medium	3	medium	3	medium	3	medium	3	medium	3	medium	3	medium	3	medium	3	medium	3	medium	3
Groundwater	dry	15	dry	15	dry	15	dry	15	dry	15	dry	15	dry	15	dry	15	dry	15	dry	15
TOTAL	GOOD ROCK	66	GOOD ROCK	74	GOOD ROCK	72	MEDIUM ROCK	52	GOOD ROCK	62	GOOD ROCK	74	MEDIUM ROCK	57	GOOD ROCK	69	GOOD ROCK	63	GOOD ROCK	74

Table 5.2: Site A117 where geotechnical survey was performed. Parameters carried out during investigation are listed below. “Pa” and “PI” correspond to Areal persistence and linear persistence.

A117	
K1	
<i>Dip</i>	229
<i>Inclination</i>	79
<i>Spacing (m)</i>	6
<i>Schmidt Hammer</i>	33.9
<i>Type</i>	Joint
<i>JRC (Barton & Choubey, 1977)</i>	8 to 10
<i>Opening (mm)</i>	152 - 101 - 12.7
<i>Filling</i>	Completely filled soil
<i>Alteration</i>	Slightly weathered
<i>Filtration</i>	None
<i>PI</i>	>90%
<i>Pa</i>	25-80%
<i>Directional length (m)</i>	4.57
<i>Directional immersion (m)</i>	5
<i>Termination</i>	Td-Tx
K3	
<i>Dip</i>	310
<i>Inclination</i>	73
<i>Spacing (m)</i>	7.5
<i>Schmidt Hammer</i>	45.5
<i>Type</i>	Joint
<i>JRC (Barton & Choubey, 1977)</i>	12 to 14
<i>Opening (m)</i>	2
<i>Filling</i>	soil
<i>Alteration</i>	Slightly weathered
<i>Filtration</i>	None
<i>PI</i>	>90%
<i>Pa</i>	25-80%
<i>Directional length (m)</i>	7
<i>Directional immersion (m)</i>	4
<i>Termination</i>	Tx

5.2.5 BULK VOLUME AND DENSITY VALUE

We performed bulk volume for lava, autoclastic breccia and breccia samples, in order to assess density value, using the device, Geopyc 1360. We obtained the envelope volume through multiple cycles of measuring. The density was directly acquired from the device as ratio between mass and volume (Section 4.8.3). The following tables indicate volume and density values for each sample:

Table 5.3: Breccia samples

Breccia samples	Density (g/cm ³)	Density (KN/m ³)	Standard deviation	Volume (cm ³)
1	2.073	20.73	0.003	2.93
2	2.105	21.05	0.003	6.06
3	2.021	20.21	0.004	1.32
Average	2.07	20.66	0.003	3.43

Table 5.4: Autoclastic Breccia samples

Autoclastic breccia	Density (g/cm ³)	Density (KN/m ³)	Standard deviation	Volume (cm ³)
1	2.6851	26.85	0.006	10.05
2	2.6376	26.37	0.005	5.74
3	2.5994	26.59	0.006	1.68
Average	2.6407	26.60	0.0055	5.82

Table 5.5: Lava samples

Lava samples	Density (g/cm ³)	Density (KN/m ³)	Standard deviation (3 cycles)	Volume (cm ³)
1	2.8726	28.726	0.01	5.19
2	2.9484	29.484	0.01	4.32
3	2.8689	28.689	0.006	8.09
Average	2.90	28.97	0.01	5.87

5.2.6 SCHMIDT HAMMER VALUE (JCS)

At the 10 sites where structural surveys were performed (fig.15), an estimate of the compressive strength was also obtained using the Schmidt hammer. At every site, 20 Schmidt hammer rebound measurements were made to compute an average estimate of the uniaxial compressive strength. The result is given in table 5.6 indicate that:

- For all data established on lava rocks, the mean compressive strength was $\sigma_c = 62 \pm 13$ MPa;
- For autoclastic breccia clast-supported, the mean compressive strength is $\sigma_c = 15 \pm 5$ MPa.

In section 4.3.1.2 the autoclastic breccia characteristics are explained, which are used to subdivide breccia layers into two classes: block-supported, matrix-poor, good interlocking; and clast-supported, matrix-rich. A global behavior able to explain the mechanical rheology of this layer is missing. In addition, the fact that the calculation of rock mass quality is difficult is well recognized (Petro et al. 2007). In my opinion both mechanical classes should be consider in order to obtain an average value representing large-scale geotechnical investigation. Individual, breccia clasts that are not fractured are considered to be an autoclastic breccia intact rock unit (Petro et al. 2007). Few clasts were suitable for Schmidt hammer tests (only along 3 site studied) but most were significantly smaller and could not be tested. The evaluation of some of the properties of rocks, such as Young's modulus (E) and uniaxial compressive strength (UCS) involves the preparation of several cores and the use of complex laboratory equipment (I. Dincer et al. 2004). Dincer's study demonstrates an empirical relationship between Young's modulus, Schmidt hammer rebound number (N), and the uniaxial compressive strength, for volcanic rocks. An Ismail correlation is implemented in Table 5.6 in order to compare and strengthen our result with those empirically obtained using Ismail Dincer formula.

Table 5.6: Schmidt hammer tests on field survey: uniaxial compressional strength

Site	Litotechnichal Units	Schmidt Hammers		Ismail Correlation		
		Rebound Number (R)	Compressional Strength (Mpa)	Compressional Strength (Mpa)	Young's modulus (E) (Gpa)	GSI
LAVA						
A08	BRECCIA-LAVA	30.84	45.00	47.97	8.24	55-65
A09	LAVA-BRECCIA	43.76	80.00	83.51	14.32	65-70
A112	LAVA	36.29	57.00	62.96	10.81	70-75
A113	LAVA	34.31	55.00	57.53	9.88	70-75
A115	LAVA-BRECCIA	37.99	65.00	67.64	11.61	55-60
A117	LAVA	36.60	55.00	63.82	10.95	65-75
A118	BRECCIA-LAVA	37.28	62.00	65.69	11.27	55-60
A119	LAVA-BRECCIA	43.65	78.00	83.21	14.27	60-65
A120	LAVA-BRECCIA	32.44	48.00	52.37	9.00	55-60
A122	LAVA-BRECCIA	46.67	80.00	91.50	15.68	65-70
BRECCIA						
A09	BRECCIA-LAVA	6.75	15.00	*	*	65-70
A122	LAVA-BRECCIA	11.15	16.00	*	*	65-70
A119	LAVA-BRECCIA	8.50	15.00	*	*	60-65

*, Ismail Correlation should be used only with basalt, andesite and tuff.

5.2.7 UNIAXIAL COMPRESSIVE STRENGTH (UCS)

During the field survey, one sample each of lava and autoclastic breccia rock was collected to determine the uniaxial compressive strength in the lab and compare these values to the field observations using Schmidt Hammer. The field samples were cored for strength testing. The coring provided 12 lava and 14 autoclastic breccia samples for uniaxial compressive strength testing. An example data of uniaxial compressive test is illustrated in Fig.5.1. In Fig.5.2 compressive strength of lava samples are shown. The results of the uniaxial compressive strength test are presented in table 5.7.

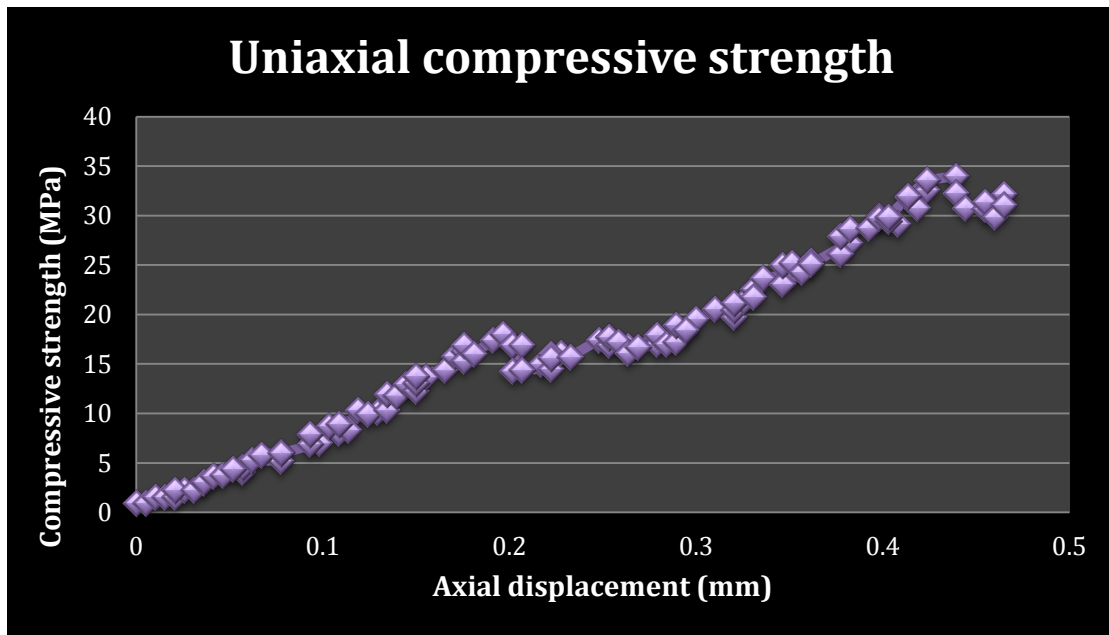


Figure 5.1: Lava sample n° 1 tested under uniaxial compressive strength. Maximum compressional strength equal to 34.00 MPa.

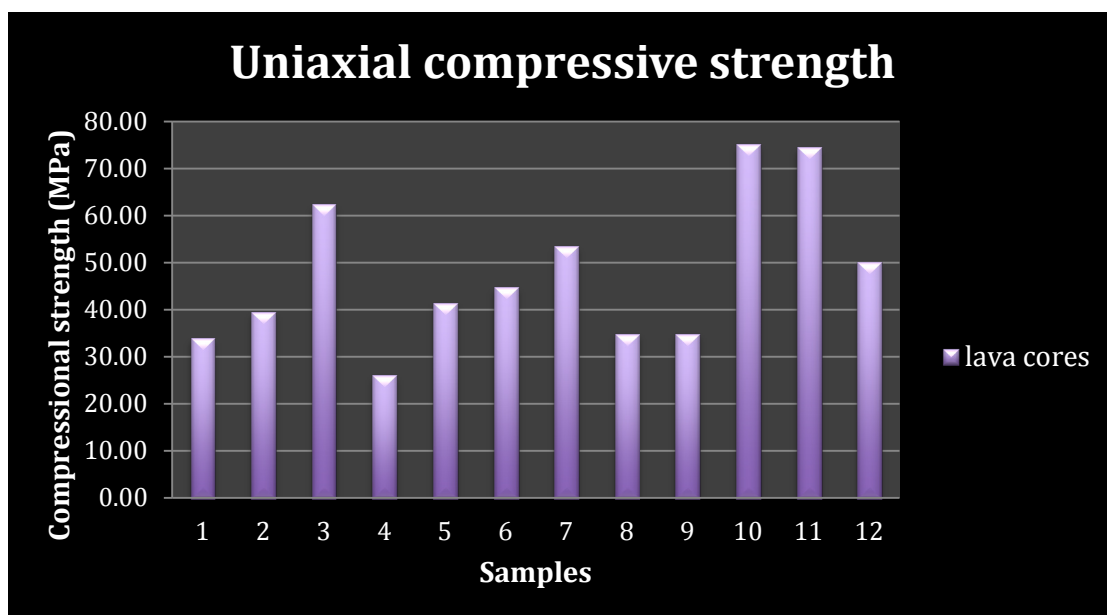


Figure 5.2: Lava cores tested under uniaxial compressive strength.

Table 5.7: Uniaxial compressional test performed on lava and autoclastic breccia

samples	sites	mass (g)	height average (mm)	length to diameter ratio (L/D)	compressional strenght (Mpa)
LAVA					
1	A08	57.74	51.25	2.23	34.00
2	A08	56.33	49.44	2.16	39.55
3	A08	59.53	52.25	2.27	62.41
4	A08	54.93	48.47	2.11	26.10
5	A08	55.7	49.11	2.14	41.48
6	A08	57.87	50.79	2.21	44.75
7	A08	55.68	49.02	2.13	53.50
8	A08	60.61	53.09	2.31	34.95
9	A08	60.55	53.02	2.31	34.93
10	A08	58.85	51.44	2.24	75.15
11	A08	59.61	52.29	2.27	74.53
12	A08	52.26	46.12	2.01	50.06
Mean					47.51 ± 16
diameter = 23 mm ; area = 414.49 mm ² ; density = 28.87 KN/m ³					
AUTOCLASTIC BRECCIA					
1	A09	35.69	49.75	2.49	31.61
2	A09	30.89	42.35	2.12	44.06
3	A09	35.55	48.09	2.40	36.22
4	A09	31.63	42.84	2.14	30.33
5	A09	30.83	41.04	2.05	27.09
6	A09	31.12	42.84	2.14	54.58
7	A09	33.04	44.53	2.23	43.04
8	A09	31.25	40.48	2.02	28.41
9	A09	39.40	50.08	2.50	54.75
10	A09	32.27	45.82	2.29	19.88
11	A09	30.89	42.21	2.11	13.58
12	A09	32.17	46.70	2.28	35.89
13	A09	30.19	40.00	2.00	19.14
14	A09	28.12	40.14	2.01	27.45
Mean					33.29 ± 13
diameter = 20 mm ; area = 314.16 mm ² ; density = 26.64 KN/m ³					

5.2.8 UNIAXIAL COMPRESSIVE STRENGTH (UCS) ULTIMATE

The field compressive strength obtained using the Schmidt hammer was validated by lab testing. Comparable result is found between field and lab compressive strength, for lava rocks. However, a significant difference was observed on breccia rocks, between field and lab compressive strength (Table 5.8). The solution implemented in this study is as follows:

- Lava rock sampled at A08 site, tested on the lab under uniaxial compressive strength shows average UCS value (Table 5.7) that resampling value determined at the field in the same sampling location A08 (as shown in Table 5.6). For this reason, global compressional strength for lava rocks is assessed directly from field data. A comprehensive strength of complete area investigated is preserved considering average value originated from every field data.

Lava UCS ultimate= 62.5 MPa

- Compressional strength for breccia layer is determined by combining field and lab data, and obtaining an average between them, reflecting variable mechanic characteristics as discussed above.

Breccia UCS ultimate= 24.5 MPa

Table 5.8: Evaluation between uniaxial compressional strength from laboratory and field data. Comparable result for lava sample.

Sites	Samples	Compressional Strength UCS (Mpa) from Field data	Compressional Strength UCS (Mpa) Ismail Dincer	Compressional Strength UCS (Mpa) from Laboratory data
A09	breccia	16 (*)	*	33.29 ± 13 ^(Av')
A08	lava	45 (*)	47.97 (*)	47.61 ± 16 ^(Av')

* , Ismail Correlation should be used only with basalt, andesite and tuff, Av' , average from all cores for correspondent sites; (*), value from Rebound Number (R) on site; Average from all field sites: 62.5

5.3 LITHOTECHNICAL UNITS

As discussed in Section 4.4, the distinction in lithotechnical units was based on the different percentage of autoclastic breccia fraction vs. lava deposits. In addition, three main lithotechnical units were defined as follows:

1. Lava unit (L): lava layer (80-100%) with rarely thin layer of breccia;
2. Lava-Breccia unit (LB): alternation of lava (ranging from 65-80%) and breccia layers;
3. Breccia unit (B): alternation of lava (less than 50%) and breccia layers;

In order to proceed with the computing the geotechnical parameters of lithotechnical units, the strength values of lava and autoclastic breccia units are required. GSI, density and UCS ultimate values are mentioned in Section 5.2.3, 5.2.5, and 5.2.8 separately. These ultimate properties, with the corresponding percentage of lava and breccia were used to define the properties of the lithotechnical units. Lithotechnical unit properties are input in the Hoek-Brown criterion (2002 edition) in order to calculate rock mass strength and its elastic parameters (Section 5.3.1). The computed physical and mechanical properties of each lithotechnical units are reported in table 5.9. The GSI of each lithotechnical units is reported in Fig.5.3.

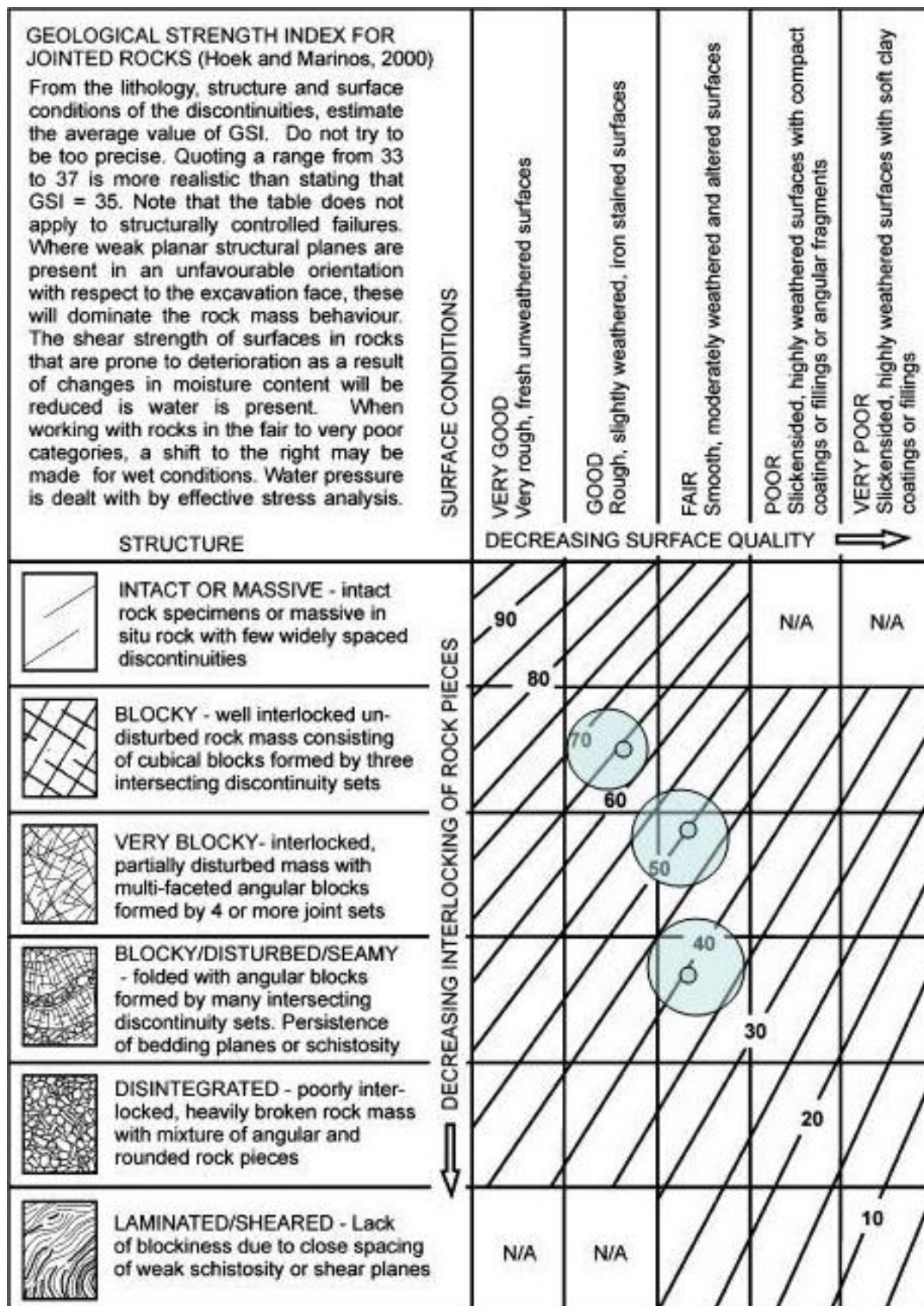


Figure 5.3: Geological Strength Index (GSI), modified from Marinos and Hoek (2001).

5.3.1 HOEK AND BROWN STRENGTH PARAMETERS AND ELASTIC PROPERTIES

The rock mass strength and elastic parameters were determined using the *RocScience* software, mentioned in Section 2.4.1, (*RocData*). “*RocData* implements the most recent update (2002 edition) of the Generalized Hoek-Brown criterion. In most cases, it is practically impossible to perform triaxial tests on rock masses at a scale, which is necessary to obtain direct values of the parameters in the Generalized Hoek-Brown equation” sourced from (<http://www.rocscience.com>). Consequently, ways of practically estimating the Hoek-Brown material constants mb , s and a are needed. The latest research indicates that the Generalized Hoek-Brown criterion are given from empirical equations [Hoek, Carranza-Torres & Corkum (2002)]. The mb parameter is a reduced value of the material constant m_i (for the intact rock). The s and a are constants which depend upon the characteristic of rock mass. The parameters used as input are: uniaxial compressive strength (σ_{ci}); material constant (m_i) based on the petrographical and textural characters (intact rock); the GSI parameter of the rock mass; the disturbance factor D due to blasting or stress release and the intact modulus of deformation (E_i) *i.e.* directly obtained from the modulus ratio (MR).

$$E_i = MR \cdot \sigma_{ci}$$

This relationship is helpful when there are no direct measurements of intact deformation modulus or when undisturbed sampling to determine the E_i is difficult. The values of MR are chosen from literature estimate through *RocData* list (MR breccia = 500 ± 0 ; MR lava = 350 ± 100). The m_i and D factor are determined as well by literature value obtained directly from *RocData*. “*RocData* provides a simple and intuitive implementation of the Hoek-Brown failure criterion, allowing users to easily obtain reliable estimates of rock mass properties and to visualize the effects of changing rock mass parameters on the failure envelopes” sourced from (<http://www.rocscience.com>). Estimated m_i values (m_i lava = 25 ± 5 ; m_i breccia = 19 ± 5). D factor ranges from 0 (no-disturbance) to 1 (high-disturbance). The disturbance factor D is considered to account for disturbances from blasting in tunneling and hence in this case the $D=0$ was assumed. The rock mass parameters results obtained directly from Hoek-Brown criterion are (as shown in table 13):

- Tensile Strength (σ'_{tm}) that represent the rock strength in biaxial tension condition ($\sigma_1 = \sigma_3 = \sigma_t$);
- Uniaxial compressive strength (UCS_m) setting $\sigma_3 = 0$;
- Global Strength (σ'_{cm}) which is useful for the overall behavior of a rock mass rather than the detailed failure propagation process;
- mb , s and a ;
- Modulus of deformation (E_m).

The deformation modulus, Young's Modulus, is a required input parameter for different numerical analyses as finite element method, which will be address in paragraph 6.4. For that reason, it is very important to obtain realistic values of deformation modulus for analysis that involves deformations.

5.3.2 MOHR-COULOMB STRENGTH PARAMETERS

We computed the equivalent Mohr-Coulomb parameters for the Hoek-Brown failure envelope. A stress range σ_3 is established to UCS/4 based on the observation that the brittle failure happen when the σ_3 is less than a quarter of the UCS [[Hoek, Carranza-Torres & Corkum \(2002\)](#)]. The stress range, from 5 to 15 MPa, is used to calculate:

- Friction angle ϕ ;
- Cohesion c ;

These factors are applied and incorporated into numerical models and limit equilibrium programs.

5.3.3 SUMMARY

The aim of this chapter was to determine geotechnical properties required to aid interpretation of the stability of Pacaya. The main mechanical and physical properties of each lithotechnical unit are reported in Table 5.9. The mean value was used for the stability analysis and is presented in brackets.

Table 5.9: Physical and mechanical properties of the lithotechnical units: established rock mass values of friction angle, cohesion, strength and elastic parameters from input data necessary to define the Mohr-Coulomb equivalent

	UNIT 1	UNIT 2	UNIT 3
	lava	lava-breccia	breccia-lava
Percentage lava (%)	85-100% (100%)	65-85% (70%)	< 50% (45%)
Density γ_d (KN/m ³)	28.97±0.006 ^(lb)	26.47 ^(lb,average)	24.39 ^(lb,average)
Intact rock UCS (Mpa)	62.5 ^(s,average)	51 ^(s,average)	41.5 ^(s,average)
mi	25±5 (25) ^(Tr)	22±5 (22) ^(Tr)	19±5 (19) ^(Tr)
Geological Strength index GSI	60-70 (65) ^(s)	45-55 (50) ^(s)	35-45 (40) ^(s)
Disturbance factor D	0-0.6 (0) ^(s)	0-0.6 (0) ^(s)	0-0.6 (0) ^(s)
Hoek-Brown failure criterion and Mohr -Coulomb equivalent parameters function of σ_{3max} (5-15 Mpa)			
mb	7.163	3.689	2.229
s	0.020	0.004	0.001
a	0.502	0.506	0.511
Friction angle ϕ (°)	42.9261	37.331	33.0211
Apparent cohesion c (Mpa)	5.02724	3.22065	2.16805
Tensile Strength σ'_{tm} (Mpa)	-0.178602	-0.0523994	-0.0236935
Uniaxial compressive strength UCS _m (Mpa)	8.87325	3.07236	1.37241
Global strength σ'_{cm} (Mpa)	23.083	13.018	7.98961
Modulus of deformation E _m (Mpa)	13818.9	6658.25	3312.78
Lb, laboratory tests; S, in situ direct tests and evaluations; Tr, Theoretical data; Un, uncertain data; in brackets, input data for stability analysis			

CHAPTER 6: MODELING

6.1 INTRODUCTION

This chapter explains how the slope stability program ROCSCIENCE was used to analyze the most hazardous 2D sections along the Pacaya volcano. A first slope analysis was performed over different sections of volcano to identify the slopes that are more likely to fail. Sections AA' and BB' were selected as the most unstable. The two dimensional stability analysis of Pacaya volcano was carried out using limit equilibrium and finite element methods. Limit equilibrium method is one of the most widely used approaches for slope stability analysis. For the limit equilibrium analysis a rigid-plastic material behavior is assumed. However, the limit equilibrium method doesn't provide information on the deformation and progressive failures. Therefore, we analyze the stability of Pacaya volcano using the Finite Element Method (FEM) also. Finally, we compare the results from the limit equilibrium and FEM to understand the stability of Pacaya volcano.

6.2 MODELING DEFINITION

For ROCSCIENCE to model the stability of a slope, model parameters must first be defined. Parameters of each model that require definition include material and water properties, slope profile, internal structures, scenarios analyzed and analysis methods. The parameters selected above are addressed in this section. The analysis was conducted based on the assumption that the problem is uniform to the perpendicular direction to the cross-section considered. Section AA' and BB' shown in Fig.4.1 is the selected cross-section which present worst scenarios in terms of safety factor obtained from primary analysis.

6.2.1 SLOPE PROFILES

The 2-D slope stability analysis was carried out on 2 different models of the topography that was developed from a series of digital elevation models (DEMs) from 1954, 2001, and 2006. The assumption used for the topographic model is that the elevation doesn't change from 2006 to present for the cross-sections taken into account. Section AA' and BB' slope profiles were studied considering their precarious stability assessed in the first analysis (Fig.6.1 and Fig.6.2). Section BB' represent the lower value of safety factor among the two sections investigated. Besides section AA' is perpendicular to the main direction of magma upwelling, which results in applying the

whole magma pressure on this section. The procedure executed in order to derive these sections is discussed in Section 4.2.2.

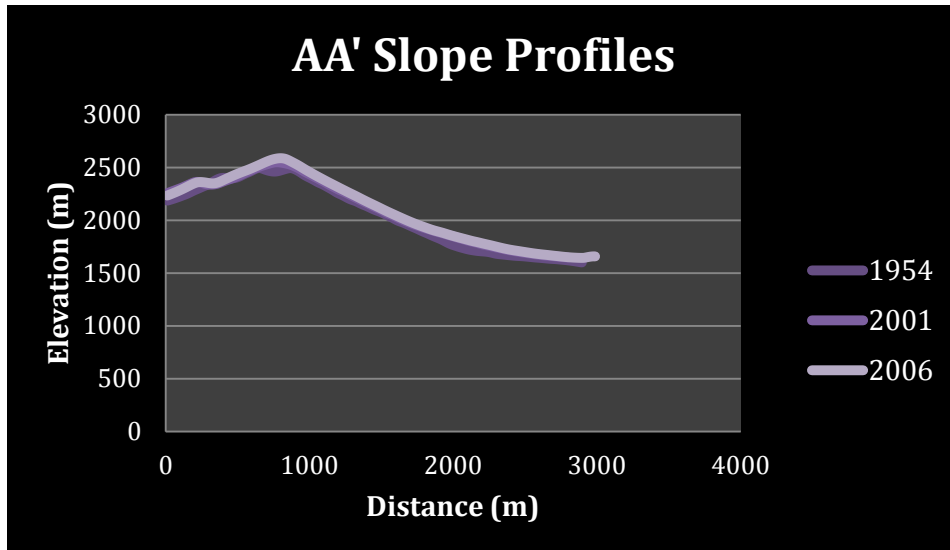


Figure 6.1: AA' section representing the slope surface investigated. Topographic surfaces come from 1954-2001-2006 DEMs.

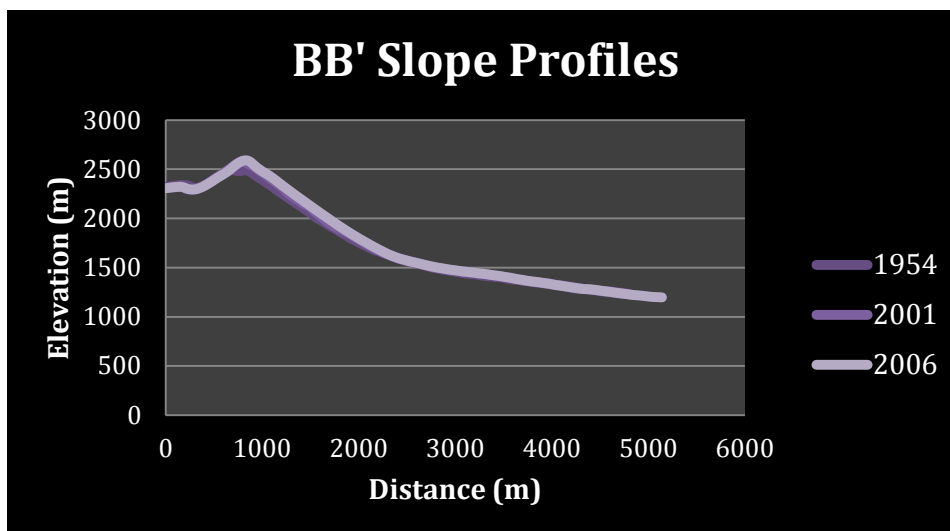


Figure 6.2: BB' section representing the slope surface investigated. Topographic surfaces come from 1954-2001-2006 DEMs.

Comparing profiles coming from different DEM, 1954 to 2006, a latest geomorphologic evolution of the surface of Pacaya volcano is derived.

6.2.2 MATERIAL AND WATER PROPERTIES

ROCSCIENCE allows material properties, or strength parameters, to be defined in the form of Hoek-Brown (UCS, and material constants m and s) or Mohr-Coulomb (c and ϕ) parameters. The latter were used for this study. Unit weights of materials are also required. These values were previously determined for each lithotechnical unit, and summarized (Table 12). The elevation of the ground water was determined from a nearby river (El Chupadero river, Fig.4.1), and is concluded that the ground water table is significantly below the slope and it doesn't affect the stability of the volcano at Pacaya. Therefore, in this study the rocks mass properties refer to dry conditions. This assumption is based on river location, river elevation under the section analyzed, the absence of springs, the general dry state of outcrops investigated, and the rare or absent precipitation in Guatemala during the dry season.

6.3.3 IN SITU STRESS RATIO (K)

The stresses undergone by a rock mass at depth is a resultant of the weight of the overlying strata and from locked in stresses from tectonic origin. The vertical stress is estimated by simple relationship:

$$\sigma_v = z \gamma$$

Where γ is the unit weight of the overlying rock, σ_v is the vertical stress, and z is the depth below surface. However, determining the horizontal stresses acting on a rock mass at a depth z below the surface is more difficult than the vertical stress determination. Therefore a ratio of the average vertical stress to horizontal stress is used and denoted by k :

$$\sigma_h = K \sigma_v$$

Based on uncertain horizontal stress distribution within slope, a good assumption is leaving the horizontal stress ratio equal to the hydrostatic initial stress.

6.2.4 INTERNAL STRUCTURES

To account for the uncertainty in the internal structure four different models were built on the basis of the field survey, previous work, and the hypothesis of the stability analysis (Fig.6.3 and Fig.6.4). The lithotechnical subdivision, completed along old scarp, reflects the ancient volcano structure that has been projected on the cross-section in order to create the third model (as shown in Fig.6.3c). The projection angle for this model is obtained from the stratigraphic contact (S1). The second model (Fig.6.3b) is a result of a homogeneous distribution of the lithotechnical units. Field observations, which revealed the predominant presence of breccia deposit in the sub-superficial flank of the volcano and missing thickness of lava flow, comparing total lava flow thickness with DEM, suggest breccia layer to be prominent in the internal structure of the volcano. Therefore, the first model is built on lava-breccia unit (as shown in Fig.6.3a). Lava flow thicknesses were calculated from 1961 to 2009 (Gomez et al. 2010) and different sums of them have been compared with DEM subtraction elevation. Thickness difference was found out from this investigation. It is reasonable to assign this difference to breccia layer because of eruptive behavior at Pacaya (Eggers 1972; Eggers 1975). This assumption of interspersed structure of lava and breccia layer along the depth is reasonable. The last model, fourth model, is built on breccia-lava unit enhancing the predominant presence of breccia deposit up to 50% at Pacaya volcano (Fig.6.3d). The worst scenario by using the poorest mechanical properties is assessed. Further, precautionary reasons call for poorest mechanical properties model to be evaluated. Internal depth structure reconstruction was inferred from W. I. Rose's knowledge of progressive history of Pacaya volcano growth. In figure 6.4 (a - d) four equivalent models for section BB' are presented.

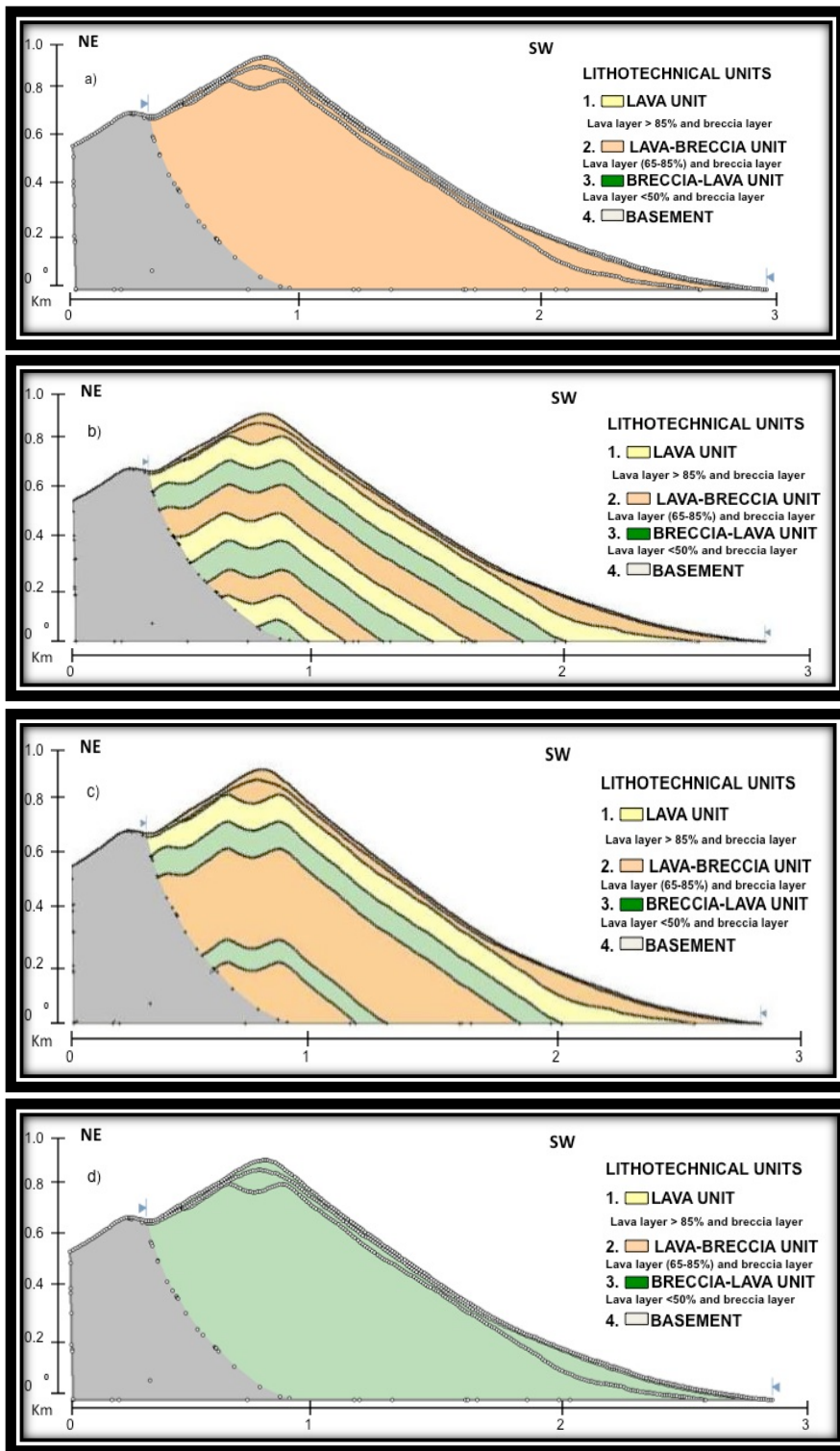


Figure 6.3: Section AA'. a) first model; b) second model; c) third model; d) fourth model.

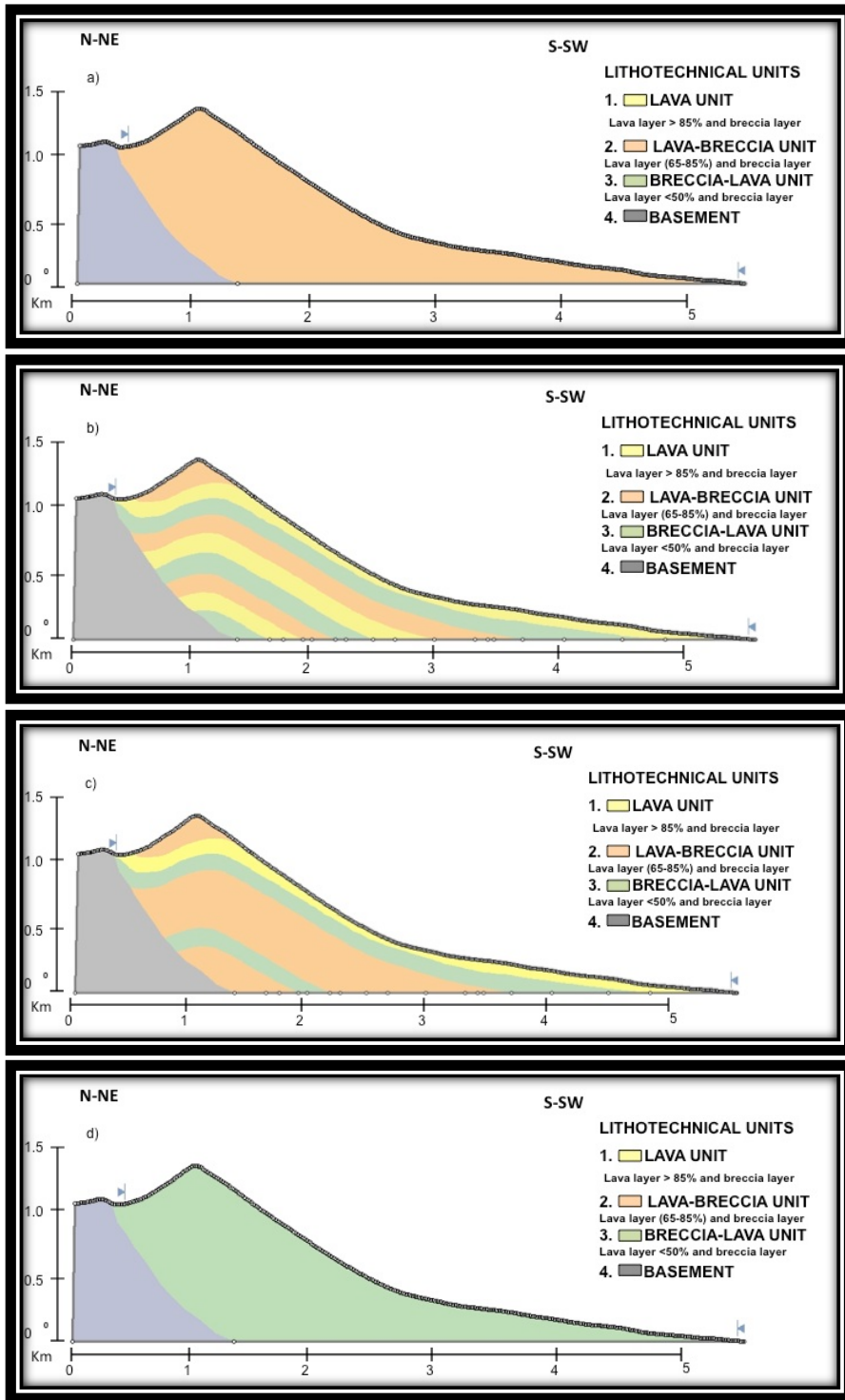


Figure 6.4: Section BB'. a) first model; b) second model; c) third model; d) fourth model.

6.2.5 SCENARIO ANALYZED

In this study four cases were investigated:

- 1) Static conditions;
- 2) Magma pressure applied to the crack of tremor source;
- 3) Seismic force applied to the edifice;
- 4) Magma pressure with seismic force.

The stability of the Pacaya volcano, in the static conditions, is assessed considering only gravity force. The stability analysis was performed accordingly to the geotechnical properties of the lithotechnical units involved. Magma pressure is computed using the formula modified by Iverson (1995):

$$P = \rho_m z \cos \beta + p_0$$

Where ρ_m is the magma unit weight (26.5 KN/m^3 from F.Batini et al. 2001), z is the crack depth (822 m), β is the angle between magma feeding system direction and the sections analyzed and p_0 is excess magma pressure component (considered equal to zero). The magma-static component is $P=21783 \text{ KN/m}^2$ for AA' section. Otherwise the BB' section reveal angle $\beta=40^\circ$ which correspond to magma-static component of $P=16686 \text{ KN/m}^2$. Triangular load distribution depth dependent is employed.

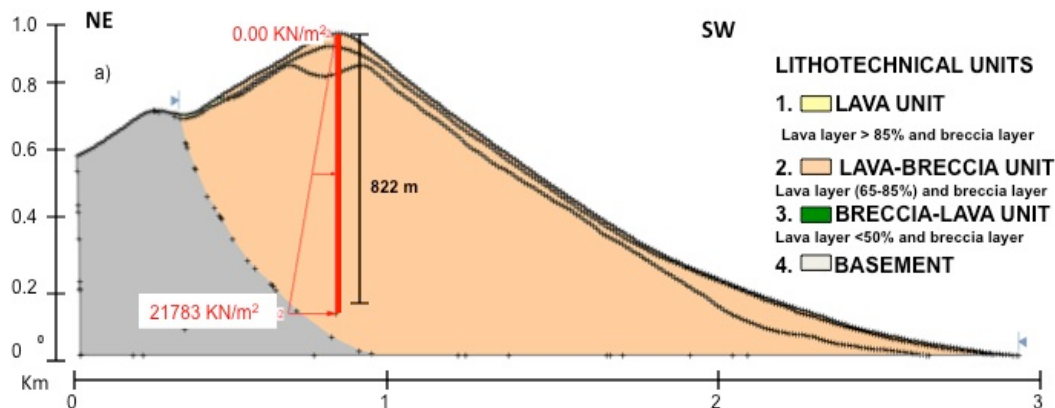


Figure 6.5: Section AA' (first model) with magma pressure applied corresponding to 21783 KN/m^2 . Magma conduit depth from field investigation.

Surface magma source depth was inferred from structural survey. Long cracks or dykes-system hypothesis, connecting new vent with old vent at the Pacaya volcano propose magma conduit depth as the elevation variance between them. Shallow magmatic system as dykes or cracks may affect the slope stability by magma pressure applied on wall-conduit. Magma pressure was applied by using a tension crack filed of water with defined density as magma. This process was implemented only in the Limit Equilibrium Method (SLIDE) because in Finite Element Method (PHASE 2) tension crack is not supported and moreover cannot apply zero strength material with possible hydrostatic forces to the surface. We get over this problem using multiple joints, in which constant value of pressure will be applied within each joint. This pressure has been used to simulate the pressure due to magma. Each joint is defined by setting slip criterion to “none” and assuming “normal stiffness and shear stiffness” equal to zero, which means to consider joints interface with strength properties assumed null. An elastic behavior is expected by joint interface subjected to a magmatic pressure. This particular setting was established to carry out the edifice response under horizontal pressure. Seismic horizontal acceleration $a=0.26$ g was used which incorporates the effect of pseudo-static loading caused by the earthquake in the limit equilibrium analysis. The coefficient is based on Peak Ground Acceleration (PGA) and obtained from seismic hazard evaluation “evaluación regional de la amenaza sísmica en centro américa”, 2008 (UPM) and rationalizing seismic coefficient method (Hynes & Franklin, 1984). The PGA evaluated in this study represent an earthquake of moment magnitude equal to 6.5 Mw with recurrence interval of 500 yr. Seismic force is directly obtained by multiply the seismic coefficient, (or seismic horizontal acceleration), per unit weight on each slices. In the past, some studies have explored the volcanic eruptions triggered by earthquakes that are far from the volcano. A classic example to support this observation is the 1992 Landers earthquake (S. California) that caused seismicity at large distances, which also included the volcanically active Long Valley caldera which experienced concurrent deformation (Linde and Sacks 1998). Considering the above example, it seems appropriate to investigate the magma pressure associated with seismic load as further scenario.

6.2.6 ANALYSIS METHOD

In this study, different methods were employed to analyze the stability of Pacaya volcano using Limit Equilibrium Method (LEM) and Numerical Modeling.

6.2.6.1 SLIDE

Several LEMs have been developed for slope stability analyses. Fellenius (1936) introduced the first method, referred to as the Ordinary or the Swedish method, for a circular slip surface. Bishop (1955) advanced the first method introducing a new relationship for the base normal force. The equation for the FOS hence became non-linear. At the same time, Janbu (1954a) developed a simplified-method that accounts for non circular failure surfaces, by separating the potential sliding mass into several smaller

vertical slices. The generalized procedure of slices (GPS) was developed at the same time as a further development of the simplified method (Janbu 1973). Later, Morgenstern-Price (1965), Spencer (1967), Sarma (1973) and several others made further contributions with different assumptions for the inter-slice forces. A procedure of General limit equilibrium (GLE) was developed by Chugh (1986) as an extension of the Spencer and Morgenstern-Price methods, satisfying both moment and force equilibrium conditions (Krahn 2004, Abramson et al. 2002). Bishop and Janbu methods are reviewed in the following section, which aims to find out the key differences in the various approaches for the factor of safety (FOS) determination. All LEMs basically differ only on how the inter-slice normal (E) and shear (T) forces are determined or assumed. In addition to this, the shape of the assumed slip surface and the equilibrium conditions for calculation of the FOS are among the other parameters that vary from one LEM to the other. A summary of selected LEMs and their assumptions are presented in Abramson et al. 2002 and Nash 1987.

6.2.6.1.1 BISHOP'S

Bishop's simplified method is very common in practice for circular shear surface. This method considers the inter-slice normal forces but neglects the inter-slice shear forces (Abramson et al. 2002). In summary, the Bishop's simplified method:

- Satisfies moment equilibrium for FOS,
- Satisfies vertical force equilibrium,
- Considers inter-slice normal force,
- More common in practice, and

Applies mostly for circular shear surfaces

6.2.6.1.1 JANBU'S

Janbu's simplified method is based on a composite shear surface (i.e. non-circular) and the FOS is determined by horizontal force equilibrium. As in Bishop's, the method considers inter-slice normal forces (E) but neglects the shear forces (T). In summary, Janbu's simplified method:

- Satisfies both force equilibriums,
- Does not satisfy moment equilibrium,
- Considers interslice normal forces, and
- is commonly used for composite shear surface.

Janbu introduced a correction factor (f_o), in the original FOS (F_o), to accommodate the effects of the interslice shear forces. With this modification, Janbu's corrected method (JCM) gives higher FOS, as:

$$Ff = f_o F_o$$

6.2.6.2 PHASE

Phase 2 is used to determine the progressive deformation, stress, and strain of Pacaya volcano and to determine the likely slip surface of failure. Stability analysis investigation was executed through Phase 2, which utilizes the Finite Element Method (FEM) shear strength reduction (SSR) approach to determine the safety factor of a slope.

6.2.6.2.1 SSR'S

The FEM is widely used for slope stability analysis utilizing the SSR approach. The SSR concept is simple: a systematic reduction in the shear strength of the material is done based on a factor, and computing the FEM slope stability models until the deformations are unacceptable/solutions do not converge (Hammah et al. 2005). In SSR approach, these steps are to determine the Strength Reduction Factor (SRF) which is equivalent to the factor of safety value that evaluate slope failure potential. The instability criteria in a FEM using a SSR approach is when the solution does not converge within a specified tolerance. To perform the slope stability analysis with SSR technique the actual shear strength properties, cohesion (c) and friction angle (Φ_p) are reduced for by SRF according to equations below. The reduced strength parameters Φ_{p_r} and c_r are determined by:

$$c_r = c / \text{SRF}$$

$$\Phi_{p_r} = \Phi_p / \text{SRF}$$

This method is referred to as the “shear strength reduction technique” (Matsui et al. 1992). When the SRF defines the instability of the slope, the corresponding value is taken as the safety factor of the slope (Griffiths et al. 1999). And this stage is referred as the “critical stage”.

6.3 LIMIT EQUILIBRIUM METHOD (LEM)

The limit equilibrium analysis was carried out using *Slide* package in Rocscience. *Slide* is a 2D slope stability package used to analyze the stability or probability of failure, of various failure surfaces (both circular and non-circular) in rock or soil slopes. The application of *slide* is easy to use, and provides the ability to model complex surfaces and slope conditions (Hoek 2000). It also provides the ability to incorporate groundwater and external loading conditions into the model in variety of ways (Hoek 2000). *Slide* utilizes the vertical slice LEMs (e.g. Spencer, Janbu, etc) to analyze the stability of slip surfaces. Rigid-plastic behavior of all slices on the wedge is assumption on which Limit Equilibrium Method (LEM) works. The program provides the capability to evaluate either individual slip surfaces or to search for a critical slip surface for the given slope profile. It also provides the option to analyze the slope using safety factor (deterministic) or in terms of the probability of failure. In the LEM the assumption is that all the forces considered act through the center of each slice and the failure model is represented as translational slip. We performed a deterministic analysis using Janbu's and Bishop's methods on the volcano models represented respectively in figure 6.3 and figure .4. The main objective of the analysis was to find the global minimum slip surface that represents the failure plane with the least "Safety Factor", as well as the stability of the deep failure surfaces that could potentially cause huge destruction.

6.3.1 SENSITIVITY ANALYSIS

Sensitivity analysis was performed on the fourth model as worst scenario, for precautionary reasons in dealing with volcano properties uncertainties. Sensitivity analysis conducted on both section AA' and BB', emphasized seismic load as likely destabilizing factor that influences the volcano. The impact of seismic coefficient was verified under wide range of values. Exponential distribution as the best representative mode to investigate seismic load range (0-0.52 g) was selected. Magma pressure effect on the slip surface was analyzed using linear distribution. Then, range of values is determined between minimum and maximum around mean as deterministic input value. The range from 0 to 33372 KN/m² for the BB' cross-section and from 0 to 43566 KN/m² for the AA' cross-section were used.

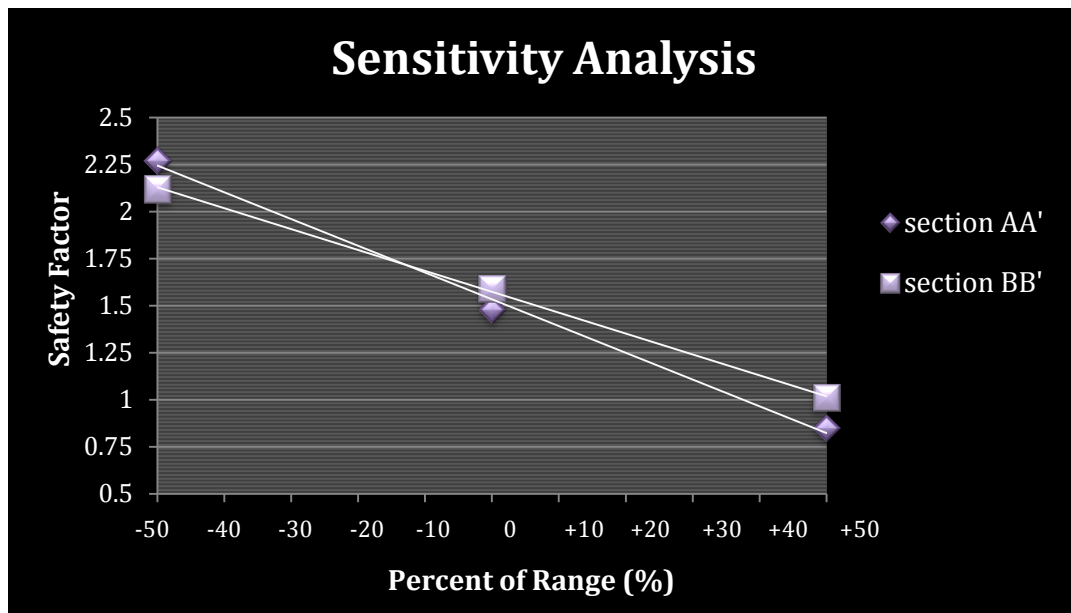


Figure 6.6: Sensitivity of the Safety Factor to variations of magma pressure component: section AA' magma load ranging from mean input $\pm 21783 \text{ KN/m}^2$. Section BB' magma load ranging from mean input $\pm 16686 \text{ KN/m}^2$

The results, Fig.6.6, indicate magma pressure doesn't destabilize the slope under most pressures evaluated. However, it is observed that the influence of magma pressure highly reduces the factor of safety. Moreover, the sensitivity analysis performed on section AA' resulted in safety factor lower than 1 corresponding to higher magma pressures applied, which destabilizes the slope. It is also worth noting that, in this scenario, the impact of over pressure is not considered. The safety factors obtained by applying the maximum magma pressures are respectively:

- i. SF=1.1 for BB' section-profiles;
- ii. SF=0.85 for AA' section profiles.

Sensitivity analyses performed using seismic load (Fig.6.7) indicate seismicity as a critical factor that significantly reduce the factor of safety. Safety factors obtained by applying the maximum seismic load are:

- i. SF=1.08 for AA' section-profiles;
- ii. SF=0.98 for BB' section-profiles.

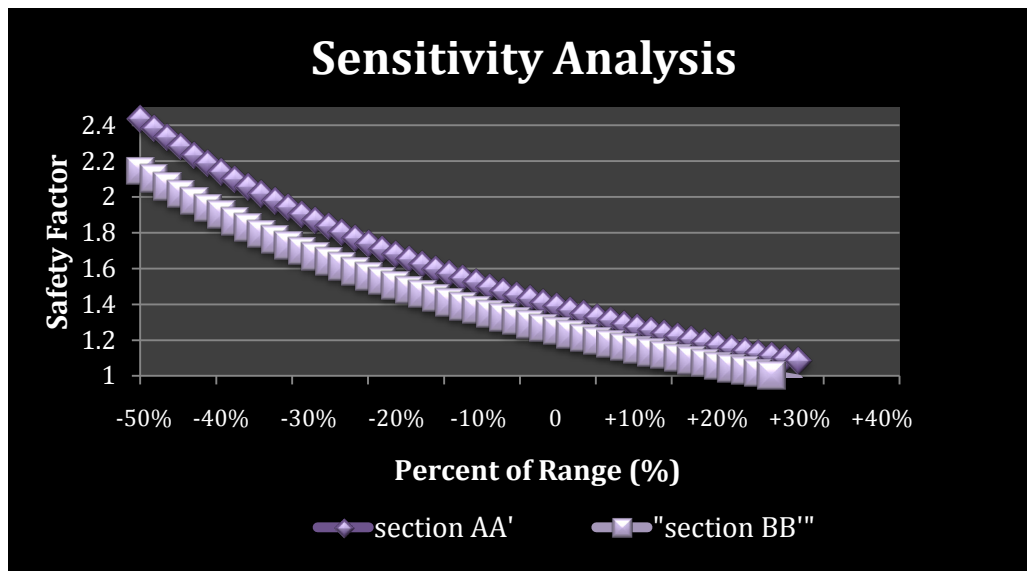


Figure 6.7: Sensitivity of the Safety Factor to variations of seismic load component: seismic load ranging from mean input ± 0.26 .

Geo-mechanical parameters sensitivity analysis results, executed on the slip surface, underline friction angle having higher sensitivity with respect to other factors. Ranges of variability of all material properties are equal for each lithotechnical unit. Different ranges were specified for different properties as friction angle, cohesion, and unit weight. The range of values is determined around mean as deterministic input value. It is evident from figure 6.8, in which third model was investigated, that the friction angle plays a critical role for the stability analysis of Pacaya volcano. The friction angle sensitivity is equal to 6:1 ratio or in other words 50% friction angle variations correspond to 16% of the safety factor. It is observed that the sensitivity of slope stability to friction angle is greater for the breccia-lava layers than the other lithotechnical units. It is also observed that the sensitivity of unit weight also plays a secondary role whereas; the sensitivity to cohesion is irrelevant. Furthermore, sensitivity analysis on geomechanical parameters was conducted on fourth model in both sections AA' and BB' in order to have a better understanding about breccia-lava sensitivity (Fig.6.9 and Fig.6.10). Since the fourth model is built on breccia-lava unit. It is observed that the friction angle sensitivity is increased to ratio equal to a 4:1 as 50% friction angle variations correspond to 25% of the safety factor. The mentioned ratio should be considered as the most reliable value corresponding to friction angle sensitivity. Besides the cohesion and unit weight acquire major consequence on the stability analysis performed on worst scenario in base of material properties. The main result achieved from sensitivity analysis is the strong safety factor dependence on the friction angle.

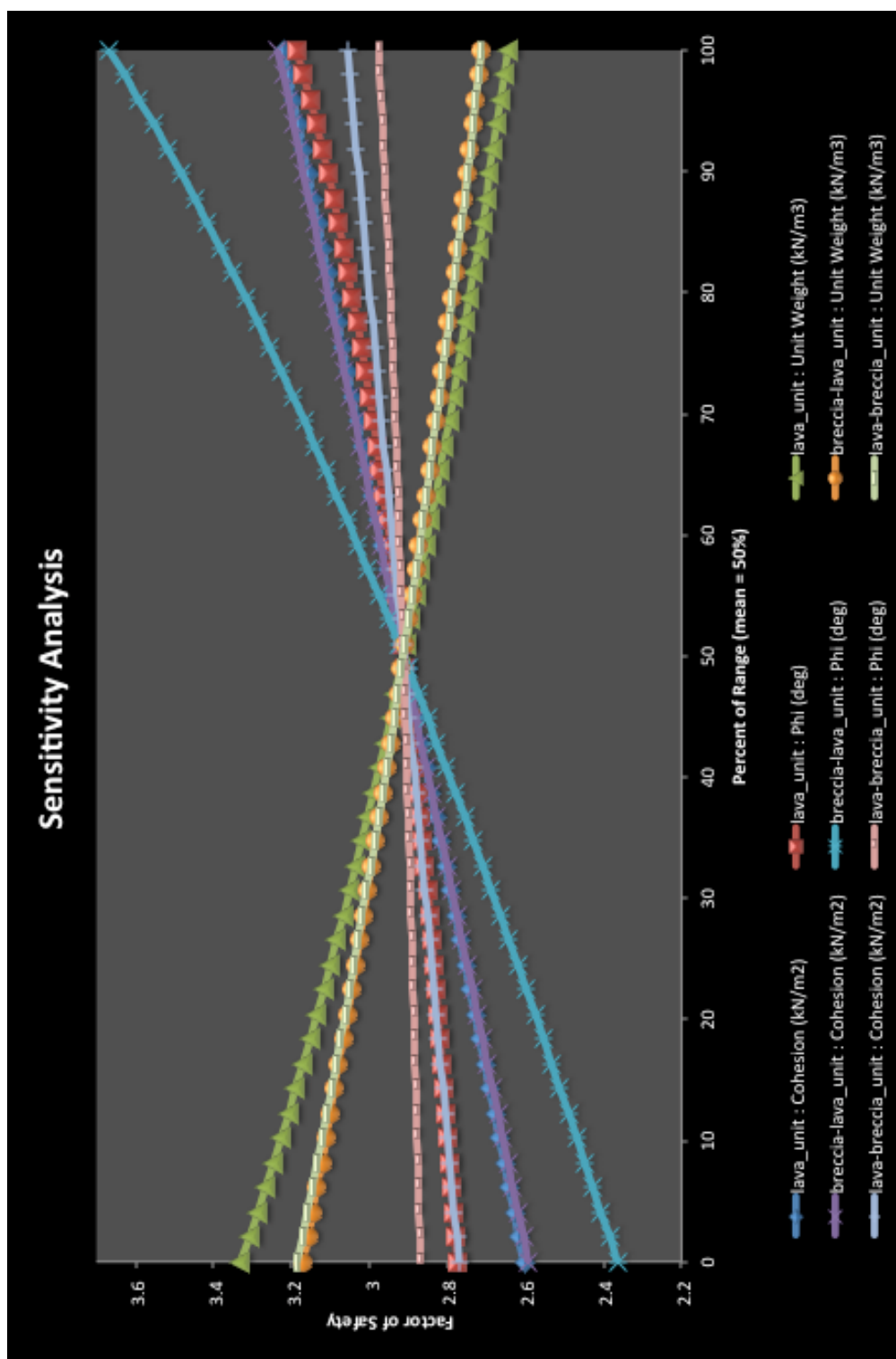


Figure 6.8: Sensitivity of the Safety Factor to variations: 1) geomechanical parameters: friction angle; cohesion; and unit weight. Mean input in base of lithotechnical unit considered.

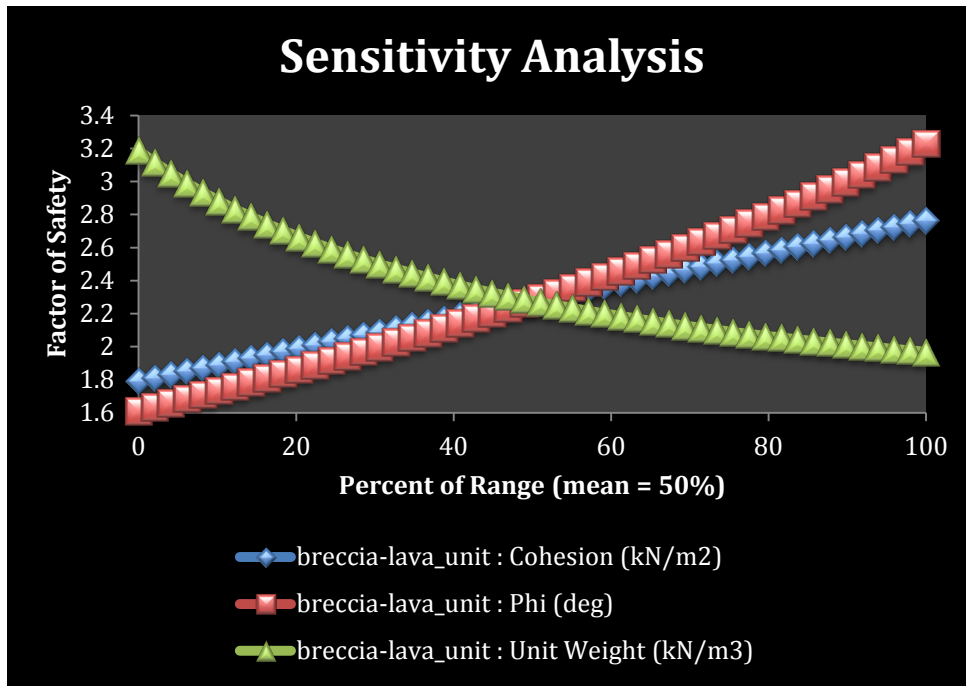


Figure 6.9: Sensitivity analysis of safety factor to variations of geomechanical parameters conducted on fourth model. Section AA'

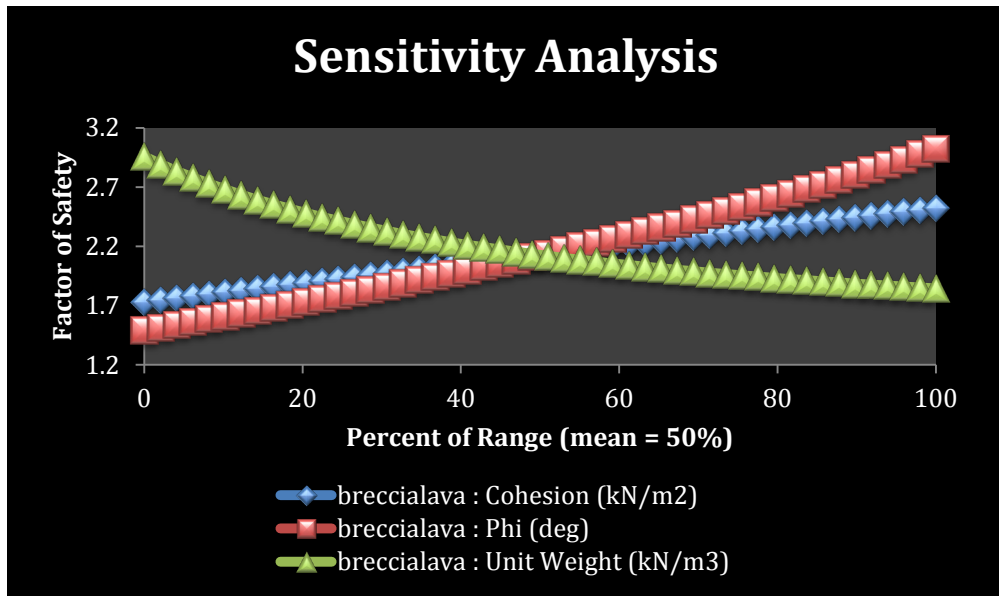


Figure 6.10: Sensitivity analysis of safety factor to variations of geomechanical parameters conducted on fourth model. Section BB'

6.3.2 LEM RESULTS

Limit equilibrium analysis is performed on four cases essentially revealed that the slope is stable under “static condition”, “magma pressure”, “seismic” and “seismic + magma” scenario. Although, the last scenario indicates proximity to unstable conditions, which is not to be neglected. Limit equilibrium results are listed in Table 6.1. In static condition, safety factors for slip surfaces, presented values always greater than 2. In section AA’ the critical slip surface presents SF=2.2-2.9 (Table 6.1). Otherwise in section BB’ the critical slip surface presents lower SF values as response of higher inclination and elevation of slope profile (shown in Fig.6.2). Corresponding volumes involved for AA’ critical slip surface is 350,000 m³ and 500,000 m³ for BB’ slip surface, considering 2-D cross section (Fig.6.11 and Fig.6.12). In 3-D examination through 100 m up to 300 m width of cross-section analyzed, the volumes ranges from 35 up to 105× 10⁶ m³ and from 50 up to 150× 10⁶ m³ respectively for critical slip surfaces AA’ and BB’. Below, slip surfaces of fourth model are presented:

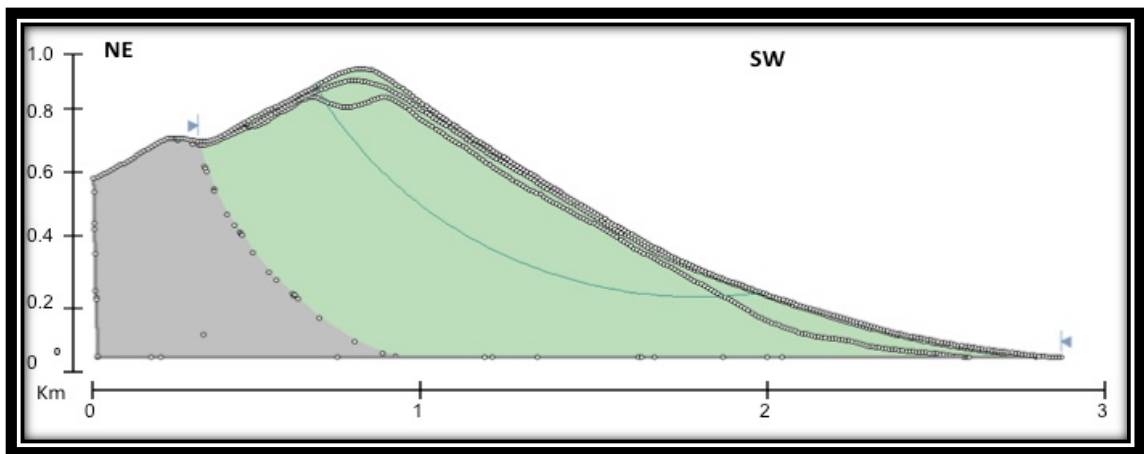


Figure 6.11: Critical slip surface of fourth model. Section AA’

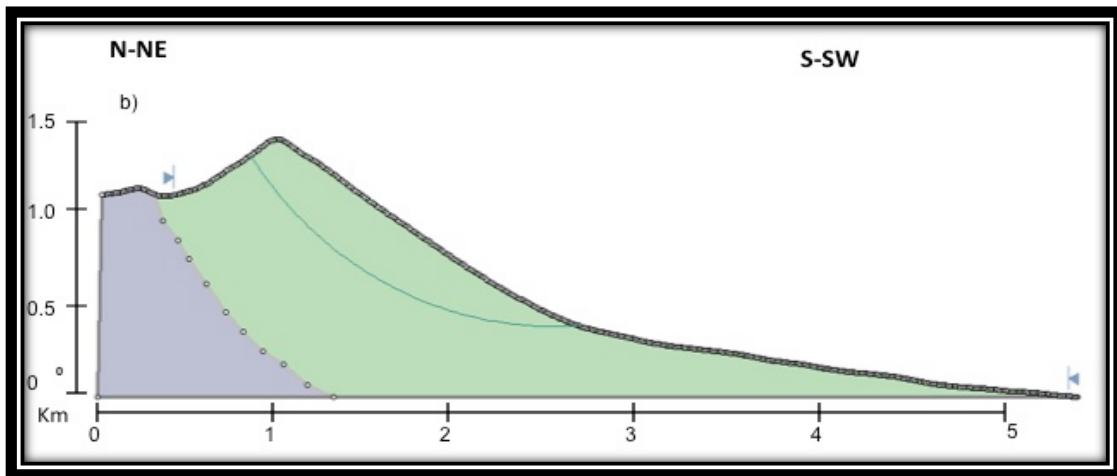


Figure 6.12: Critical slip surface of fourth model. Section BB'

Magma pressure as triangular force distribution influenced significantly the safety factor (decreasing range of 0.5 up to 1) of the slip surfaces AA' and BB' sections.. The safety factors, visible in table 14, demonstrate the decreasing to unity for the AA' section perpendicular to main direction of magma rising. Seismic regional load affects the stability of slope in a similar way with respect to magma pressure. Regional seismicity has been proposed over the years as a possible trigger of volcanic eruption. The combined activity has been addressed here. This last scenario analyzed demonstrates that seismic and magma load together may be responsible for the volcanic collapse at Pacaya. Safety factors, in Table 6.1, highlight an important reduction due to this load case, especially looking to the fourth model (SF=1.04-1.06). Janbu and Bishop methods presented similar results with little change (± 0.03) in safety factor values. The principal results achieved here indicate that magmatic and seismic load estimated, would highly reduce the stability. The worst scenario according to geotechnical parameters, fourth model, evaluated here proposes carefulness to treat these destabilizing factors in response to hazards associated. The main results from deterministic and sensitivity analysis indicate that magmatic load (as shown in Fig.6.6), seismic load (Fig.6.7) and sensitivity (Fig.6.8) would lead to reduction in safety factor and the deepening of failure surface (e.g. Fig.6.13 section AA').

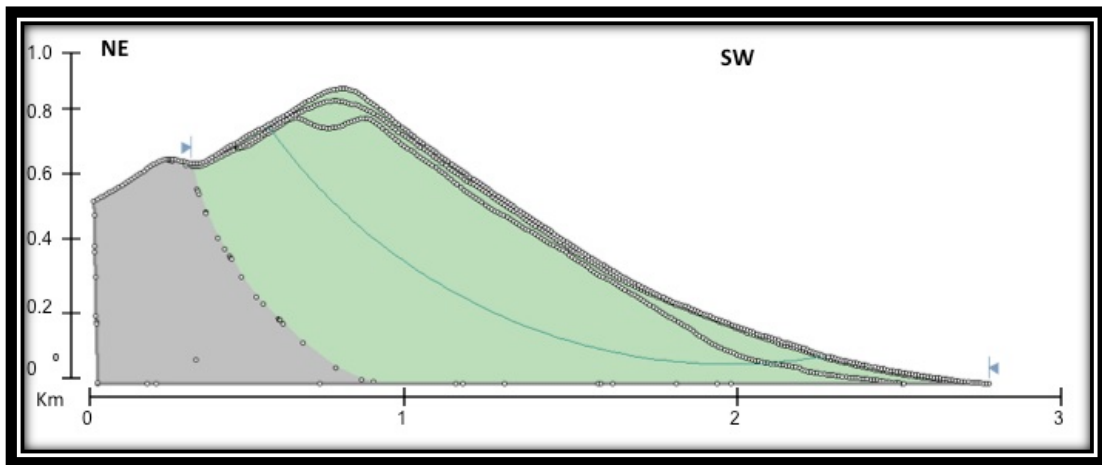


Figure 6.13: Slip surface from seismic load scenario analyzed.

Table 6.1: Results of limit equilibrium analysis.

Models	Safety Factor (SF)							
	Gravity		Seismic		Magma Pressure		Magma Pressure + Seismic	
	section AA'	Section BB'	Section AA'	Section BB'	Section AA'	Section BB'	Section AA'	Section BB'
1	2.97	2.66	1.91	1.72	1.94	2.05	1.35	1.36
2	2.91	2.56	1.93	1.7	2.04	1.99	1.41	1.32
3	2.91	2.56	1.93	1.69	1.97	2.01	1.37	1.33
4	2.27	2.12	1.53	1.38	1.48	1.59	1.04	1.06
Bishop Method for all output values; Horizontal Seismic Load Coefficient (0.26); Triangular Load (0-21783 kN/m2 sec AA') (0-16686 kN/m2 sec BB')								

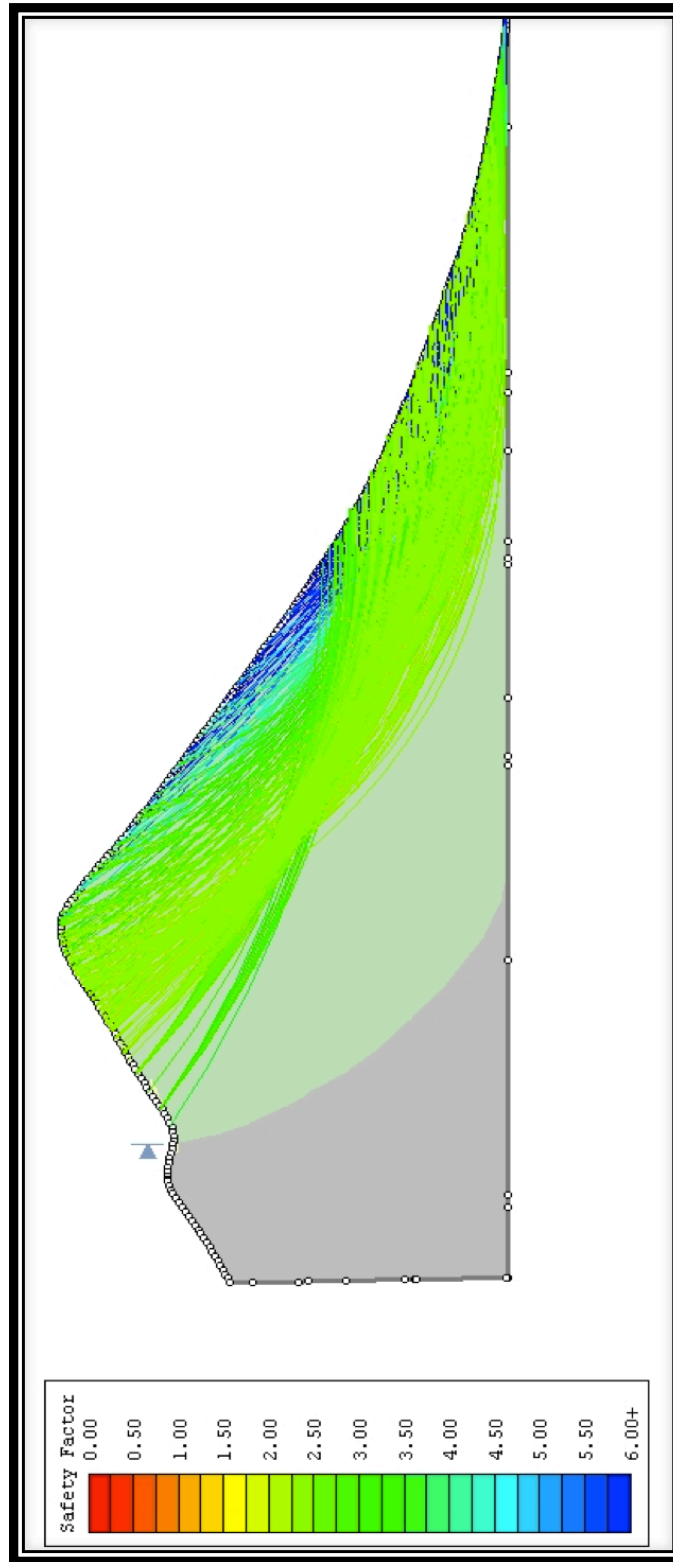


Figure 6.14: Distribution of safety factor on fourth model (section AA'). Green zone represents worst values of safety factor under static condition.

6.4 NUMERICAL MODELING: FINITE ELEMENT METHOD (FEM)

To determine the progressive deformation, stress and strain, of the Pacaya volcano and define the likely slip surface of failure we performed the numerical modeling through *Phase 2*. *Phase 2* models a system evolving in time that enables to monitor the deformation and progressive failure step by step. The main aim of this approach is to determine future scenario of the progressive deformation and how it would result in slope instability. This method in parallel with deterministic ones would be taken into account for future volcanic hazards at Pacaya volcano, because collapse events affect wide areas around volcanoes. This in turn would help to update the risk map at Pacaya taking into account collapse events. Stability analysis was performed using Phase 2, which is used to derive the safety factor of a slope relating to its strength reduction factor. In order to perform the two-dimensional numerical modeling, elastic-plastic behavior is assumed. The model was generated using a 2-dimensional finite element mesh generator, which automatically generates meshes based on either triangular or quadrilateral elements. In all models, recommendation in Wyllie and Mah (2004) by Loren Lorig, was adopted to ensure that boundaries were distant enough so as not influence analysis results. Basement was added to each model in order to avoid mesh distortions due to constrain boundary (Fig.6.15). Basement influence to models deformation was deleted through elastic properties selected.

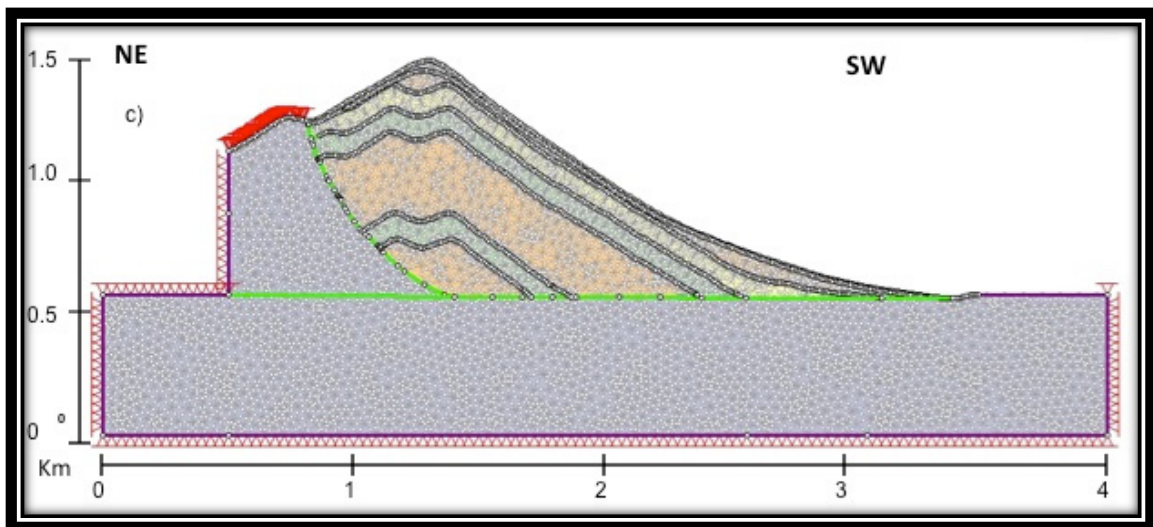


Figure 6.15: Third model generated using a 2 dimensional automatic finite element mesh. Section AA'.

6.4.1 STRESS

Based on uncertain horizontal stress distribution within slope, a good assumption is leaving the horizontal stress ratio equal one as hydrostatic initial stress. Then using “actual ground surface” as option of gravity stress field type, the program will determine the vertical stress in every finite element based on the weight of material above it. Since the initial stress condition and the body forces does not indicate an equilibrium state within the slope, the material within the slope will undergo deformation due to its own weight and stress conditions. It is observed that the material will deform in the horizontal direction away from the surface of the slope because the initial stresses are not in equilibrium. Therefore, “the final vertical stress distribution within the slope will be a gravitational stress distribution with the horizontal stress component caused due to some unloading and redistribution of stress due to the Poisson effect” sourced from (<http://www.rocscience.com>). The Poisson value for all materials is assumed 0.3 ± 0.02 from literature (Riccardo Castellanza’s handsout, UNIMIB).

6.4.2 STAGE OF ANALYSIS AND FAILURE SURFACE

We performed static condition, magma pressure, seismic load and magma + seismic analysis using numerical modeling. Friction angle and cohesion were employed as reduction parameters to apply shear strength reduction method. Each lithotechnical unit parameter, listed above, is investigated as each model is considered into analysis procedure. Geotechnical engineering slope stability, involve large uncertainties related to inaccuracies in measurements and due to the differences between laboratory and field data. In such environment, strength reduction offers a means for dealing with uncertainty. The FEM analysis consists of 10 stages of progressive shear strength reduction. The strength parameters are reduced by strength reduction factor, and the stresses are analyzed by finite elements for each of the reduced conditions. This step is repeated for various values of SRF, till the model is unstable. The model is determined unstable when the results of the analysis do not converge and the SRF corresponding to this state is the critical strength reduction factor (critical SRF), and is equivalent to the safety factor, of the slope (figure 6.17). Griffiths et al. 1999 tell: “The critical SRF of a slope is defined as the factor by which the original shear strength parameters must be reduced in order to bring the slope to failure”. The Maximum Shear Strain contours, presented in fig.6.17 highlight the “failure” of the slope at the critical SRF or at the corresponding material parameters (table 15). Here above, a progressive evolution of SSR method performed on fourth model (AA’ section) under static condition. Different stages of SRF are presented:

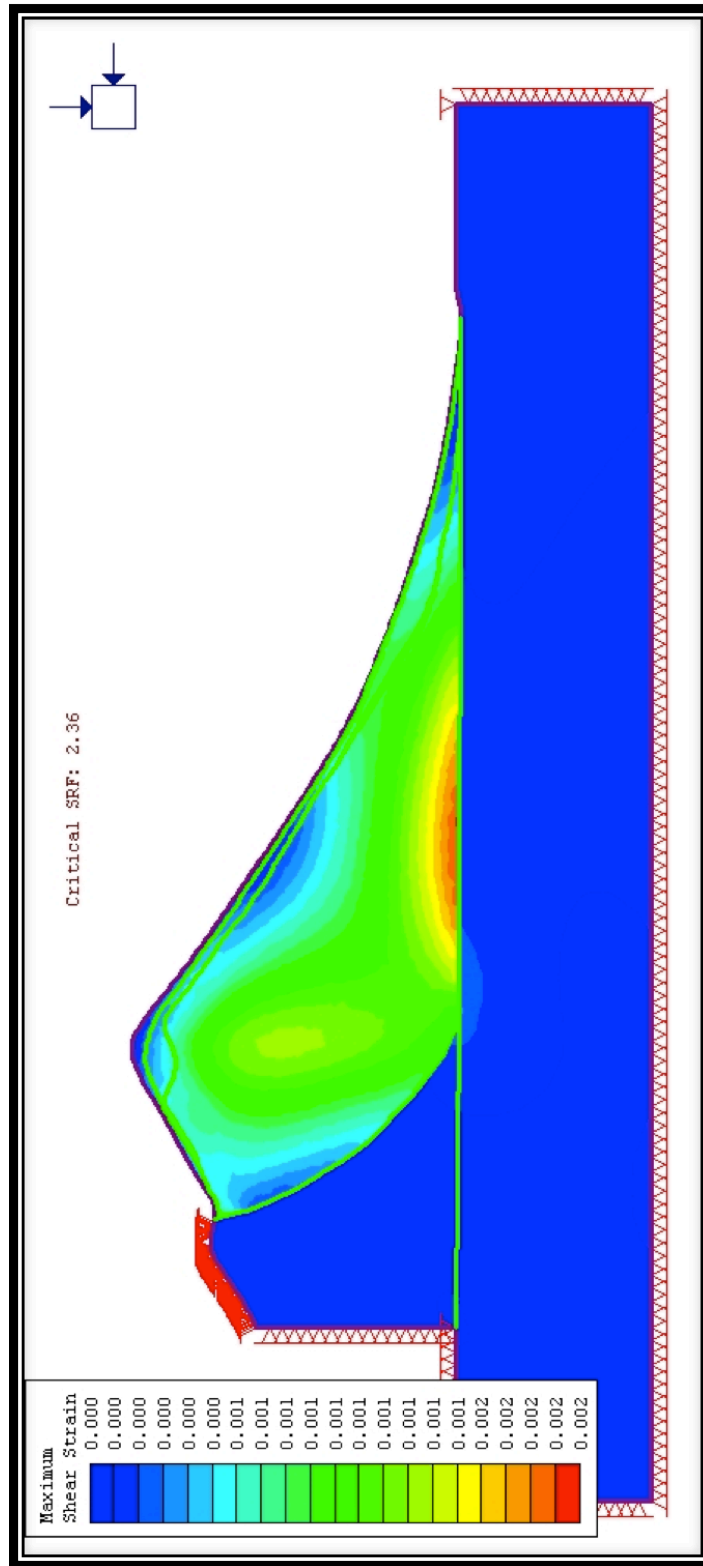


Figure 6.16: Initial shear strength stage. Maximum shear strain presented. Fourth model section AA' analyzed under static condition.

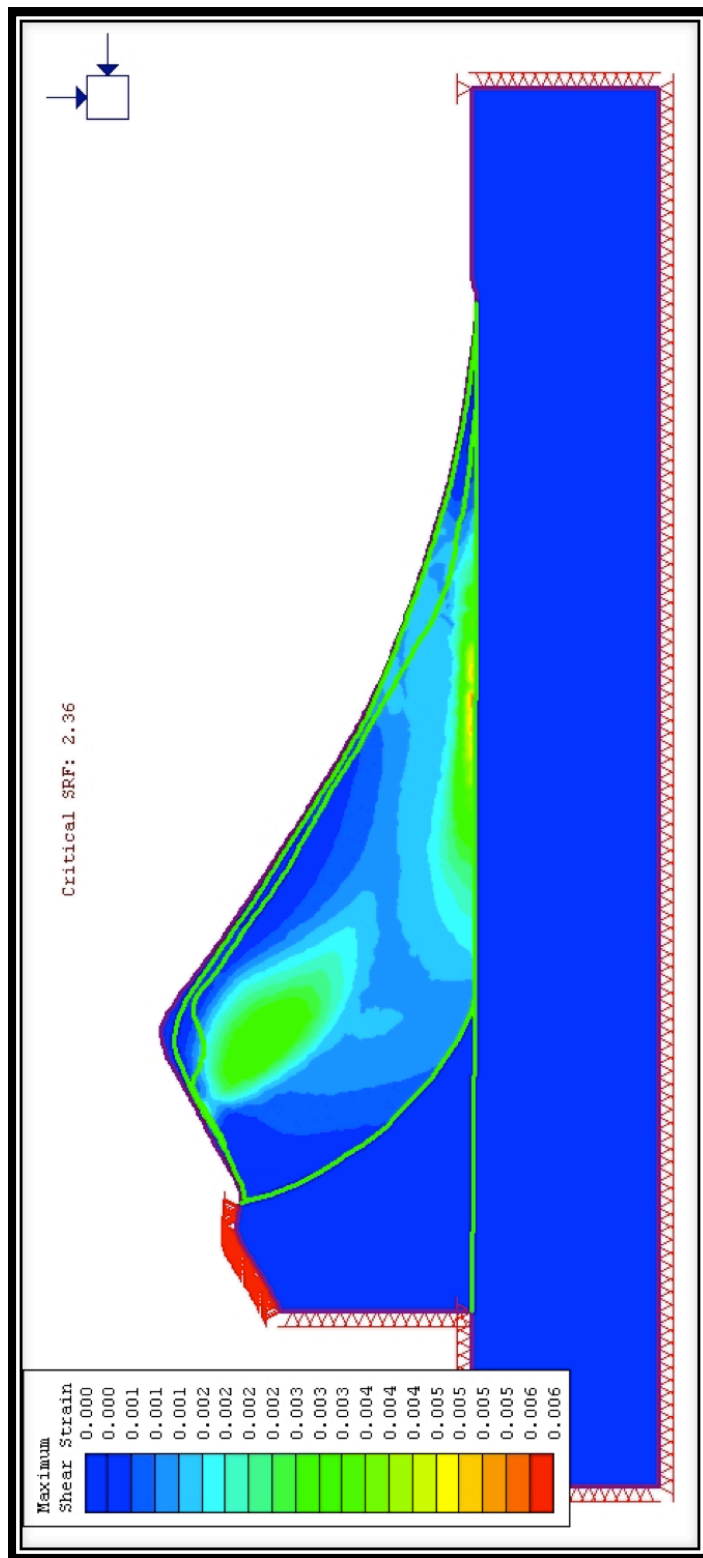


Figure 6.17: Critical shear strength stage (strength reduction factor). Maximum shear strain presented. Fourth model section AA' analyzed under static conditions

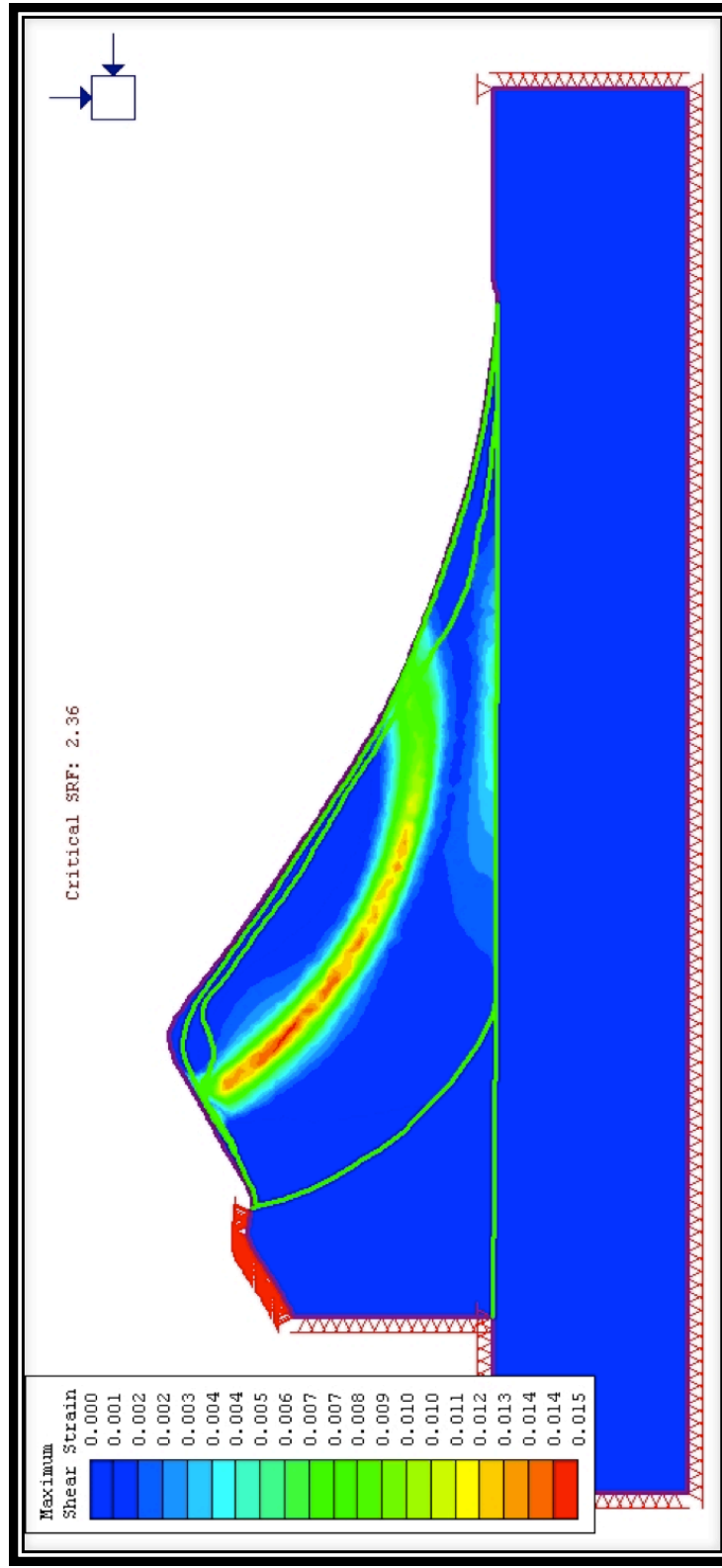


Figure 6.18: Final shear strength stage. Maximum shear strain presented. Fourth model section AA' analyzed under static condition.

Final stage models evolution of progressive deformation along time and represents future scenarios of progressive deepening of slip surface that leads to trigger of a collapse (fig.6.18). Consequently, slip surface underline preferential weak zone on the slope. Each model, not presented here, show the slip surfaces that are demonstrated to correspond for both limit equilibrium and finite element method. Subsequently weak zone are delineated at each model investigated. Maximum deformation contours highlight different range of strain propagation as response unlike material properties involved in each model. Then different range of strain is determined by different strength reduction factor computed according to material properties involved. For example, I present first and fourth model constructed using section AA' respectively in fig.6.19 and fig.6.18.

Maximum shear strains are:

- i. First model maximum shear strain = 0.12;
- ii. Fourth model maximum shear strain = 0.015

Slope angle, topography, material properties, and the internal structure are critical factors that affect the volcano stability, even though simple internal structure is examined here. The most sensitive geo-mechanical parameter, friction angle, for the slip surface is pretty similar at least for three of models even if diverse lithotechnical units are employed. The average value of friction angle acting on slip surface, crossing through only one lithotechnical unit, for the first model is 37.33°; the second one is 38.77°; third one is 38° comprised of different ratio of lithotechnical units crossed. Same trend is observed for the cohesion as well, highest cohesion for the second model and lowest for the first model. Otherwise fourth model presents different friction angle, which correspond to 33.02. Maximum shear strain determined through SSR, presented higher shear strain for the model that is the most resistant to failure, which corresponds to the model with higher friction angle, cohesion, etc. In other words, the maximum shear strain is expression of the highest SFR required in order to produce failure of the model contemplated. Higher shear strain value is exhibited for the second model (higher friction angle), medium for the third and lower in the first model. Lowest value is obtained for the fourth model. This pattern corresponds to the variation in material properties, especially in friction angle as the most sensitive factor. The small strain variation emphasized, in different structure models investigated, reflect the low sensitivity to material parameters as well as the internal structure of the volcano. The location of slip surfaces, observed in each model analyzed, support the inference that slope angle and geometry play critical role to determine the weak zone. The ability to animate the progression of failure by cycling through the various SRF tabs clearly indicated a deepening of failure surfaces for all models analyzed.

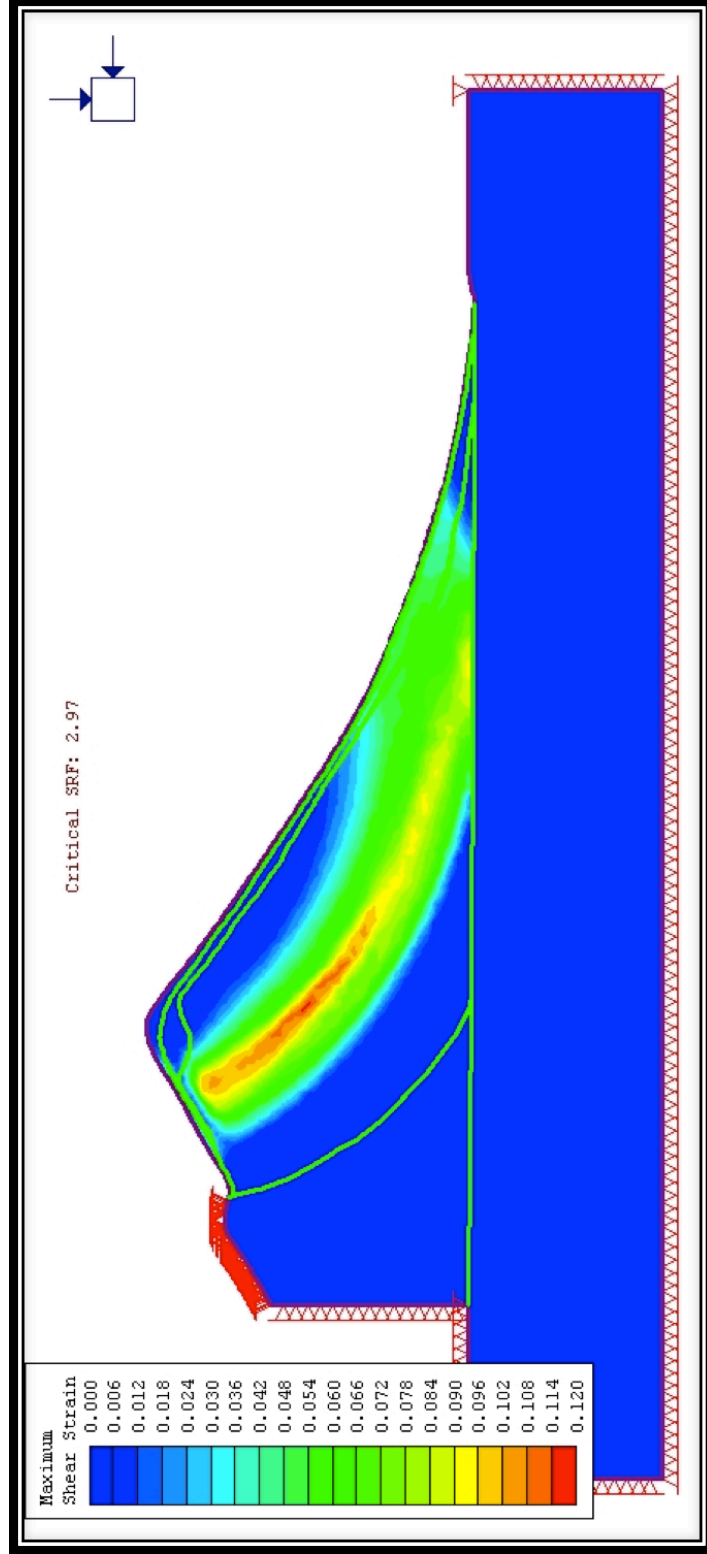


Figure 6.19: Final shear strength stage. Maximum shear strain presented. First model section AA' analyzed under static conditions

The importance of internal structure and the distribution of litotechnical units is defined from the shear strain along the third model computed at the different stages of SSR (Fig.6.20, 6.21, and 6.22). The initial, critical, and final stages are presented in Figures 6.20, 6.21, and 6.22. The presence of “layers” of breccia-lava unit in the third model drives the shear strain distribution of the model. Breccia-lava unit represent the poorest mechanical properties employed in developing models. Maximum shear strain is constantly associated to breccia-lava “layers” as response to the larger reduction of its mechanical properties. This means that the weak “layers” at equivalent SRF for the model considered, are more deformed than others “layers or units”. Furthermore, looking at third model stage evolution it is evident that the slip surface is deepening through multiple shear strength reduction steps, following the weakest “layers” existing in the model. Shear strain distribution explains the critical role on the volcano stability of weak “layers” as the breccia-lava unit, which may be the main factor that controls instability. Further, deformation and displacement at the fourth model are analyzed. In Fig.6.23 the deformation vectors indicate the vertical deformation at the volcano summit, above 2400 m., delimiting an “active” wedge with a vertical shear zone. Below, a predominant downward deformation is determined resampling outward slip displacement. On the other side of the volcano slope a likely initial tensile fracturing is observed. It is well expressed by horizontal displacement in Fig.6.24. The deformation contours, in Fig.6.25, emphasized this displacement of huge volume of material downward to the slope. Information of the displacement involved during SSR method is presented at the critical stage and final stage in Fig.6.26 and 6.27, which give an idea of the total displacement that we can encounter during collapse due to possibly hydrothermal weathering. Last stage displacement represents a future scenario occurring for determined mechanical properties shown in table 16a.

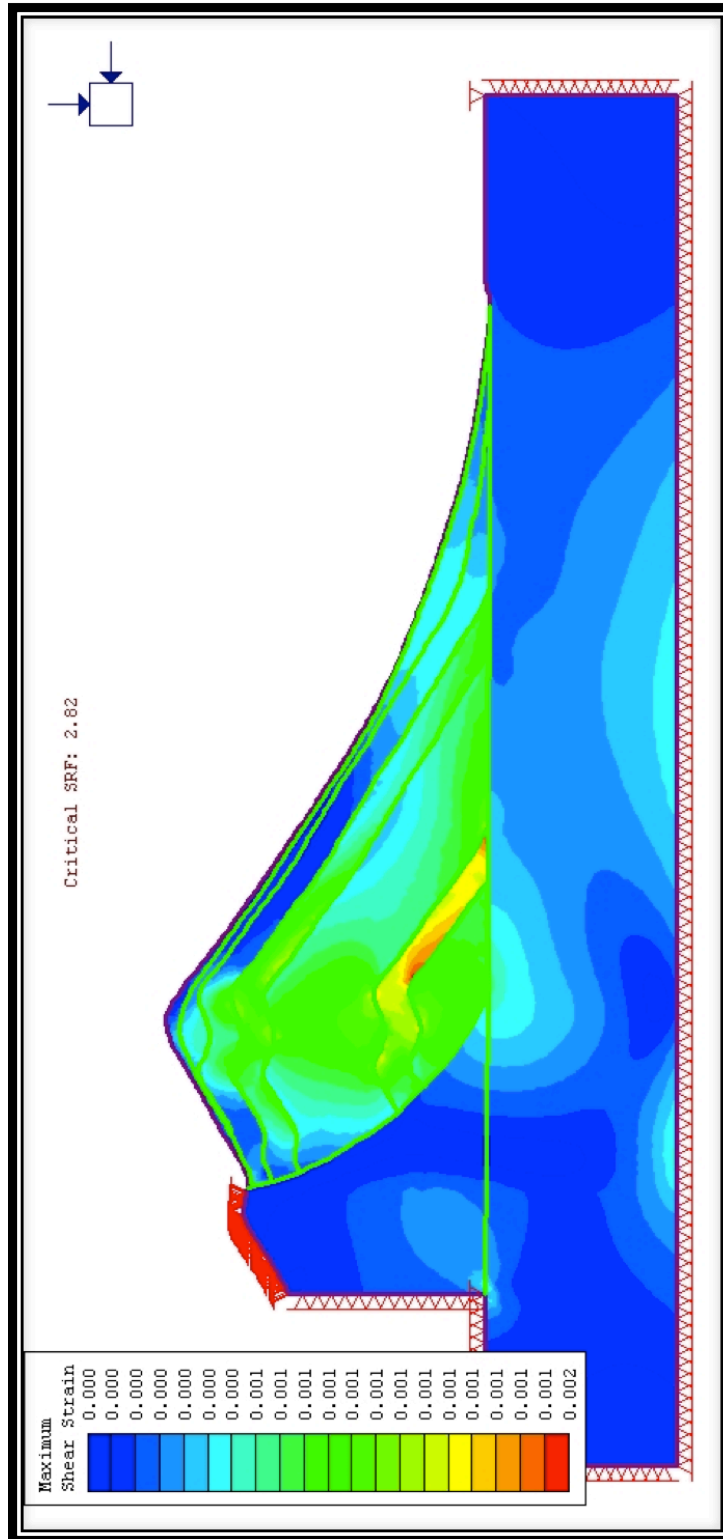


Figure 6.20: Initial shear strength stage. Maximum shear strain presented. Third model section AA' analyzed under static condition

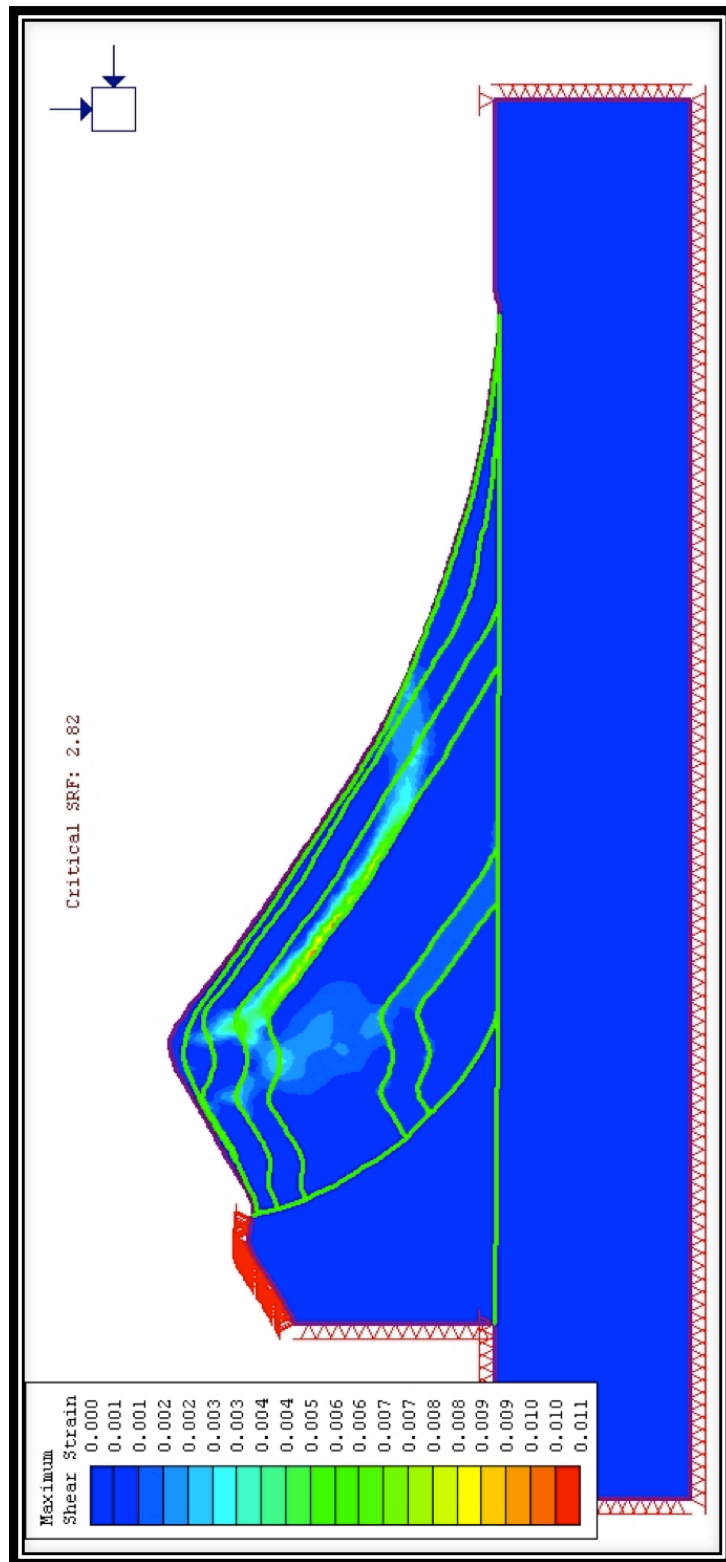


Figure 6.21: Critical shear strength stage (strength reduction factor). Maximum shear strain presented. Third model section AA' analyzed under static conditions

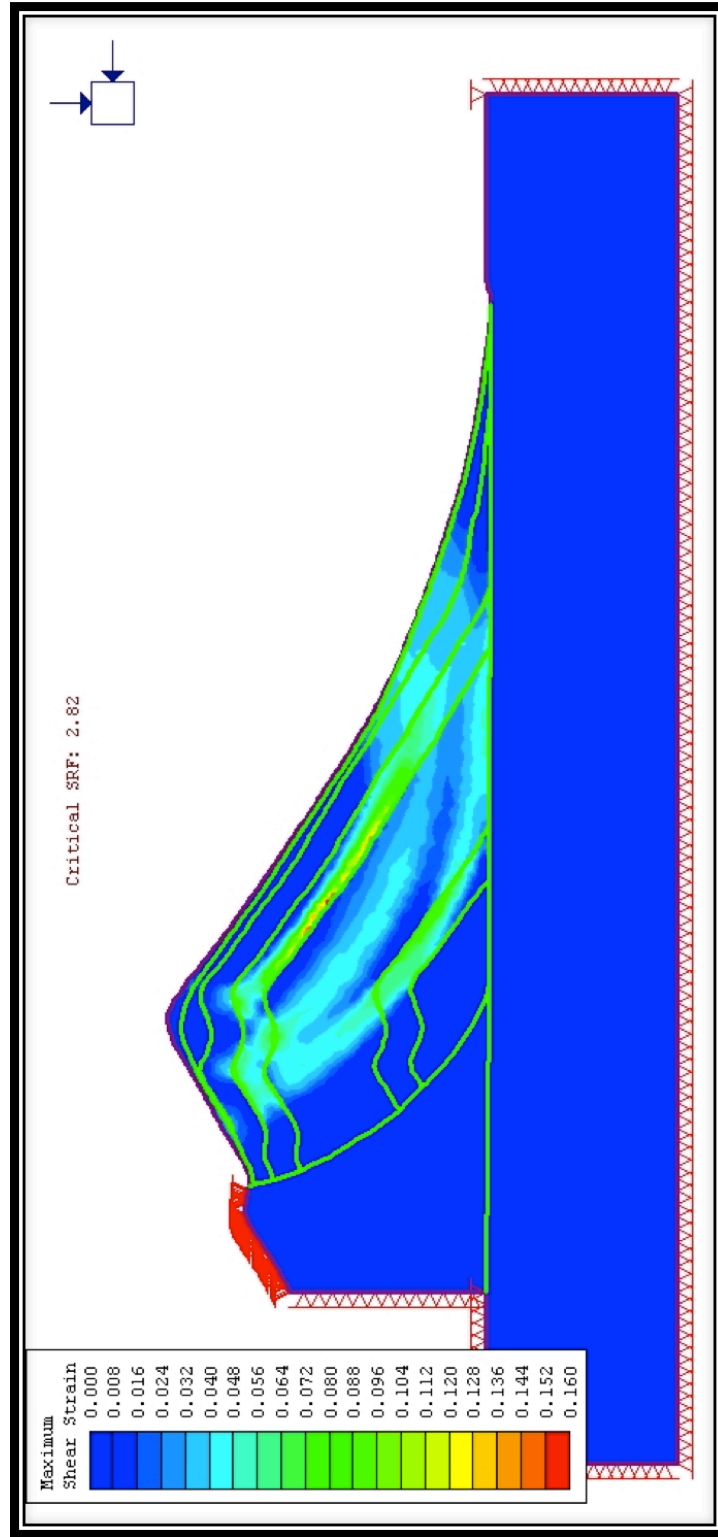


Figure 6.22: Final shear strength stage. Maximum shear strain presented. Third model section AA' analyzed under static condition

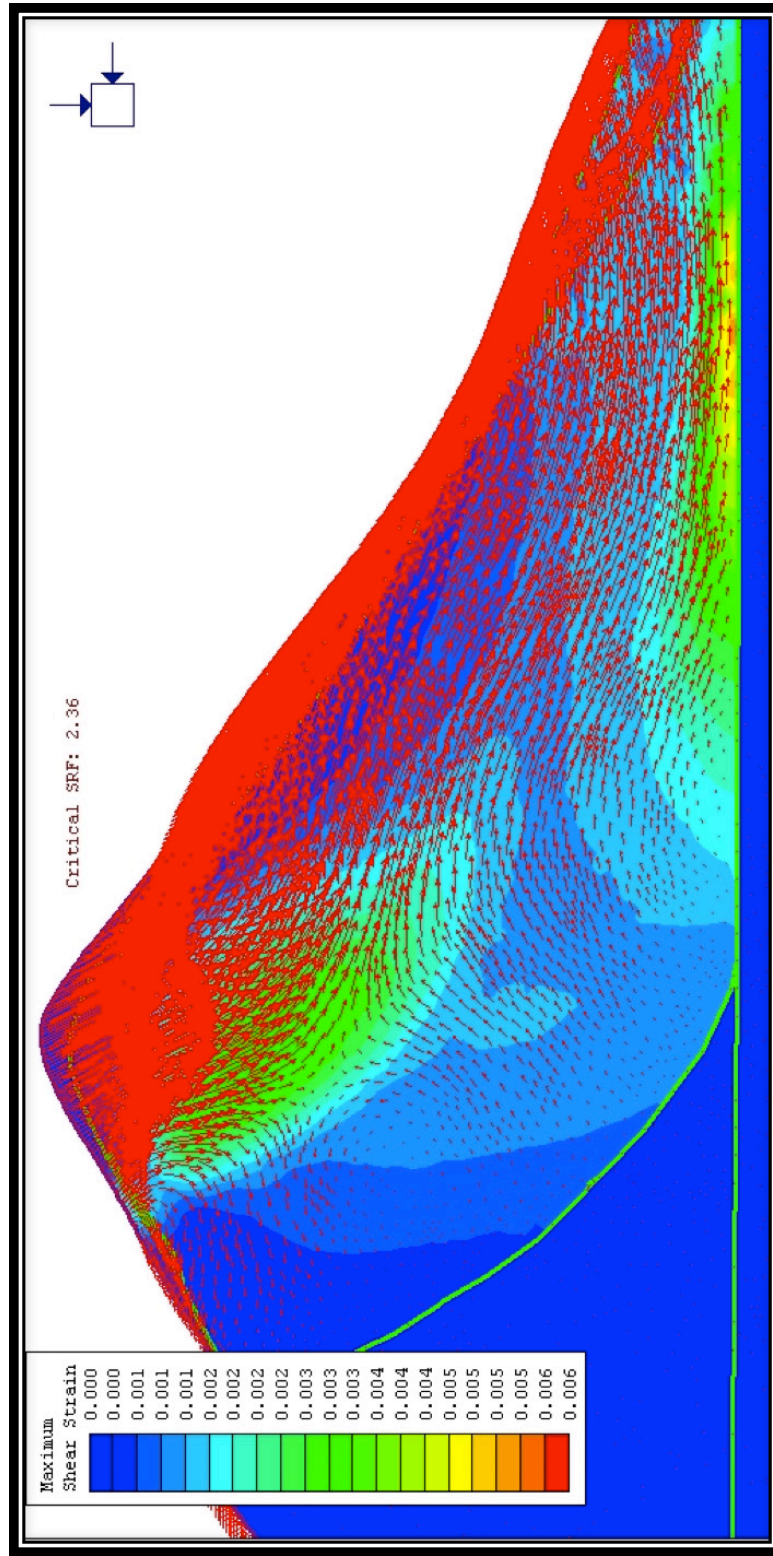


Figure 6.23: Deformation vectors indicate strain direction and distribution. Fourth model section AA'.

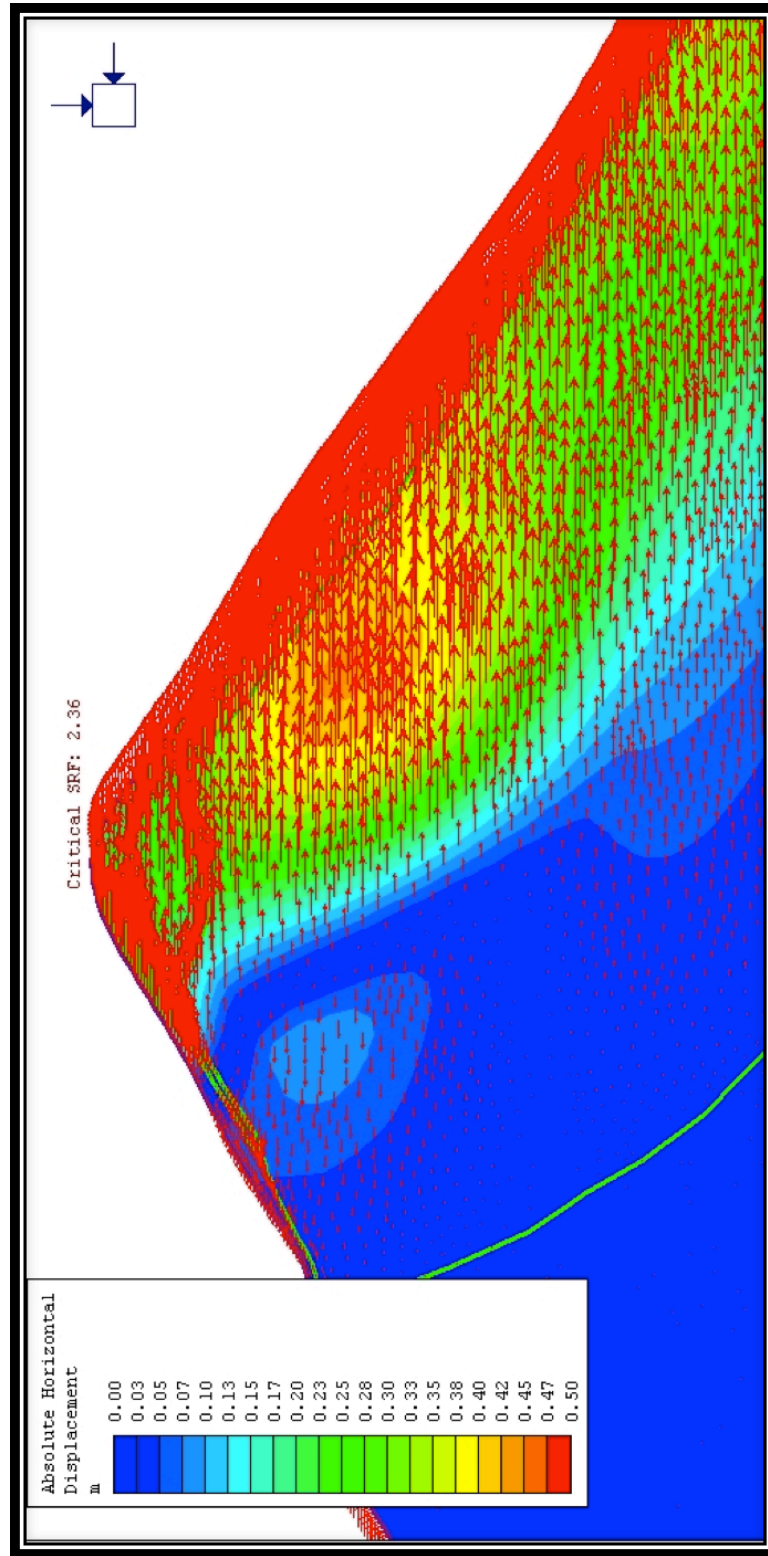


Figure 6.24: Horizontal displacement at the critical stage. It is observed opposite direction of displacement arrows in the upper slope, indicate tensile fracturing. Fourth model section AA'

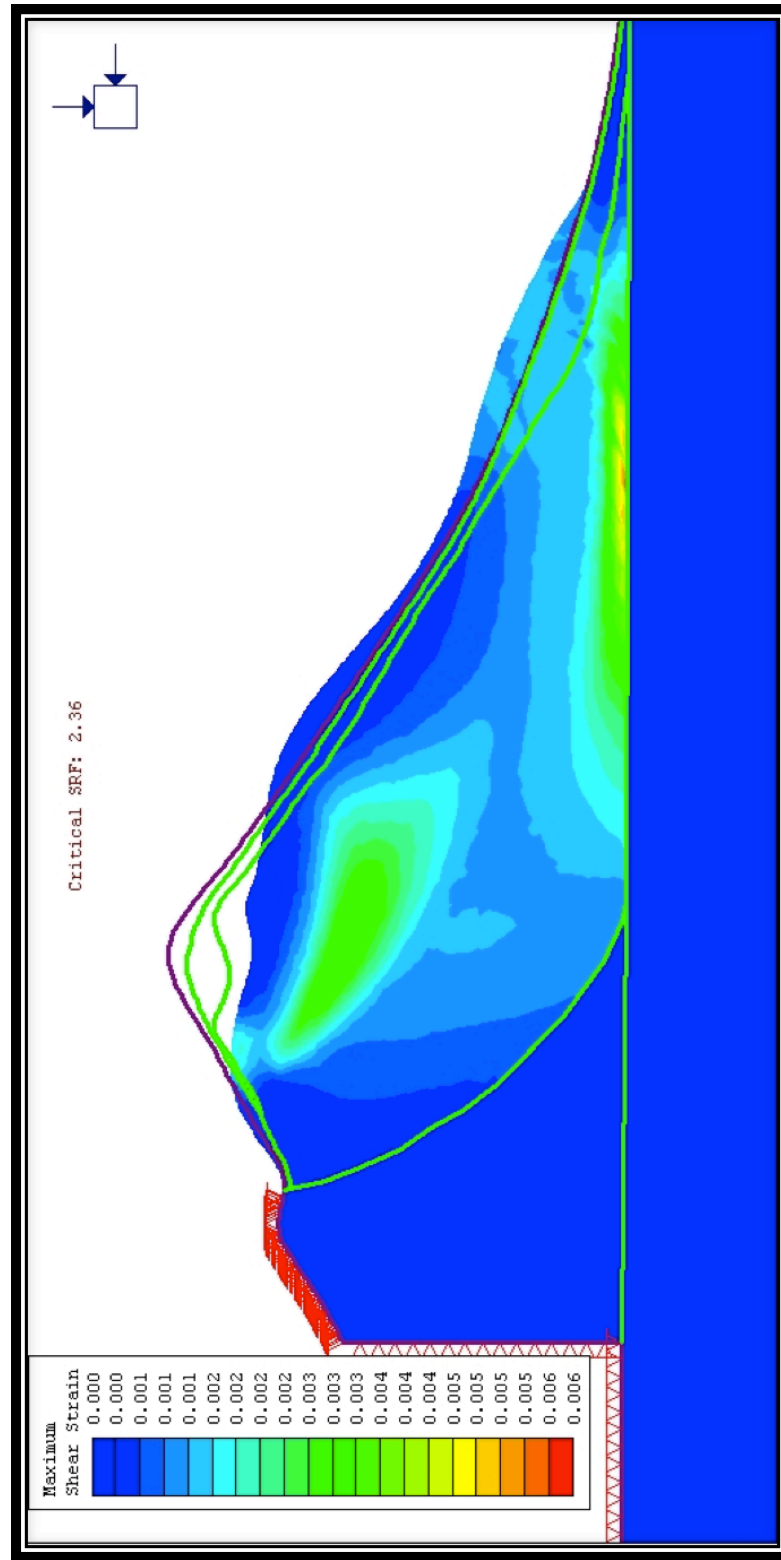


Figure 6.25: deformation contour indicated material volume slip direction. Fourth model section AA'

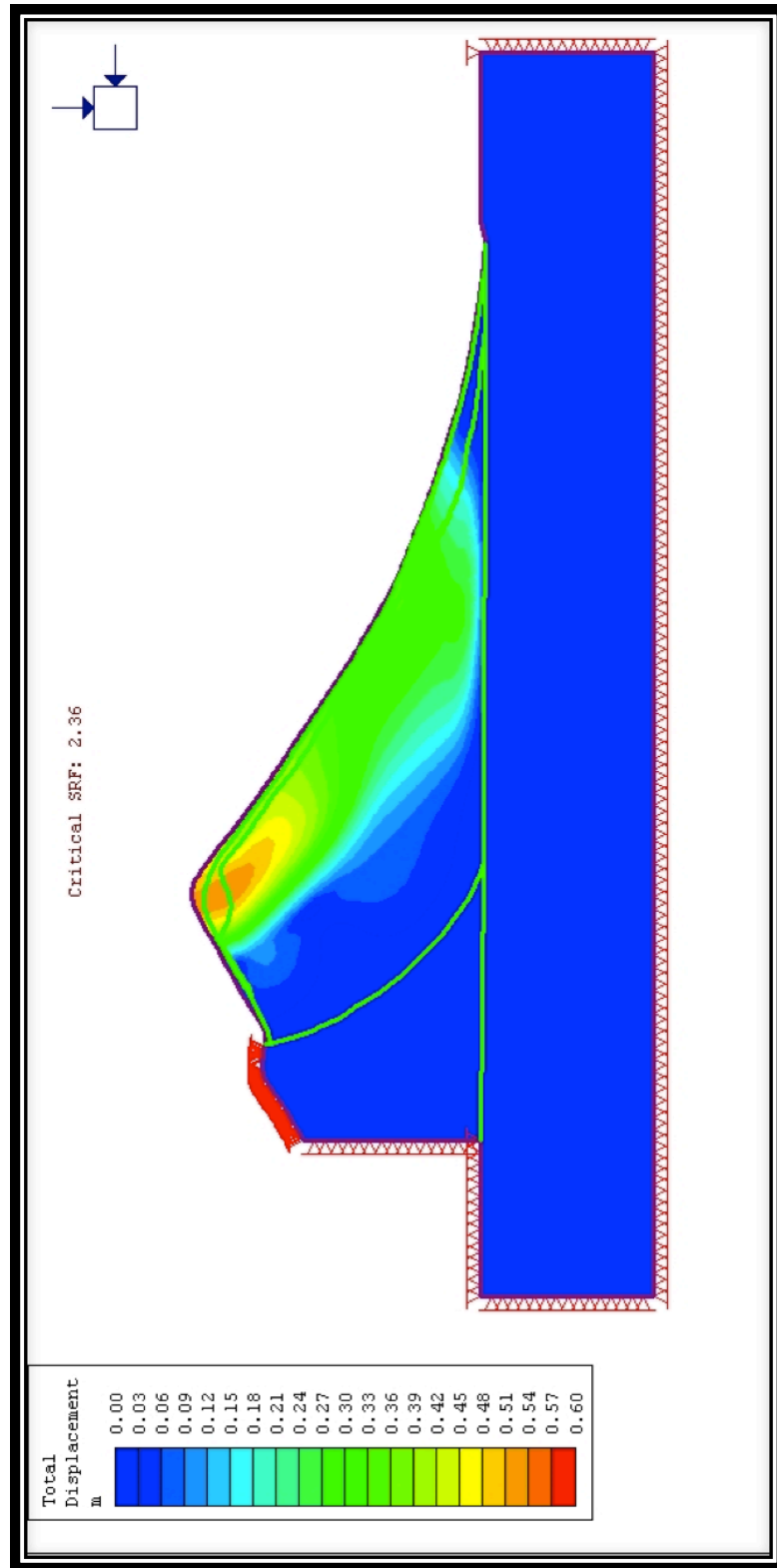


Figure 6.26: Total displacement at the critical stage. Fourth model section AA'

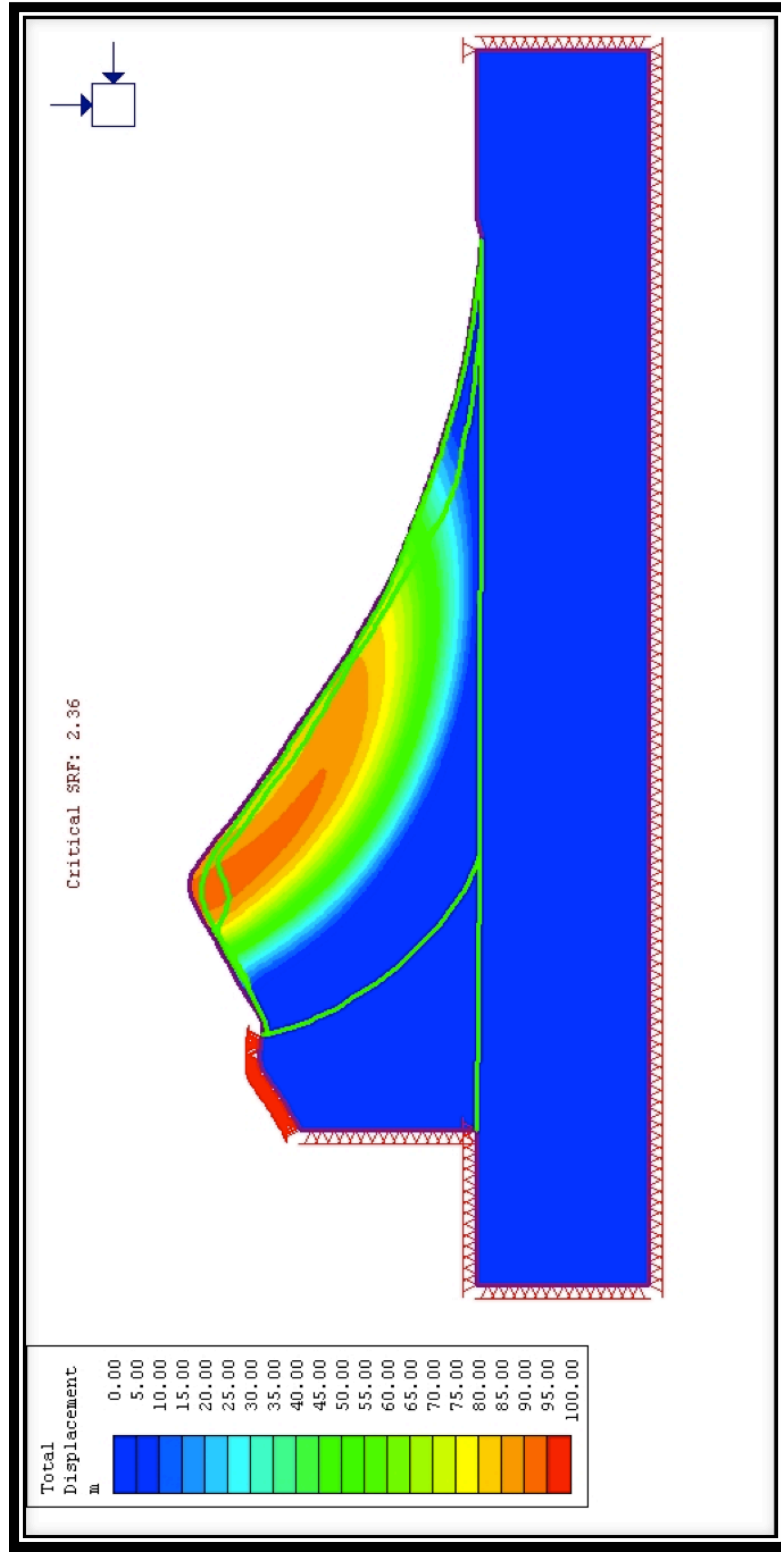


Figure 6.27: Total displacement at the final stage. Fourth model section AA'

6.4.3 FEM RESULTS

The critical stage properties represent parameters before the model becomes unstable. The progressive reduction in material parameters involved in this analysis satisfy the uncertainty in material properties that occurs in volcanic environments due to alterations. An assortment of volcano deformations (e.g. 1°, 3°, 4° models) is presented (Fig. 6.18-6.19-6.22) as response to a wide range of properties examined. The FEM results compare well with limit equilibrium method (Table 6.2). Factor of safety values obtained from both method employed are very similar, except for the magma scenario in which different features were used to model magma pressure (see Section 6.2.4). SSR “polygonal search area” allowed to focus the SSR analysis on any particular region and assesses more important global failure potential. Seismic and magma pressure affect the whole slope stability in terms of a destabilizing factor, as the SRF (“critical stage”) is decreased approximately to 1.00 under magma pressure and seismic load applied. The same behavior is expected in the “final stage”, in which SRF is decreased of 1.00 as well. In effect the material properties, in the “critical and final stage”, are higher than the correspondent “critical and final stage” where gravity alone is investigated (Tab.6.3-6.4). So the slip surfaces (maximum shear strain) begin to fail as a response to the extra load applied. Scenario seismic + magma affects the slope stability and the SRF is reduced to values close to 1. Additionally, considering the fourth model the slope is found unstable, SF=0.8 is obtained. Comparing both, LEM and FEM, results on figures 6.14 and 6.18 (e.g. fourth model) it is evident that the distribution of safety factor (color distribution) underline the same slip surface highlighted by strain contours in the numerical modeling analysis. Finite elements method models deformation in the entire slope. It is able to explain, especially looking at third model, (critical and final shear strength reduction stage, fig.6.21 and 6.22) the importance of layers with poor properties in the volcano internal structure. Deformation, in the third model, is deepening to reach poor layer of breccia-lava unit. Accordingly, here it is revealed how important it is to deal with diverse internal structure in modeling slope stability analysis. Future investigation, using seismic survey, might be useful to constrain poor layers in different level of volcano interior. Furthermore, the main utility of SSR method is to analyze the significance of reduction in input strength parameters potentially hydrothermally weathered specially in environment as volcanoes. Further study focused on rocks mass alteration may implement this investigation.

Table 6.2: Results of Numerical Modeling Analysis. Strength Reduction Factor (SRF) correspond to Safety Factor (SF)

Models	Critical Strength Reduction Factor (SRF) or Safety Factor (SF)							
	Gravity		Seismic		Magma Pressure		Magma Pressure + Seismic	
	section AA'	Section BB'	Section AA'	Section BB'	Section AA'	Section BB'	Section AA'	Section BB'
1	2.97	2.62	1.86	1.69	1.58	1.79	1.06	1.18
2	2.82	2.52	1.84	1.59	1.86	1.84	1.27	1.24
3	2.82	2.5	1.84	1.58	1.63	1.78	1.15	1.17
4	2.36	2.1	1.48	1.35	1.17	1.35	0.8	0.91
Shear Strength Reduction (SSR) method for all output values; Horizontal Seismic Load Coefficient (0.26); Triangular Load (0-21783 KN/m2 sec AA') (0-16686KN/m2 sec.BB')								

Table 6.3: Shear Strength Reduction Method. Gravity and Magma Pressure scenario analyzed. Result of Finite Element Method

SECTION AA'		Shear Strength Reduction (SSR)							
		Gravity			Magma Pressure				
		Friction angle (degree)	Cohesion (Mpa)	Friction angle (degree)	Cohesion (Mpa)	Friction angle (degree)	Cohesion (Mpa)		
Models	Lithotechnical units	Critical SRF or SF=2.97	Final Stage SRF (3.5)	Critical SRF or SF=1.58	Final Stage SRF (1.9)				
1	lava-breccia	14.4	1.08	12.29	0.92	25.77	2.04	21.87	1.69
Models	Lithotechnical units	Critical SRF or SF=2.82	Final Stage SRF (3.25)	Critical SRF or SF=1.86	Final Stage SRF (2.25)				
2	lava	18.25	1.78	15.97	1.54	26.56	2.7	22.45	2.23
	lava-breccia	15.13	1.14	13.21	0.99	22.29	1.73	18.72	1.43
	breccia-lava	12.98	0.77	11.31	0.66	19.26	1.16	16.11	0.96
Models	Lithotechnical units	Critical SRF or SF=2.82	Final Stage SRF (3.25)	Critical SRF or SF=1.63	Final Stage SRF (2)				
3	lava	18.25	1.78	15.97	1.54	29.70	3.08	24.94	2.51
	lava-breccia	15.13	1.14	13.21	0.99	25.07	1.98	20.87	1.61
	breccia-lava	12.98	0.77	11.31	0.66	21.74	1.33	18.00	1.08
Models	Lithotechnical units	Critical SRF or SF=2.36	Final Stage SRF (3)	Critical SRF or SF=1.17	Final Stage SRF (1.5)				
4	lava								
	lava-breccia breccia-lava	15.4	0.92	12.22	0.72	29.05	1.85	23.43	1.44
Magma Pressure Triangular Load (0-21783 KN/m²); SRF= Strenght Reduction Factor (SF in critical stage);									

Table 6.4: Shear Strength Reduction Method. Seismic and Magma + Seismic scenario analyzed. Result of Finite Element Method

SECTION AA'		Shear Strength Reduction (SSR)					
		Seismic Load			Seismic + Magma		
Models	Lithotechnical units	Friction angle (degree)	Cohesion (Mpa)	Friction angle (degree)	Cohesion (Mpa)	Friction angle (degree)	Cohesion (Mpa)
		Critical SRF or SF=1.86		Final Stage SRF (2.15)		Critical SRF or SF=1.06	Final Stage SRF (1.4)
1	lava-breccia	22.29	1.73	19.53	1.50	35.73	3.04
						28.58	2.30
Models	Lithotechnical units	Critical SRF or SF=1.84		Final Stage SRF (2.25)		Critical SRF or SF=1.27	Final Stage SRF (1.7)
2	lava	26.81	2.73	22.45	2.23	36.21	3.95
	lava-breccia	22.51	1.75	18.72	1.43	30.98	2.54
	breccia-lava	19.45	1.17	16.11	0.96	27.10	1.70
Models	Lithotechnical units	Critical SRF or SF=1.84		Final Stage SRF (2.29)		Critical SRF or SF=1.15	Final Stage SRF (1.4)
3	lava	26.81	2.73	22.10	2.19	38.96	4.37
	lava-breccia	22.51	1.75	18.42	1.41	33.55	2.80
	breccia-lava	19.45	1.17	15.84	0.94	29.47	1.88
Models	Lithotechnical units	Critical SRF or SF=1.48		Final Stage SRF (1.75)		Critical SRF or S=0.8	Final Stage SRF
4	lava						
	lava-breccia						
	breccia-lava	23.71	1.46	20.37	1.23	not converge	not converge
Magma Pressure Triangular Load (0-21783 KN/m ²), SRF= Strength Reduction Factor (SF in critical stage);							

6.5 SCENARIO FOCUSED (MAGMA OVERPRESSURE)

Magmatic system, better known as volcanic plumbing system, is one of the most critical feature required to understand the volcanic behavior. It controls the eruption intervals due to replenishment of magma from deeper source or crystallization (Tait et al. 1989). Moreover, the volume of the magmatic chamber affects the volume and eruption frequency. Further the depth and size of magma reservoir are significant factors for volatile exsolution and magma differentiation, and the stress field caused by the magmatic overpressure (Pinel V. and C. Jaupart 2003). Stress field produced by growing of larger volcano at the surface may affect the upper crust of the volcano causing magma overpressure in a shallow reservoir. Another cause for magma overpressure could be the sealing of the conduit. The height of a strato-volcano often exceeds 2 km, and that amount to a load on the surface of approximately 50 MPa. And these surface loads are causing the stress changes to happen in the upper crust that are of similar magnitude or greater to tectonic stresses (Van Wyk de Vries and Matela 1998). The overpressure caused at the beginning of the eruption depends strongly on the edifice dimension as explained in V. Pinel et al. (2003). It should be noted that the overpressure would be greater than the strength of the enclosing rock to produce the deformation on the edifice and to trigger the failure. Pacaya is a stratovolcano, that which experienced small repetitive collapse in the last years. A possible mechanism responsible for these collapses would be the magma overpressure generated by the edifice load over the year. Here we want to analyze the influence of this factor on the instability of volcano applying a constant force along the conduit that feeds the summit of volcano vent (Fig. 6.28). Magma overpressure feeding dyke is smaller than the overpressure that exist in a reservoir (Iverson 1995). Iverson assumed range of overpressure feeding conduit of 0-10 MPa. Overpressure computed along Swarthuggens dikes intruded in to the enclosing rocks, and suggest a range of 4-40 MPa (Daniel et al. 2012). In this research a 2 and 2.5 MPa of overpressure was applied at Pacaya volcano. The overpressure may correspond to different conditions. Here we want to address the cases of magma venting through surface fissure where the overpressure represent the excess pressure, which causes the flow within the magma conduits. This condition seems to fit the characteristic at Pacaya volcano, which is classified as an “open vent” volcano. To be mentioned is the case where the overpressure represents the increasing pressure due to conduit obstructed or intrusion of dykes in enclosing rocks. This last case was examined using greater values of overpressure as 10-20-30-40 MPa, following Daniel et al. (2012).

6.5.1 CASES ANALYZED AND RESULTS

Here, we present the magma overpressure scenario particularly for the fourth model. In this scenario, the magmastatic pressure discussed in the previous section was implemented with an additional pressure, which correspond to magma overpressure of 2 Mpa (Fig.6.28).

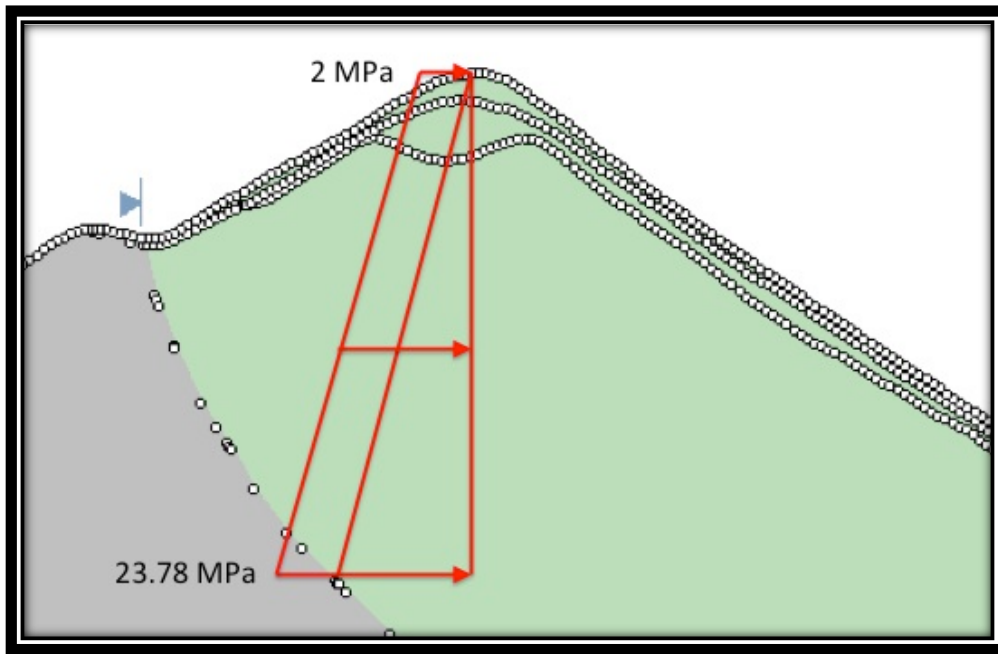


Figure 6.28: Magma overpressure component added to magmastatic one. Fourth model section AA'.

The result achieved here, by applying the magma overpressure component, shows that the slope is unstable under this extra load. Overpressure due to magma venting through surface conduit could very well represent the condition at Pacaya volcano. This extra load could be responsible for the recent collapse that occurred in 2010. The value of the factor of safety that triggered failure of the slope correspond to $SF=0.95$. Furthermore, specific attention was addressed to analyze shallow zone of volcano, which is the most predisposed area to be affected by magmatic overpressure. A unique joint, with constant pressure of 2.5 MPa, represents the magmatic or dike conduit. The dyke conduit was modeled as a discontinuity in the rock mass. Different joint setting was implemented here, using Mohr-Coulomb slip criterion and assuming “normal and shear stiffness” different from zero. An elasto-plastic behavior is expected by joint interface subjected to a magma overpressure. This particular setting permit to observe shear strain at the magma conduit that would generate a new shallow slip surface. To account for the uncertainties in the strength properties of magma conduit two values of normal and shear stiffness

were performed. In the following figures 6.29 and 6.30, shear strain and deformational vector are indicated. Range of normal and shear stiffness from 10-100 MPa for discontinuity, that would represent the magmatic conduit was considered (D.R Wines et al. 2003). Further, in Apuani et al. 2008 the magmatic conduit interface present normal stiffness and shear stiffness of 45 and 18 MPa respectively.

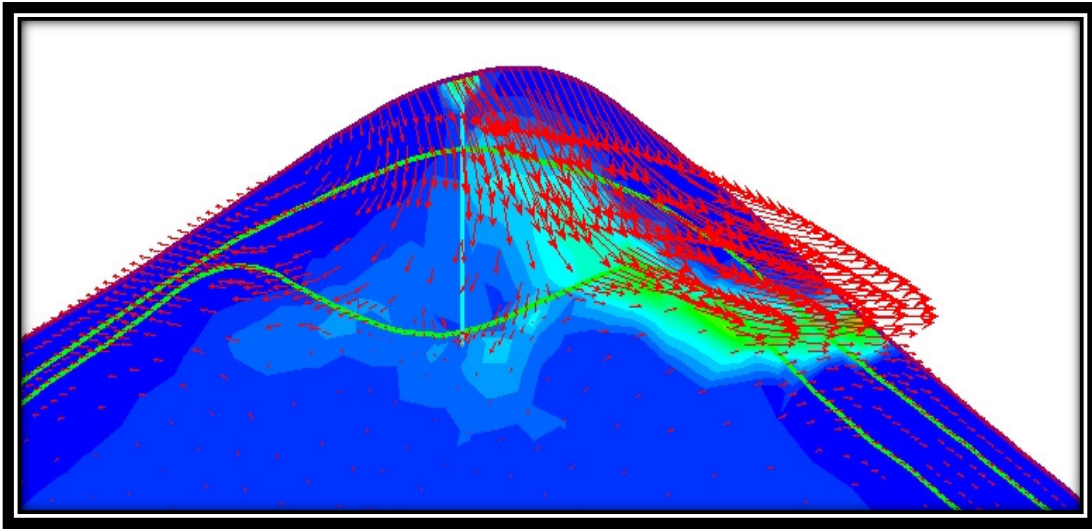


Figure 6.29: Magma overpressure of 2.5 MPa. Joint Normal and shear stiffness equal to 10 MPa

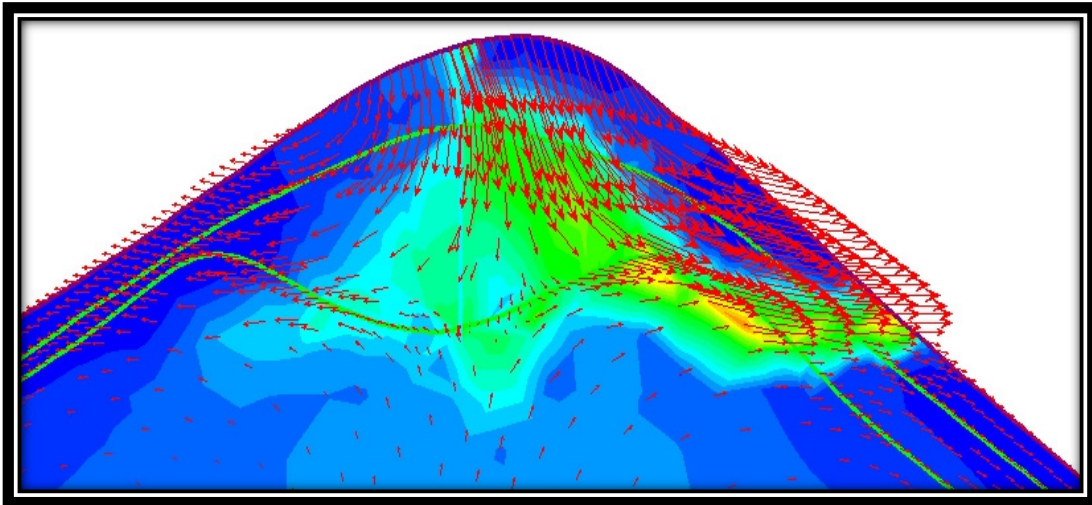


Figure 6.30: Magma overpressure of 2.5 MPa. Joint Normal stiffness equal to 45 MPa and shear stiffness equal to 18 MPa.

The deformational vectors indicate the displacement produced in the shallow zone during magma venting through surface fissure where the overpressure represents the excess pressure that causes the flow in the magma conduits. This scenario may explain repetitive small collapse that Pacaya has suffered. The excessive magma pressure component acting at the superficial zone of volcano would be the force that causes the magma wall paths to be enlarged producing deformation on the volcano edifice. The results addressed in this section demonstrate the critical role of magma overpressure as destabilizing factor, which contribute during eruption or after and deforming the volcano edifice triggering collapse

CHAPTER 7: CONCLUSION

The results from limit equilibrium and finite element methods are concordant and both propose that the least stable sector is on the south-western flank of the volcano. The lowest safety factor value suggests that the edifice is stable under gravitational loading alone and the estimated magma pressure in the dykes doesn't destabilize the Pacaya volcano slope. Furthermore, the estimated seismic load doesn't destabilize the slope as well. Although seismic and magma pressure significantly reduced the stability of Pacaya volcano. The magma and seismic loads combined together representing earthquakes that trigger volcanic eruption indicate to be one possible destabilizing factor, especially looking at fourth model, which is unstable. In this study the influence of magma overpressure is also analyzed and indicates to be a destabilizing factor and likely responsible of small collapses that happened in the last years. Moreover, the FEM analysis presents progressive evolution of failure surface and demonstrates the significance in the reduction of strength parameters leading to the deeper propagation of collapse. The FEM strength reduction method presents an opportunity to analyze the significance of the reduction in the input properties potentially due to hydrothermal alteration (especially in friction angle). Phase 2 models the evolution of the system along time, and allows a step by step monitoring of progressive failure and deformation. The approach helps in determining the future scenario of progressive deformation that leads to the trigger of a collapse.

REFERENCE

- Apuani T, Corazzato C, Cancelli A, Tibaldi A. 2005. Stability of a collapsing volcano (Stromboli, Italy): Limit Equilibrium analysis and numerical modeling. *Journal of Volcanology and Geothermal Research* 144:191-210.
- GNGTS-Trieste [internet]. 1999. Pisa (IT): Dipartimento di Science della terra, Universita di Pisa. The petrophysic applied to the definition of geologic nature of crustal structures. Available from:
<http://www2.ogs.trieste.it/gngts/gngts/convegniprecedenti/1999/>
- Bieniawski, Bieniawski ZT. 1989. Engineering rock mass classification. John Wiley and Sons. New York (1989), p.251.
- Borgia A et al. 2002. The volcano-tectonic evolution of Concepci_n, Nicaragua. *Bulletin of Volcanology* 65: 248–266.
- Burkart B, Self S. 1985. Extension and rotation of crustal blocks in northern Central America and effect on the volcanic arc. *Geology* 13: 22–26.
- Carr M, 1976. Underthrusting and Quaternary faulting in northern Central America. *Geological Society of America Bulletin* 87: 825–829.
- Conway M. 1995. Construction patterns and timing of volcanism at the Cerro Quemado, Santa María, and Pacaya volcanoes, Guatemala. Ph. D. Dissertation. Michigan Technological University, Houghton, Michigan. 152 pp.
- Day SJ. 1996. Hydrothermal pore fluid pressure and the stability of porous, permeable volcanoes. In: McGuire WJ, Jones AP, Neuberg J eds. *Volcano instability on the Earth and other planets*. Geological Society of London,

Special Publication 110.

- Dincer I et al. 2004. Correlation between Schmidt hardness, uniaxial compressive strength and Young's modulus for andesites, basalts and tuffs. *Bulletin of Engineering Geology and the Environment* 63: 141-148.
- Duncan JM. 2000. Factor of Safety and Reliability in Geotechnical Engineering. *Journal of Geotechnical and Geoenvironment Engineering* 307-316.
- Eggers AA. 1971. The geology and petrology of the Amatitlán quadrangle, Guatemala. Ph. D. Dissertation. Dartmouth College, Hanover, New Hampshire. 221p.
- Eggers AA. 1975. Mapa Geologica de Amatitlán, Guatemala. Hoja 2059116. Instituto Geográfico Nacional de Guatemala.
- Elsworth D and Voight B. 1995. Dyke intrusion as a trigger for large earthquakes and failure of volcano flanks. *Journal of Geophysical Research* 100: 6005–6024.
- Ergü'n Tuncay and Nilsun Hasancebi. 2009. The effect of length to diameter ratio of test specimens on the uniaxial compressive strength of rock. *Bulletin of Engineering Geological Environment* 68: 491–497.
- Francis PW and Wells GL. 1988. Landsat Thematic Mapper observations of debris avalanche deposits in the Central Andes. *Bulletin of Volcanology* 50: 258–278.
- Franklin JA. 1985. Suggested method for determining point load strength. *International Journal of Rock Mechanics & Mining Sciences* 22(2): 53–60.
- Griffiths DV and Lane PA. 1999. Slope stability analysis by finite elements. *Géotechnique* 49: 387-403.

- Gomez et al. 2010. Volcanological map of the 1961–2009 eruption of Volcan de Pacaya, Guatemala. MS. Thesis. Michigan Technological University, Houghton, Michigan. 57 pp.
- Goudie AS. 2006. The Schmidt hammer in geomorphology research. *Progress in Physical Geography* 30: 703-718.
- Hoek E and Brown ET. 1980. Empirical strength criterion for rock masses. *Journal Geotechnical and Engineering Div., ASCE* 106: 1013-1035.
- Hoek E and Brown ET. 1980. *Underground Excavations in Rock*, London, Instn Min. Metall.
- Hoek E and Brown ET. 2002. Hoek-Brown failure criterium – 2002 edition. Rocscience Library.
- Hoek E and Marinos P. 2000. Predicting Tunnel Squeezing. *Tunnels and Tunnelling International*. Part 1 – November 2000, Part 2 – December, 2000.
- Hoek E, Carranza-Torres C, Corkum B. 2002. Hoek-Brown criterion – 2002 edition. *Proc. NARMS-TAC Conference*, Toronto, 2002, 1:267-273.
- Hürlimann M, Ledesma A, Martí J. 1999. Conditions favouring catastrophic landslides on Tenerife (Canary Islands). *Terra Nova* 11: 106–111.
- International Society for Rock Mechanics (1981) *Rock Characterization, Testing and Monitoring-ISRM Suggested Methods*. Pergamon, London.
- Iverson R M. 1995. Can magma injection and groundwater forces cause massive landslides on Hawaiian hotspot? *Journal of Volcanology and Geothermal Research* 66: 295-308.
- IGN / Eggers A. 1969-1972. Mapa Geologico de Guatemala Escala 1:50,000. Hoja 2059 II G, “Amatitlan”. First edition (map). Guatemala.

- IGN / Bonis S. 1993. Mapa Geologico de Guatemala Escala 1:250,000. Hoja ND 15 – 8 – G, “Guatemala”. First edition (map). Guatemala.
- Kuno H. 1960. High Alumina Basalt. *Journal of Petrology* 1: 121-145.
- López DL, Williams SN. 1993. Catastrophic volcanic collapse: relation to hydrothermal processes. *Science* 260: 1794–1796.
- Marinos P and Hoek E. 2001. Estimating the geotechnical properties of heterogeneous rock masses such as flysch. *Bulletin of Engineering Geology and the Environment* 60: 85-92.
- Matsui T and San K C. 1992. Finite Element slope stability analysis by shear strength reduction technique. *Soils Found* 32: 59-70.
- Matthews JA and Shakesby RA. 2008. The status of the “Little Ice Age” in southern Norway: relative-age dating of Neoglacial moraines with Schmidt hammer and lichenometry. *Boreas* 13: 333-346.
- McGuire WJ. 1996. Volcano instability: a review of contemporary themes. Geological Society, London, Special Publications 110:1-23.
- Palmstrom A. 1982. The volumetric joint count- a useful and simple measure of the degree of rock mass jointing. *Proc. 4th Cong. Int. Assoc. Eng. Geol.*, New Delhi 2:221–228.
- Pinel V and Jaupart C. 2003. Magma chamber behavior beneath a volcano edifice. *Journal of Geophysical research* 108: 2072- 2089.
- Potro R and Hurlimann M. 2008. Geotechnical classification and characterization of material for stability analyses of large volcanic slopes. *Engineering Geology* 98:1-17.
- RocScience [internet]. Products and support, Slide and Phase. Available from <http://www.roscience.com>.

- Rose WJ. 1967. Notes on fumaroles and recent activity of Volcán de Pacaya: Geological Bulletin no. 4. Instituto Geográfico Nacional de Guatemala, 31-33.
- Siebert L. 1984. Large volcanic debris avalanches: characteristics of source areas, deposits, and associated eruptions. *Journal of Volcanology and Geothermal Research* 22: 163 – 197.
- Siebert L. 1996. Hazards of large volcanic debris avalanches and associated eruptive phenomena. In: R S, Tilling R eds. *Monitoring and Mitigation of Volcano Hazards*. New York, Springer.
- Siebert L. 2002. Landslides resulting from structural failure of volcanoes. In: Evans SG, DeGraff JV eds. *Catastrophic landslides: Effects, occurrence, and mechanisms* Geological Society of America.
- Siebert L, Glicken H, Ui T. 1987. Volcanic hazards from Bezymianny- and Bandai-type eruptions. *Bulletin of Volcanology* 49: 435 – 459.
- Swanson RH, Bernier PY, Woodard PD eds. 1987. *Forest hydrology and watershed management*. Oxfordshire, United Kingdom, International Association of Hydrological Sciences.
- Tait S et al. 1989. Pressure, gas content and eruption periodicity of a shallow, crystallising magma chamber. *Earth and Planetary Science letters* 92: 107-123.
- Tibaldi A. 2001. Multiple sector collapses at Stromboli volcano, Italy: how they work. *Bull. Volcanology* 63:112-125.
- Vallance J, Siebert L, Rose WJ, Girón, Banks N. 1995. Edifice collapse and related hazards in Guatemala. *Journal of Volcanology and Geothermal Research* 66:337-355.
- Van Wyk de Vries B, Kerle N, Petley D 2000. A sector-collapse forming at Casita Volcano. *Geology* 28: 167–170.

- Van Wyk de Vries B and Matela R. 1998. Style of volcano-induced deformation: numerical models of substratum flexure, spreading and extrusion. *Journal of Volcanology and Geothermal Research* 81:1-18.
- Venzke E, Wunderman RW, McClelland L, Simkin T, Luhr JF, Siebert L, Mayberry G, Sennert S. 2009. *Global Volcanism, 1968 to the Present*. Smithsonian Institution, Global Volcanism Program Digital Information Series, GVP-4 (<http://www.volcano.si.edu/reports/>).
- Walter TR et al. 2006. Gravitational spreading and formation of new rift zones on overlapping volcanoes. *Terra Nova* 18:26-33.
- Watters RJ, Zimbelman DR, Bowman SD, Crowley JK. 2000. Rock mass strength assessment and significance to edifice stability, Mount Rainier and Mount Hood, Cascade Range volcanoes. *Pure and Applied Geophysics* 157: 957–976.
- White R and Harlow D. 1993. Destructive upper-crustal earthquakes of Central America since 1900. *Bulletin of the Seismological Society of America* 83:1115–1142.
- Williams H. 1960. Volcanic history of the Guatemalan Highlands, Univ. Calif. Berkeley Publ. in Geological Science 38:86.
- Wunderman RL and Rose WI. 1984. Amatitlán, an actively resurging cauldron 10 km of Guatemala City. *Journal of Geophysical Research* 89: 8525–8539.
- Wyllie DC and Mah CW. 2004. *Rock Slope Engineering, civil and mining*, Eds. 4. 218-244. (Lorig, L., Varona, P., “Numerical Analysis,”).

APPENDIX

APPENDIX A: ROSE DIAGRAM (DIP DIRECTION) OF PRINCIPAL DISCONTINUITIES

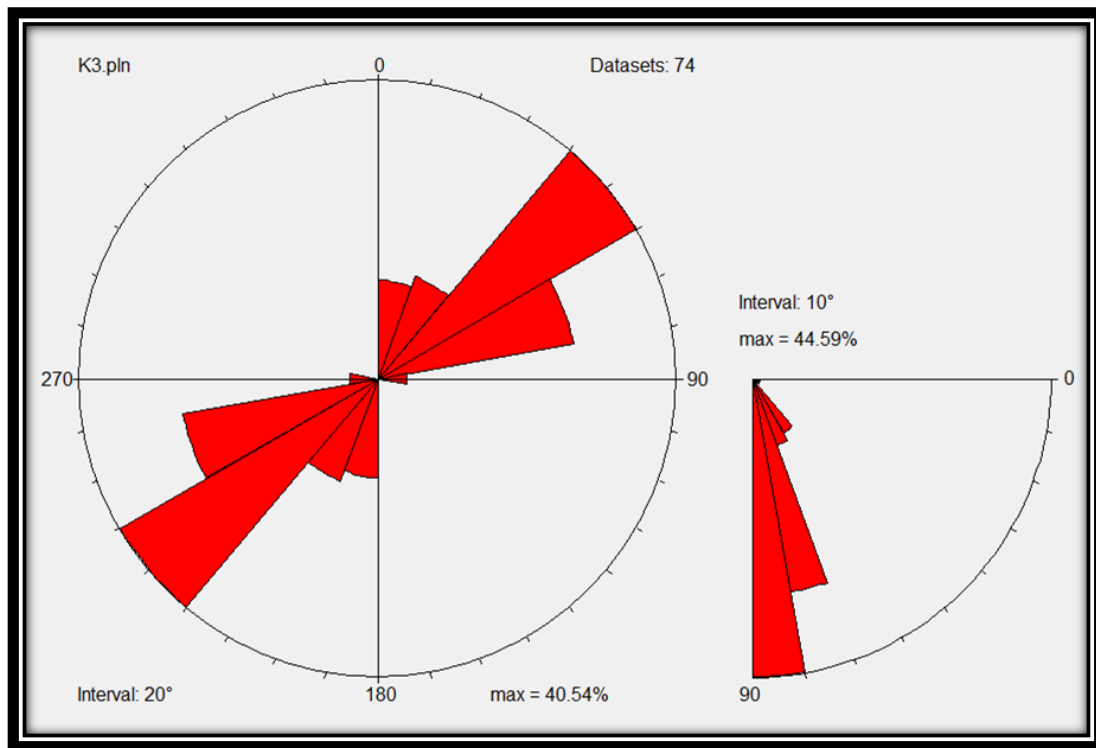


Figure A.1: Dip direction of K3 discontinuity

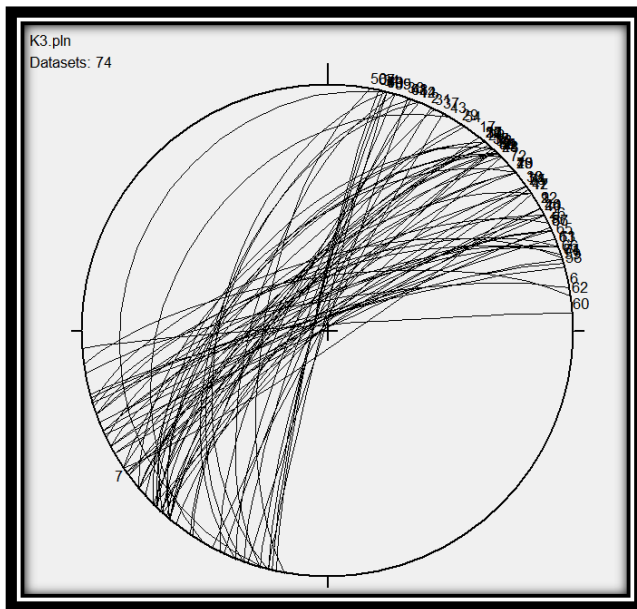


Figure A.2: Projection of all discontinuities measured on the field, representing K3.

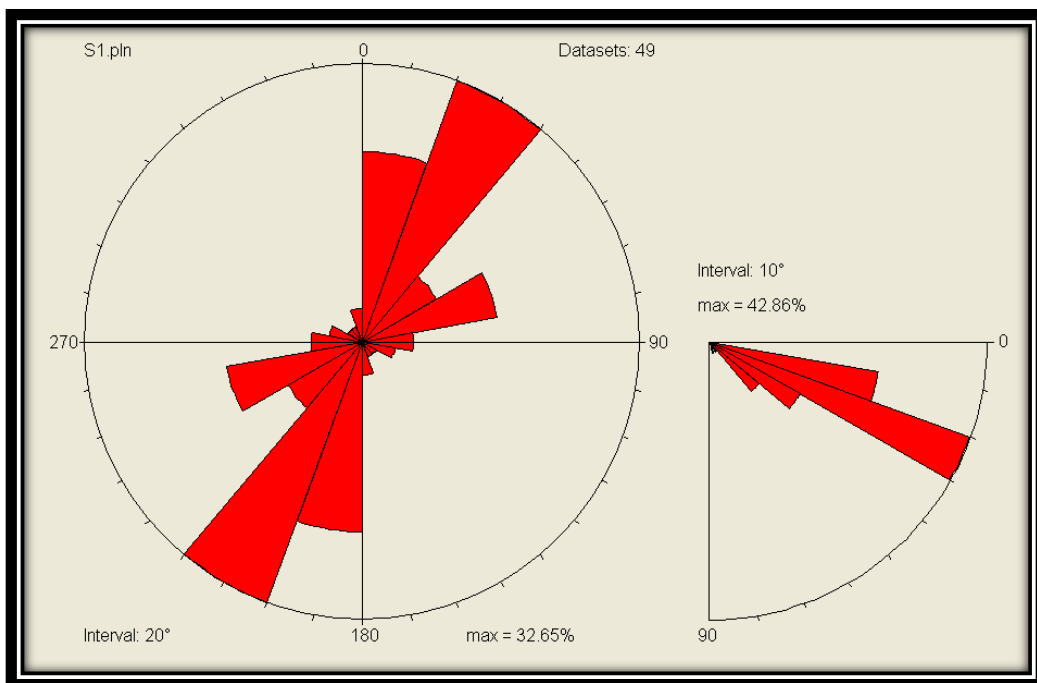


Figure A.3: Dip Direction of S1 stratigraphic discontinuity.

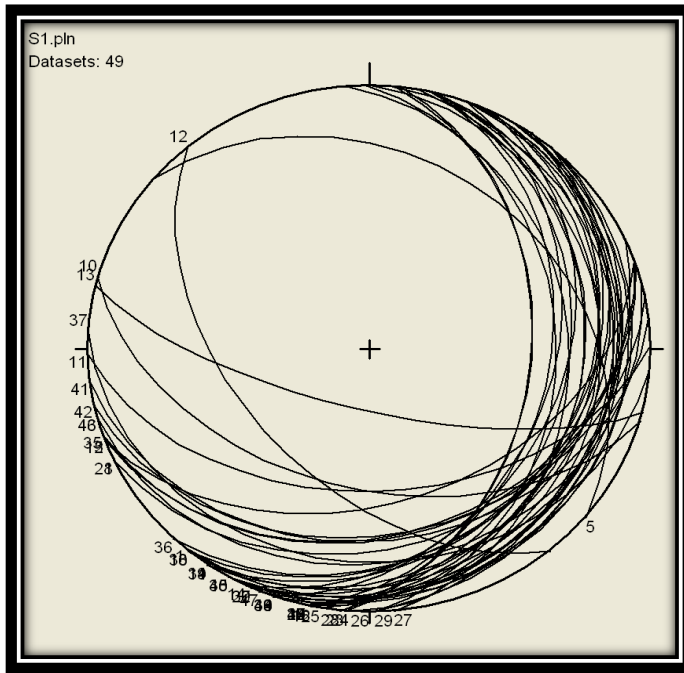


Figure A.4: Projection of all stratigraphic contact between lava and breccia layer measured on the field, representing S1.

APPENDIX B: PROJECTION ON EQUAL SCHMIDT'S STEREOGRAMS OF POLES
TO PLANES OF DISCONTINUITIES

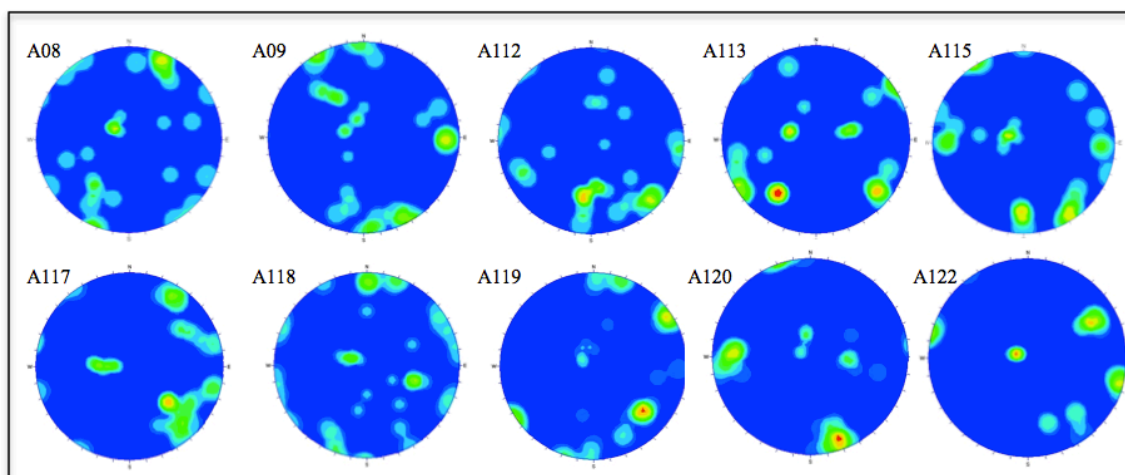


Figure B.1: Projection on equal Schmidt's stereograms of poles to planes of discontinuities for each site investigated

APPENDIX C: GEOTECHNICAL SURVEY ON SITES INVESTIGATED IN THE FIELD

Values presented here are assumed as average from a list of data determined in the field. The impossibility to obtain a representable average value due to extreme variability for some parameters, required sequential values to indicate their range.

Table C.1: A08 site

discontinuity	Dip	Inclination	Spacing (m)	Schmidt Hammer	Type	JRC	Opening (mm)	Filling	Alteration	Filtration	PI	Pa	Directional length (mm)	Directional Immersion (mm)	Termination
K1	218	77	0.9	24.0	joint	18-20	51 - 63	soil	slightly weathered	none	<50%	<25%	267	584-787	Td
K2	44	65	1.6	23.5	joint	14-16	8-76	soil	discolored	none	<50%	<25%	482	660	Td
K3	313	81	1.25	32.2	joint	16-18	13-51	soil	discolored	none	<50%	<25%	304	635	Td
S1	137	24	2	43.8	joint	10 to 12	closed	none	discolored	none	>90%	<25%	2500	762	Tx

Table C.2: A09 site

Discontinuity	Dip	Inclination	Spacing (m)	Schmidt Hammer	Type	JRC	Opening (mm)	Filling	Alteration	Filtration	PI	Pa	Directional length (m)	Directional immersion (m)	Termination
K1	263	78	1.1	43.0	joint	6 to 8	25-50	pletely filled	slightly	none	50-90%	<25%	1.5	1.7	Td
K2	16	71	1	54.3	joint	2 to 4	76	soil	discolored	none	50-90%	<25%	1.7	3.1	Td
K3	299	84	124	37.9	joint	14 to 16	12-25	soil	discolored	none	<25%	<25%	1.8	1.06	Td
K4	162	66	3.5	39.7	joint	12 to 14	25.4	soil	discolored	none	<25%	<25%	1.6	0.6	Td
S0	116	24	1	44.1	joint	21 to 14	12.5	soil	discolored	none	50-90%	<25%	30	0.25	Tx

Table C.3: A112 site

Discontinuity	Dip	Inclination	Spacing (m)	Schmidt Hammer	Type	JRC	Opening (mm)	Filling	Alteration	Filtration	PI	Pa	Directional length (m)	Directional Immersion (m)	Termination
K1	316	63	3.2	45.1	joint	6 to 8	24.5-152	partially filled with soil	discolored	none	50-90	25-80	4	8	Td
K2	136	63	5	36.4	joint	8 to 10	63-76	soil	discolored	none	50-90%	<25%	1.5	9	Td or Tx
K3	299	81	1.5	31.6	joint	14 to 16	24.5	soil	discolored	none	<25%	<25%	1.5	2	Td
K5	68	68			joint due gravity										
S1	200	53	1.166667	32.2	joint	8 to 10	closed	none	discolored	none	50-90%	<25%	3.5-4	1	Td

Table C.4: A113 site

Discontinuity	Dip	Inclination	Spacing (m)	Schmidt Hammer	Type	JRC	Opening (mm)	Filling	Alteration	Filtration	PI	Pa	Directional length (m)	Directional immersion (m)	Termination
K1	249	48	1.7	29.5	joint	10 to 12	24.5-100	soil	discolored	none	>90%	25-80 %	2	1.2	Td
K2	76	69	0.9	37.1	joint	16 to 18	closed	soil	discolored	none	50 to 90%	<25%	1.2	4.5	Td
K3	306	80	0.5	38.5	joint	14 to 16	closed	soil	discolored	none	<50%	<25%	0.5	0.5	Td
K5	59	82	0.32		joint	14 to 16	12 - 24.5	soil	discolored	none	<50 %	<25 %			Td
S1	120	35	0.04	32.3	joint	8 to 10	none	none	slightly weathered	none	50-90%	<25%	3 - 4	1	Td

Table C.5: A115 site

Discontinuity	Dip	Inclination	Spacing (cm)	Schmidt Hammer	Type	JRC	Opening (mm)	Filling	Alteration	Filtration	PI	Pa	Directional length (cm)	Directional immersion (cm)	Termination
K1	262	82	28.7	42.6	joint	8 to 10	24.5	completely filled soil	slightly	none	50-90%	<25%	24.5	17.7	Td
K2	North	77	110	40.0	joint	12 to 14	12.5	soil	slightly weathered	none	50-90%	25-80%	2.45	2.28 - 38.1	Td
K3	323	83	20	35.1	joint	14 to 16	24.5	soil	slightly weathered	none	<50%	<25%	66	43.2	Td
K5	92	63	17.7	39.6	joint	10 to 12	24.5 - 50	soil	slightly weathered	none	<50%	<25%	20	14	Td
S1	126	21	48.2	33.0	joint	12 to 14	0 - 12	soil	slightly weathered	none	>90%	25-80%	700	100	Tr

Table C.6: A118 site

Discontinuity	Dip	Inclination	Spacing (cm)	Schmidt Hammer	Type	JRC	Opening (mm)	Filling	Alteration	Filtration	PI	Pa	Directional length (cm)	Directional immersion (cm)	Termination
K1	247	81	200	45.8	joint	12 to 14	24.5 - 76	partially filled soil	slightly	none	<50%	25-80%	60	90	Tr
K2	17	61	14.6	38.3	joint	12 to 14	12.5	soil	slightly weathered	none	<50%	<25%	7.6 - 12.7	23 - 38 - 60	Td
K3	302	66	5	35.7	joint	8 to 10	12 - 24	soil	slightly weathered	none	>90%	>80%	17.7 - 33 - 56	48 - 61 - 94	Tr
K4	187	81	41	35.0	joint	14 to 16	12 - 25	soil	slightly weathered	none	<50%	25-80%	4.4 - 10 - 40	66 - 79	Td
S1	117	22	150	31.7	joint	12 to 14	none	none	slightly weathered	none	>90%	<25%	900	100	Tx

Table C.7: A119 site

Discontinuity	Dip	Inclination	Spacing (m)	Schmidt Hammer	Type	JRC	Opening (mm)	Filling	Alteration	Filtration	PI	Pa	Directional length (m)	Directional immersion (m)	Termination
K1	241	86	3	44.5	joint	12 to 14	0 - 12	partially filled soil	slightly	none	<50%	25-80%	1	5	Td
K2	North	74	2	45.1	joint	8 to 10	12.5	soil	slightly weathered	none	>90%	25-80%	3.5	5	Td-Tx
K3	313	71	1	49.8	joint	8 to 10	12.5	soil	slightly weathered	none	>90%	25-80%	3.5	5	Tx-Td
K4	193	80	none	35.0	joint	14 to 16	12 - 25	soil	slightly weathered	none	<50%	25-80%	0.13	0.8	Td
S1	142	20	1.5	44.0	joint	12 to 14	5	soil	slightly weathered	none	>90%	<25%	11	0	Tx

Table C.8: A120 site

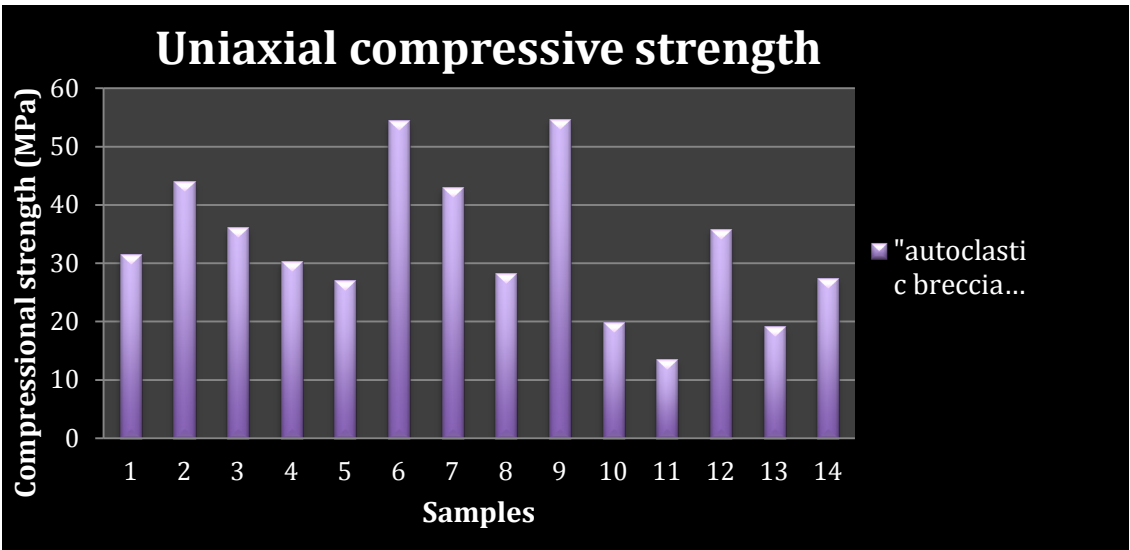
Discontinuity	Dip	Inclination	Spacing (cm)	Schmidt Hammer	Type	JRC	Opening (mm)	Filling	Alteration	Filtration	PI	Pa	Directional length (cm)	Directional immersion (cm)	Termination
K1	272	49	23	32.8	joint	16 to 18	5	partially filled soil	slightly	none	<50%	<25%	56	25.4 - 61	Td
K3	344	81	1.6	30.0	joint	12 to 14	5	soil	slightly weathered	none	50-90%	<25%	50	80	Tx-Td
K5	89	77	35	32.6	joint	12 to 14	12.5	soil	slightly weathered	none	50-90%	25-80%	30 - 114	23 - 76	Td
S1	147	21	30	35.2	joint	8 to 10	5	soil	slightly weathered	none	50-90%	<25%	100 - 200	30	Tx-Td

Table C.9: A122 site

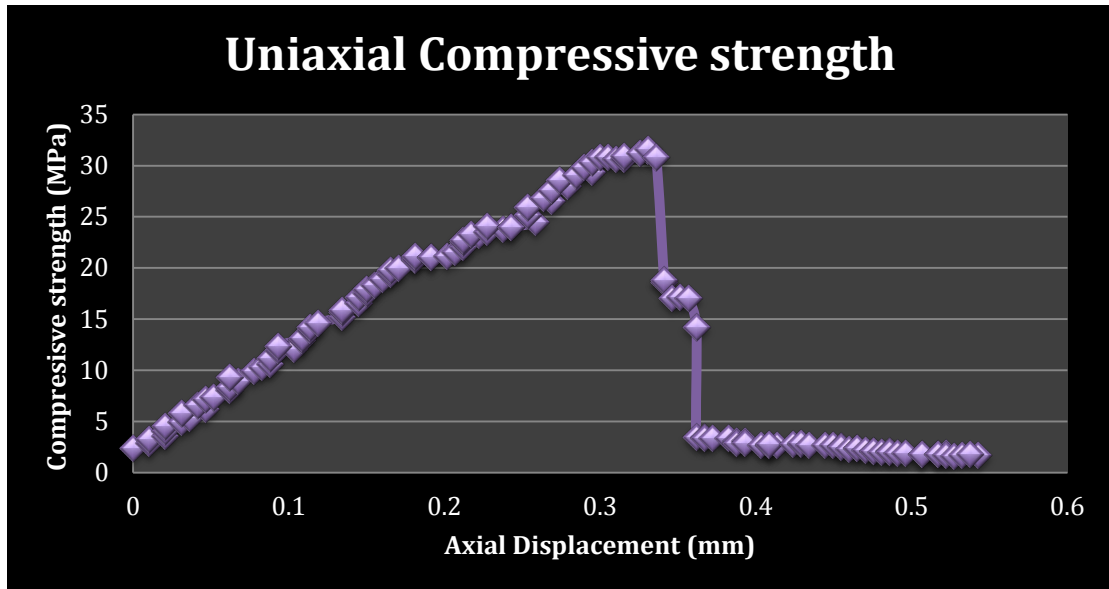
Discontinuity	Dip	Inclination	Spacing (m)	Schmidt Hammer	Type	JRC	Opening (mm)	Filling	Alteration	Filtration	PI	Pa	Directional length (m)	Directional immersion (m)	Termination
K1	240	72	2.5	51.3	joint	4 to 6	25.4 - 76	partially filled soil	slightly	none	>90%	>80%	2	2.5	Td-Tx
K3	310	80	2.1	47.5	joint	8 to 10	37	soil	slightly weathered	none	>90%	>80%	2.6	4	Tx-Td
S1	111	14	0.5	41.3	joint	12 to 14	none	none	slightly weathered	none	50-90%	<25%	10	2.5	Tx

APPENDIX D: LIST OF UNIAXIAL COMPRESSIVE TEST PERFORMED IN THE
LABORATORY

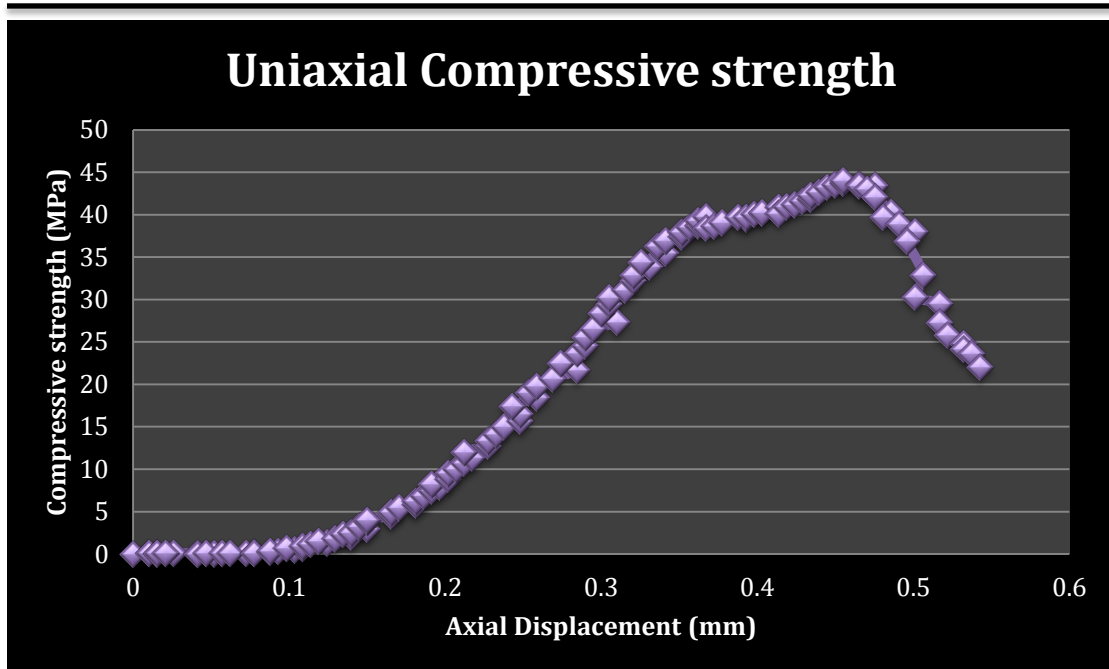
Figure D.1: Autoclastic Breccia cores (1-14)



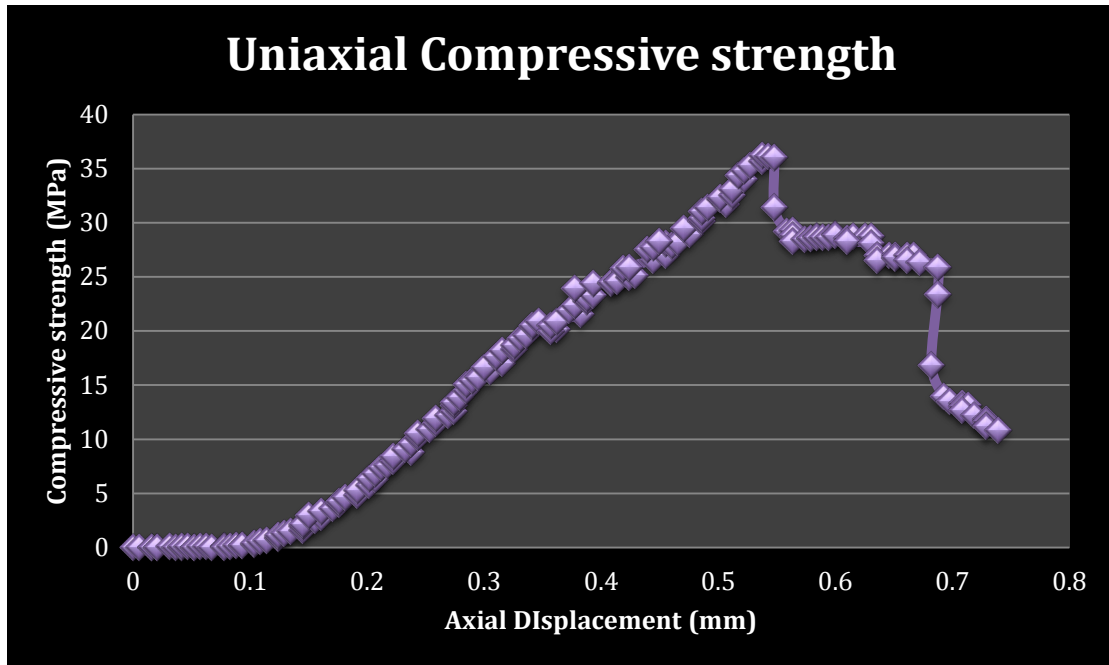
Autoclastic Breccia core Number ° 1



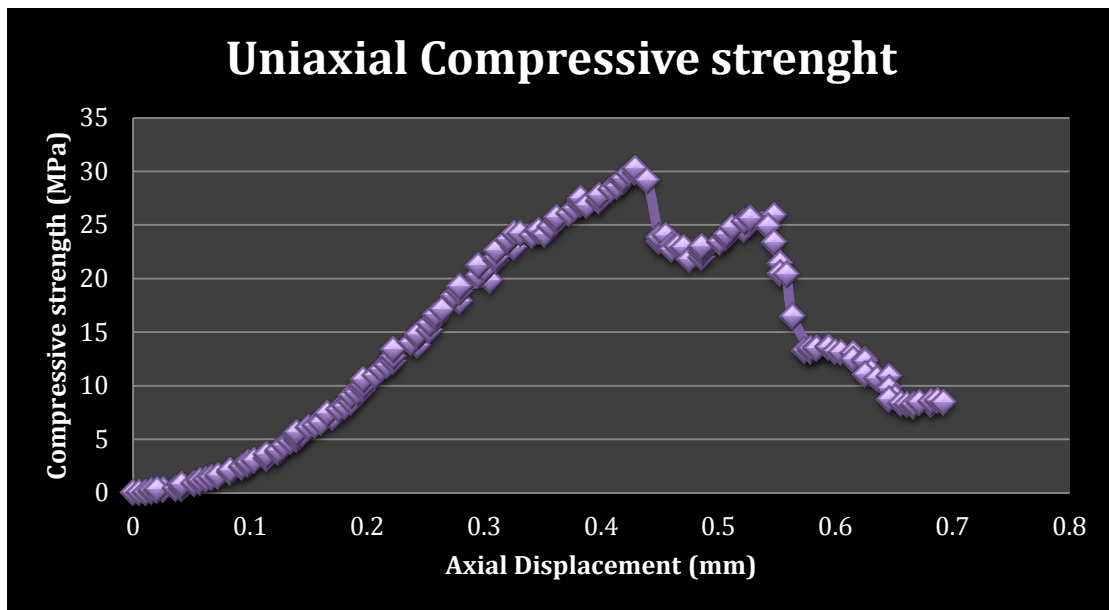
Autoclastic Breccia core Number ° 2



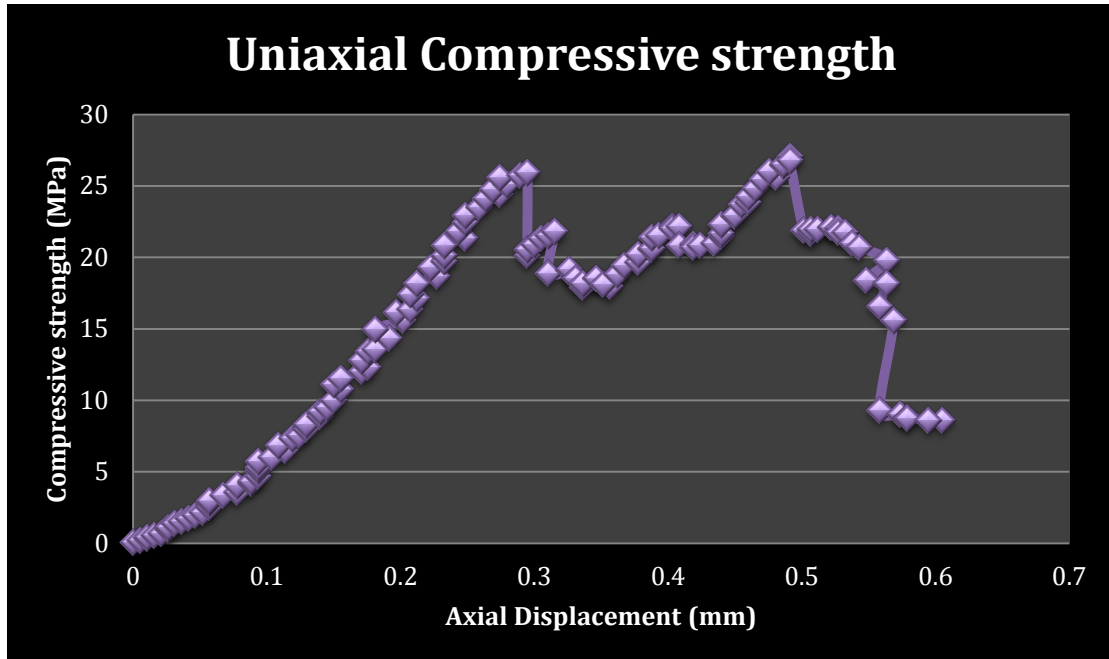
Autoclastic Breccia core Number ° 3



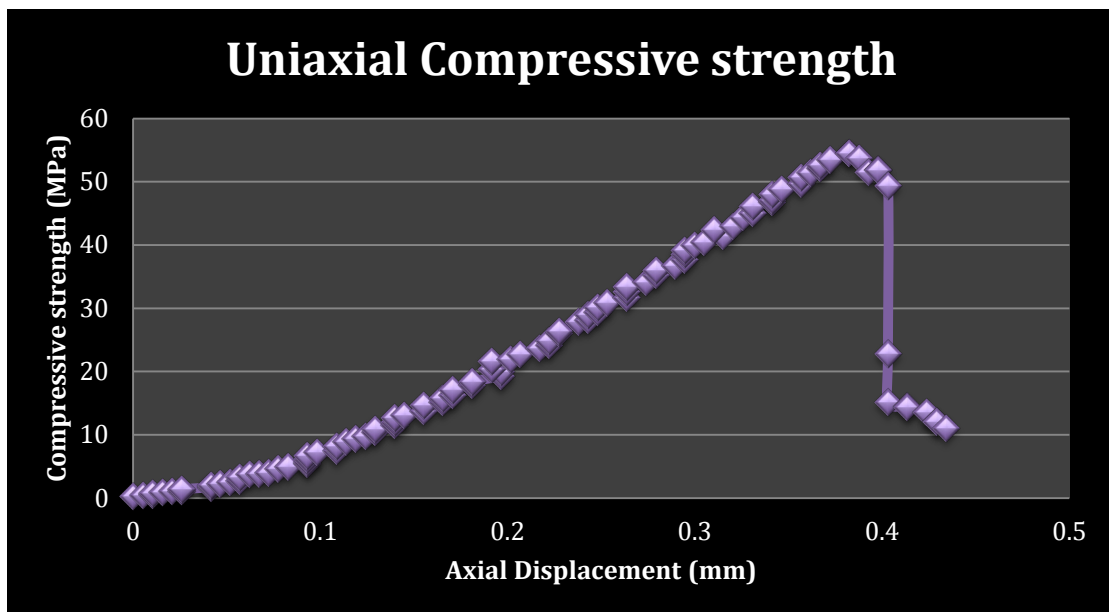
Autoclastic Breccia core Number ° 4



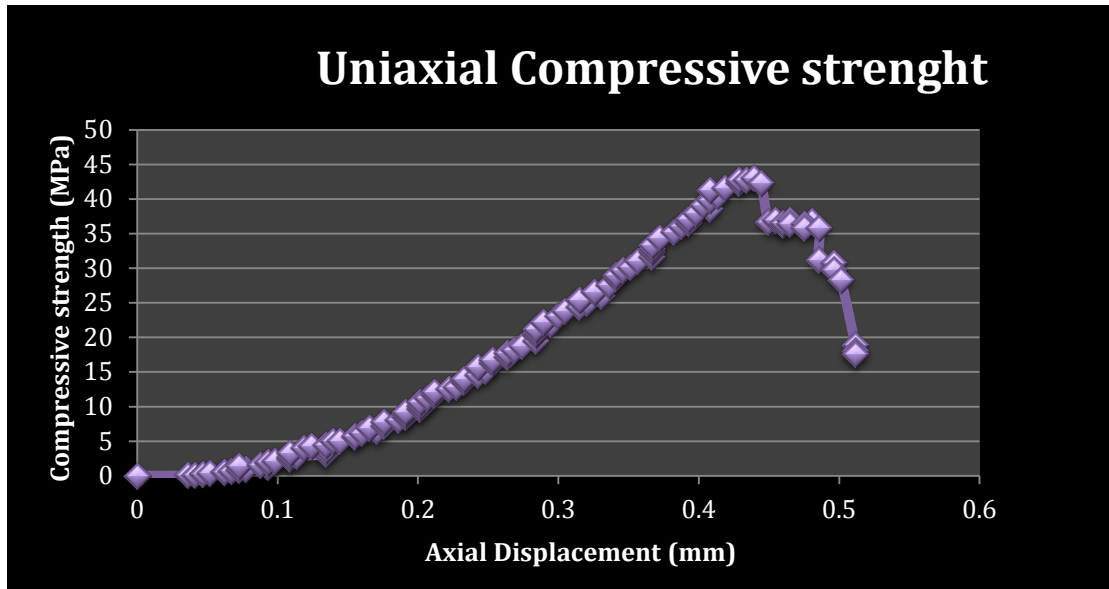
Autoclastic Breccia core Number ° 5



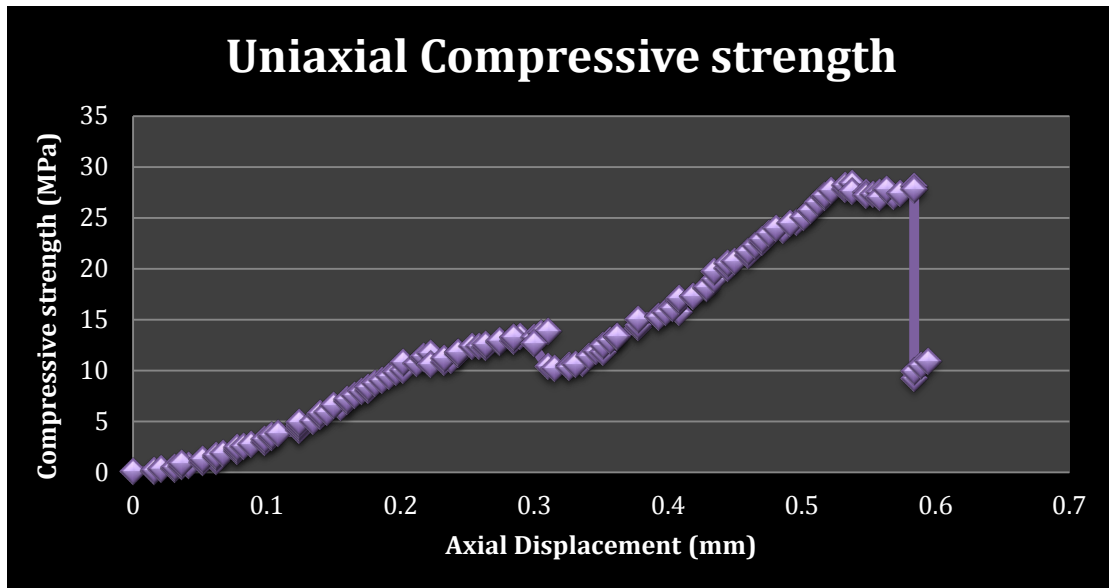
Autoclastic Breccia core Number ° 6



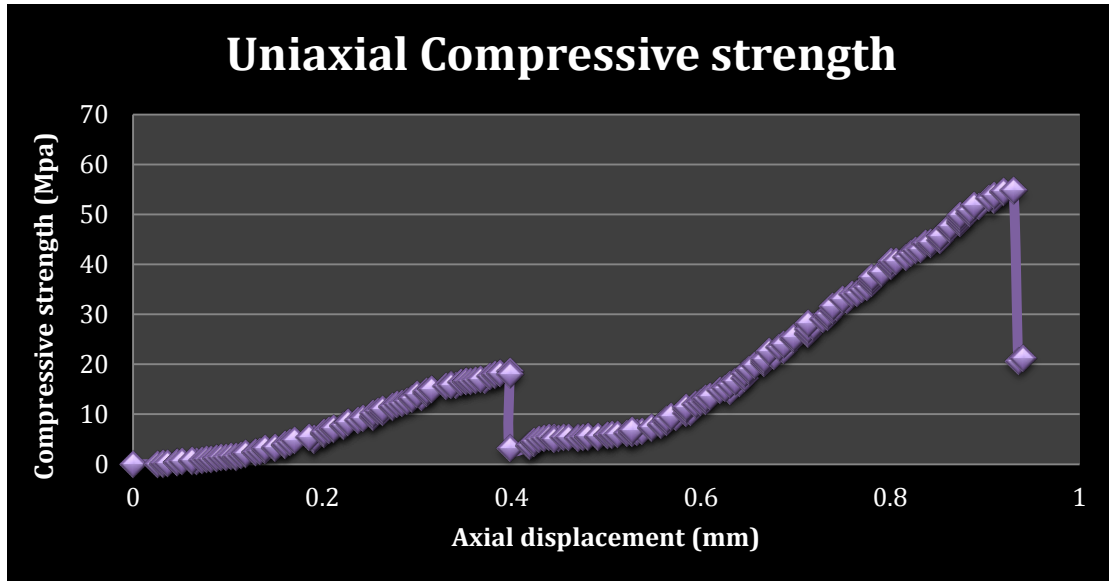
Autoclastic Breccia core Number ° 7



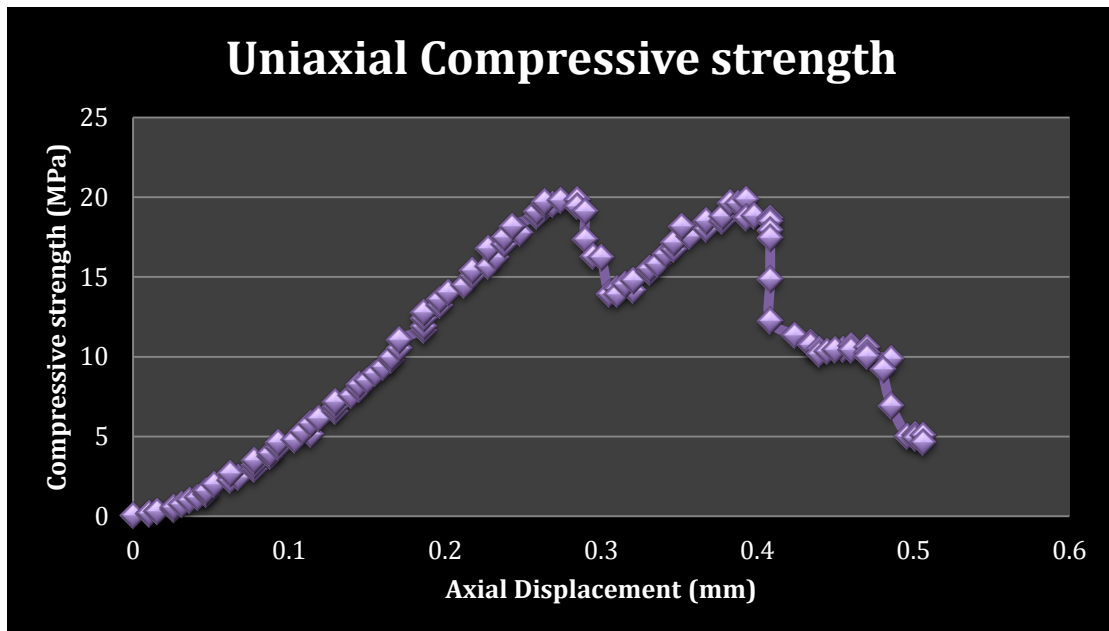
Autoclastic Breccia core Number ° 8



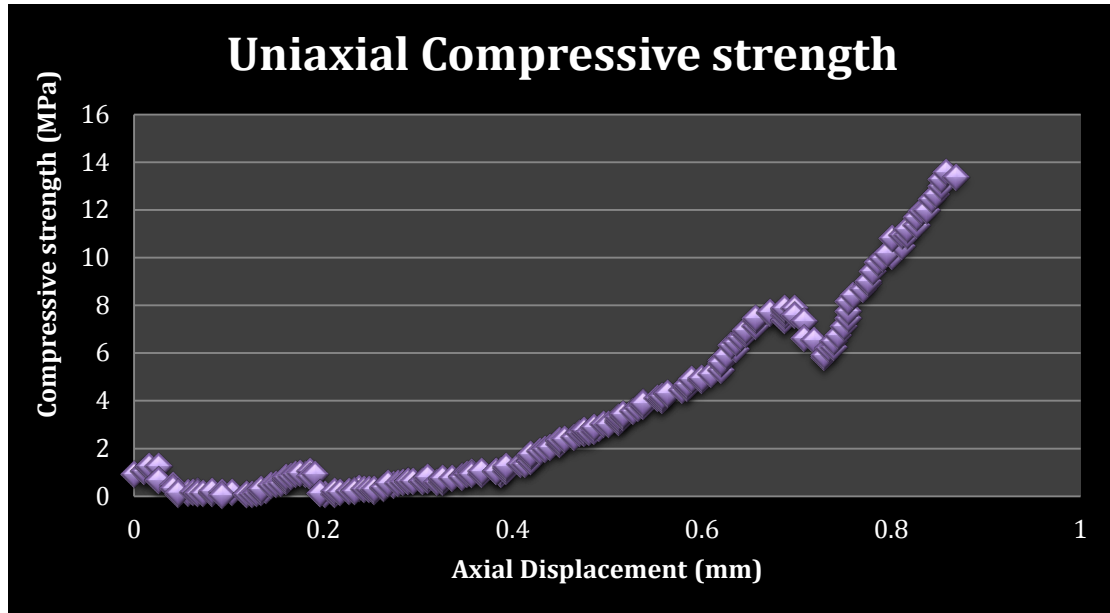
Autoclastic Breccia core Number ° 9



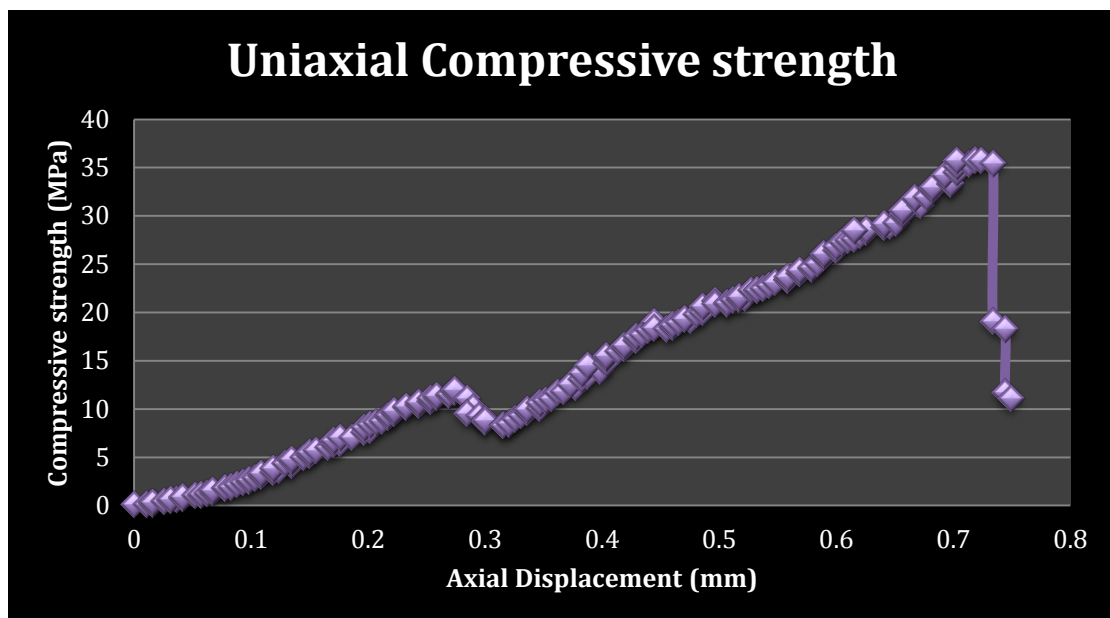
Autoclastic Breccia core Number ° 10



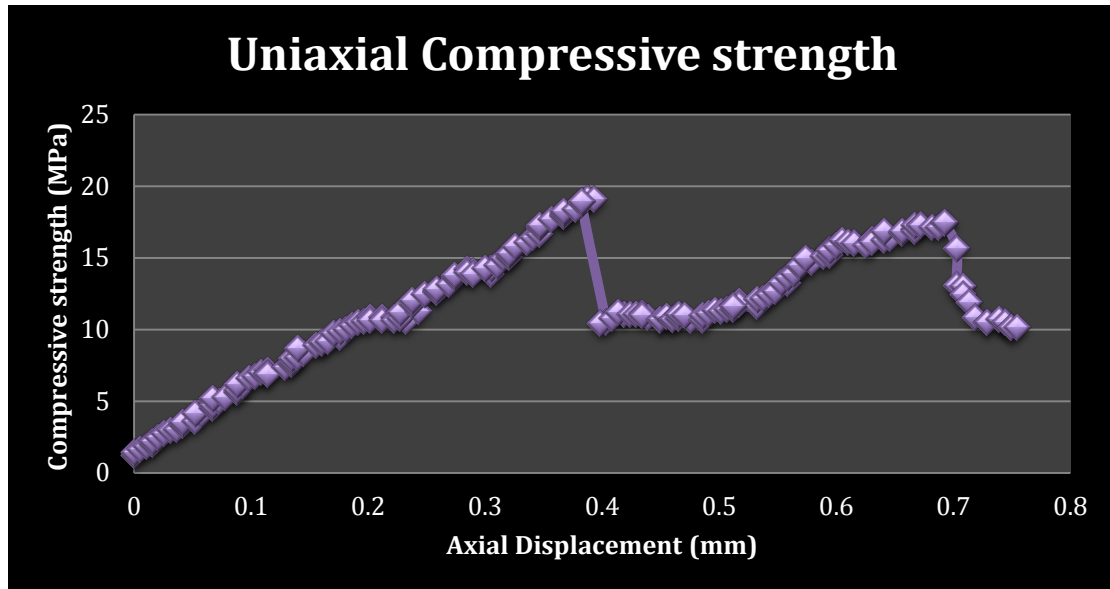
Autoclastic Breccia core Number ° 11



Autoclastic Breccia core Number ° 12



Autoclastic Breccia core Number ° 13



Autoclastic Breccia core Number ° 14

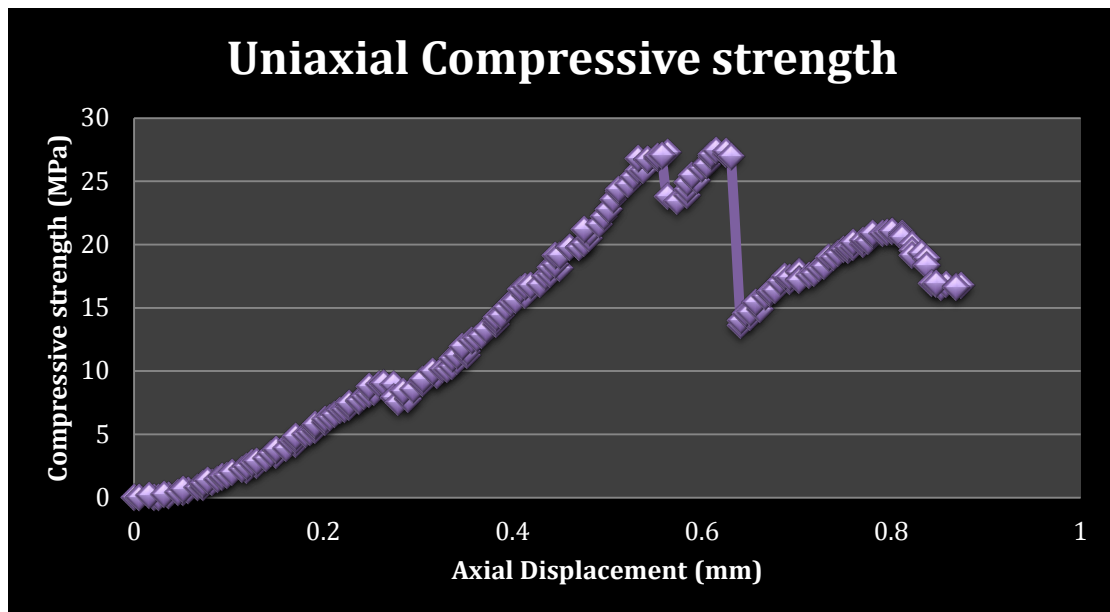
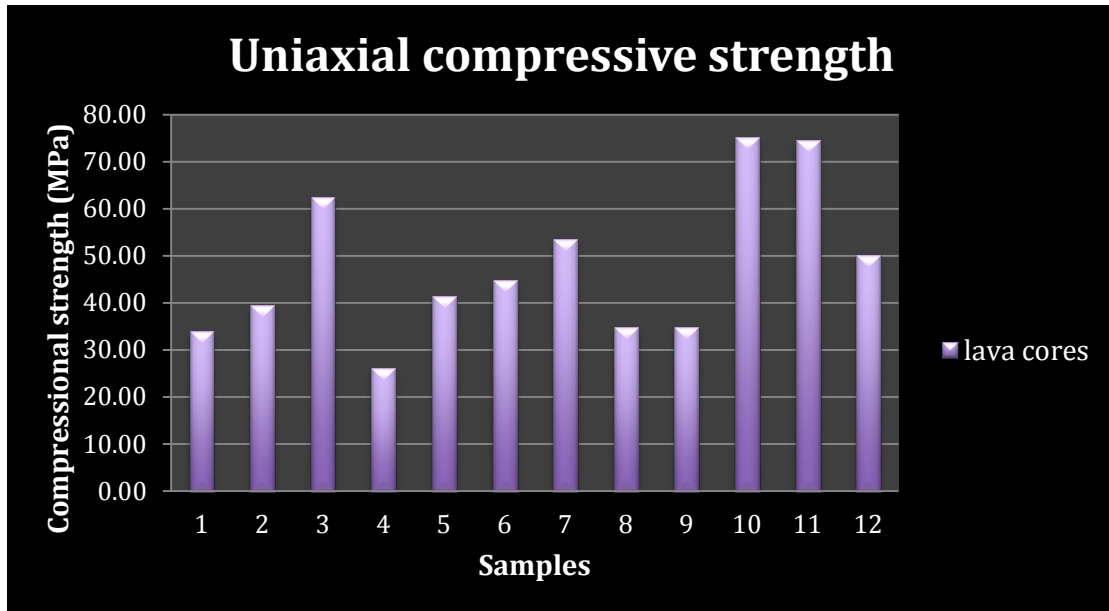
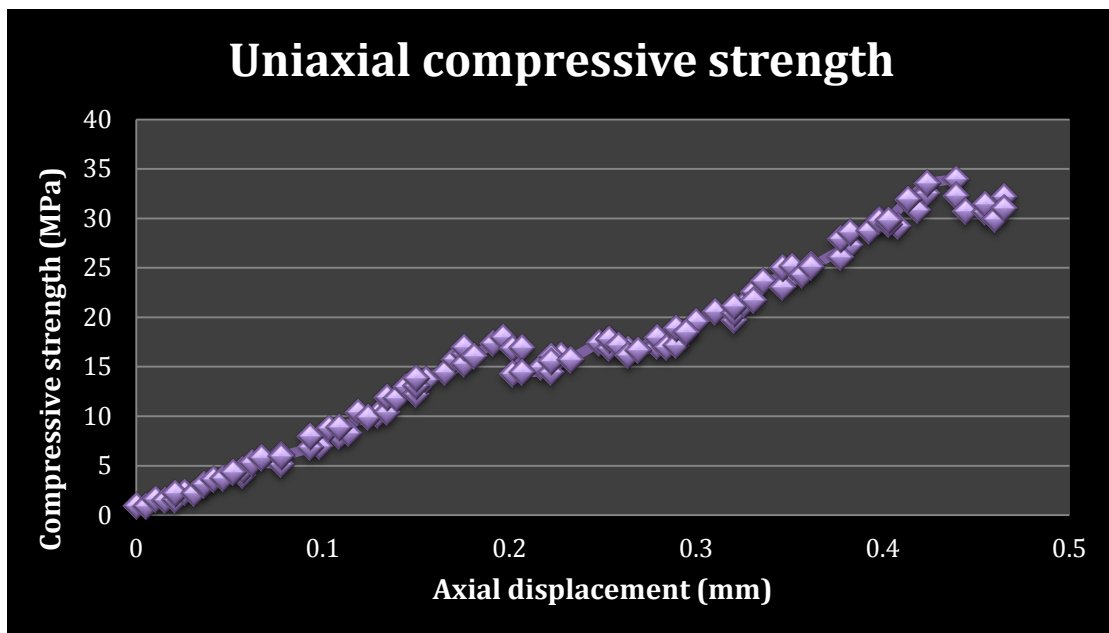


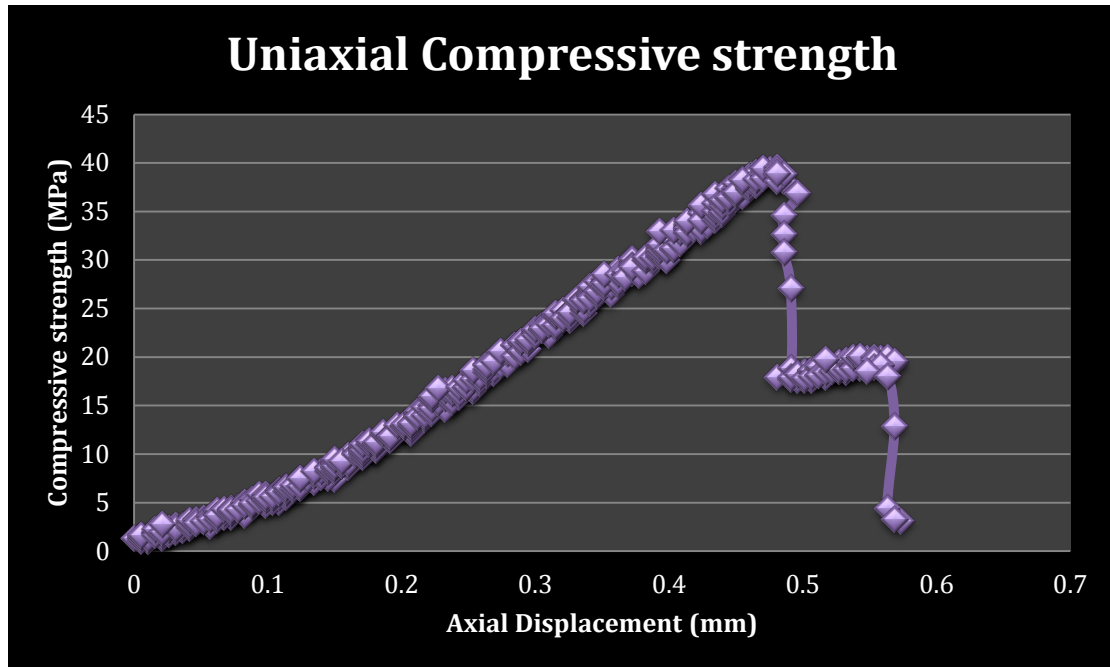
Figure D.2: Lava cores (1-12)



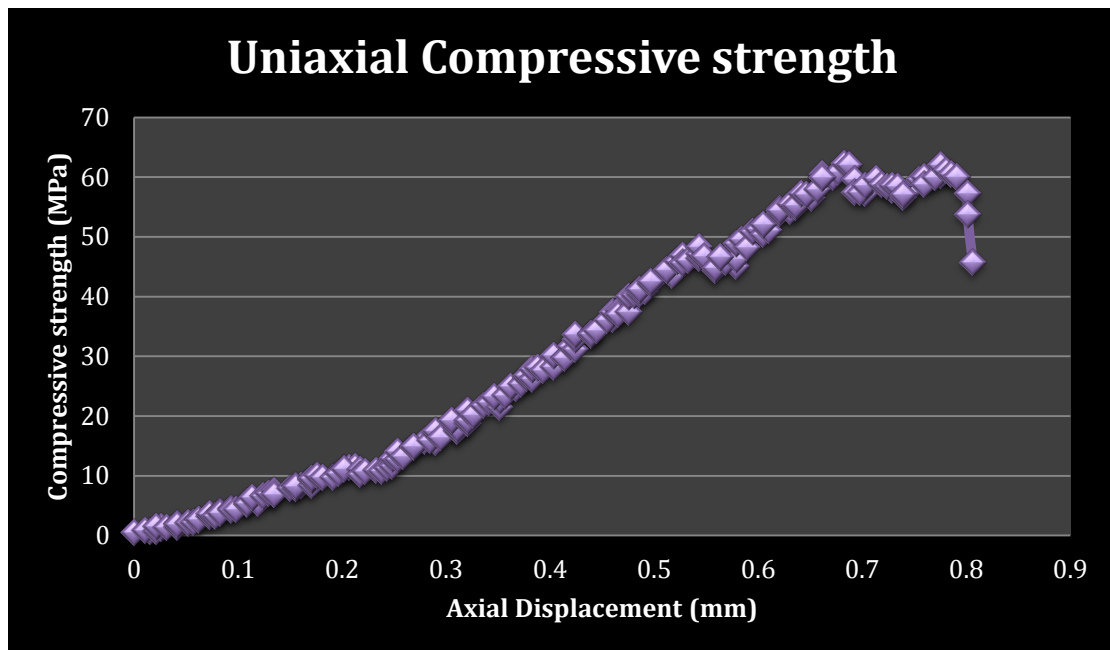
Lava core Number ° 1



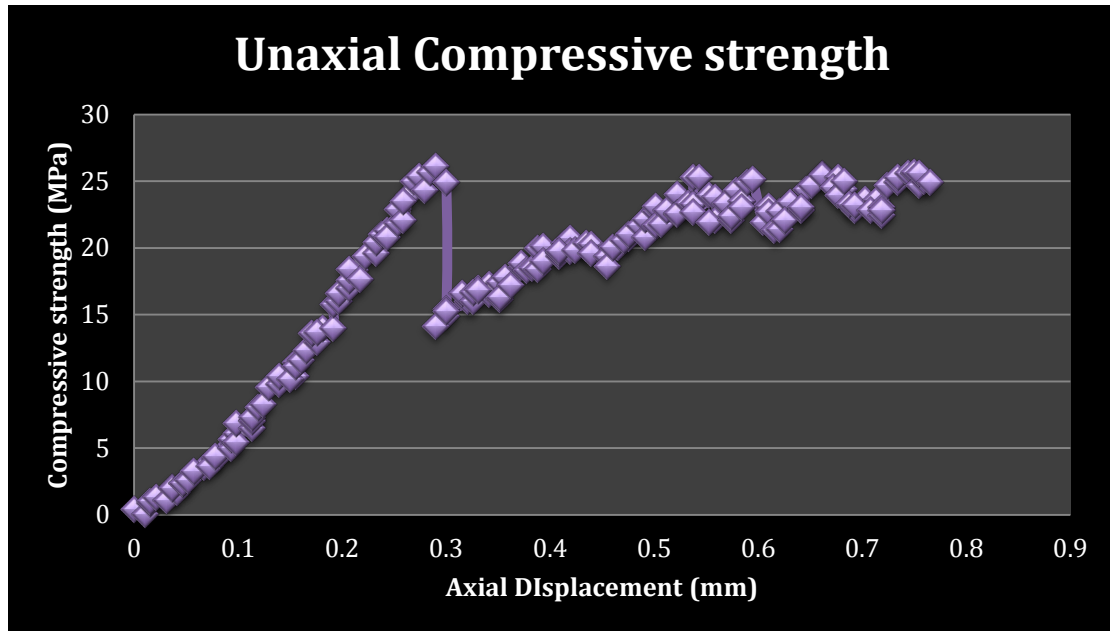
Lava core Number ° 2



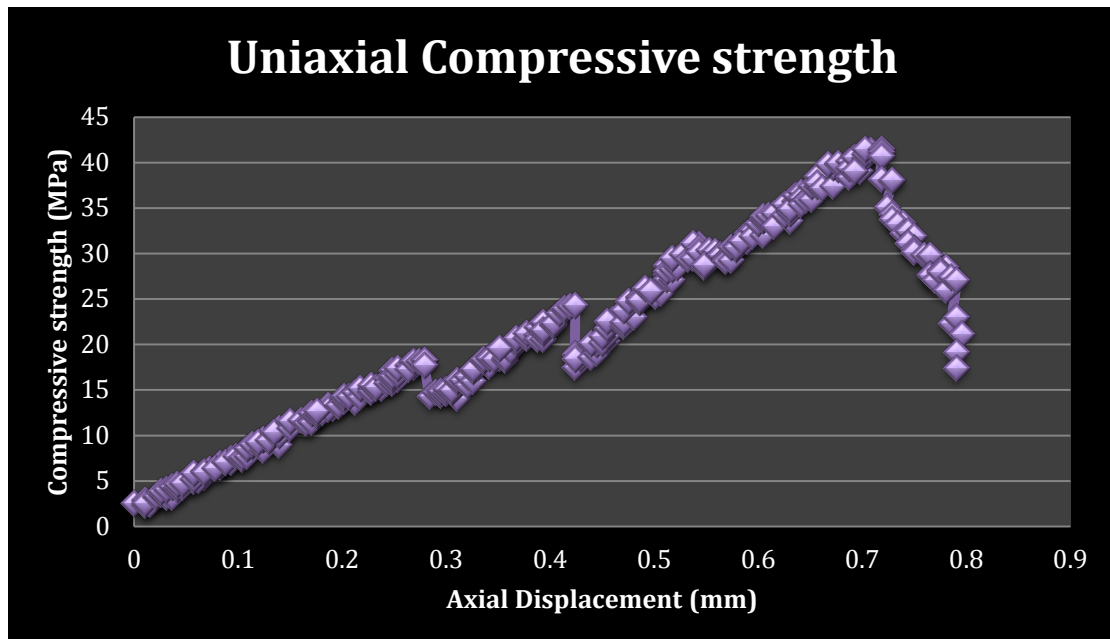
Lava core Number ° 3



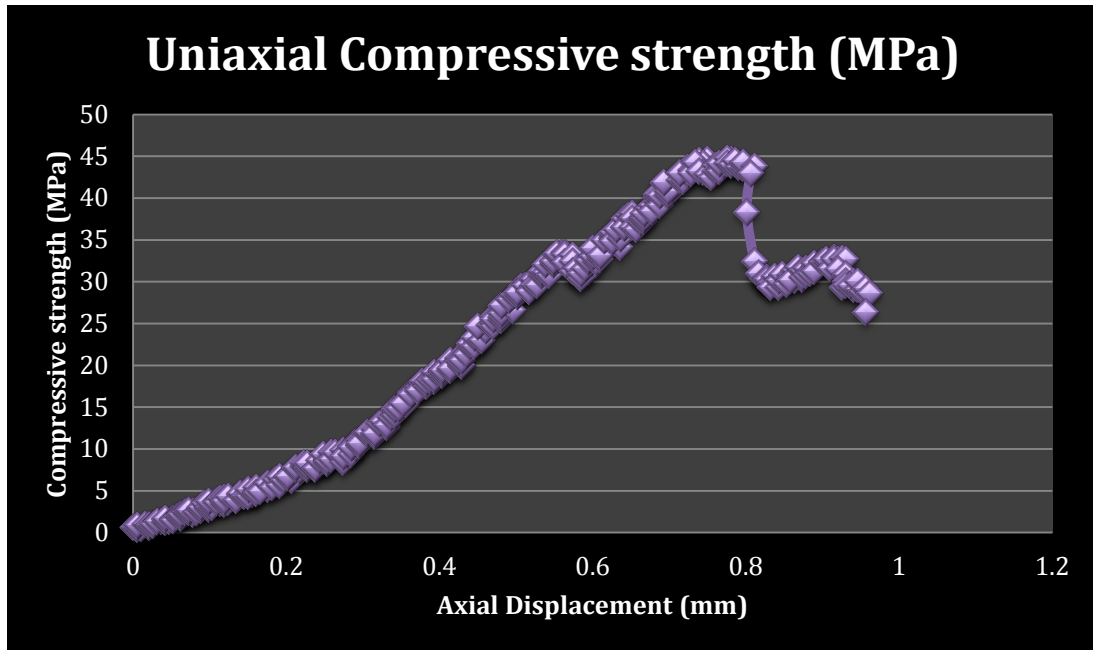
Lava core Number ° 4



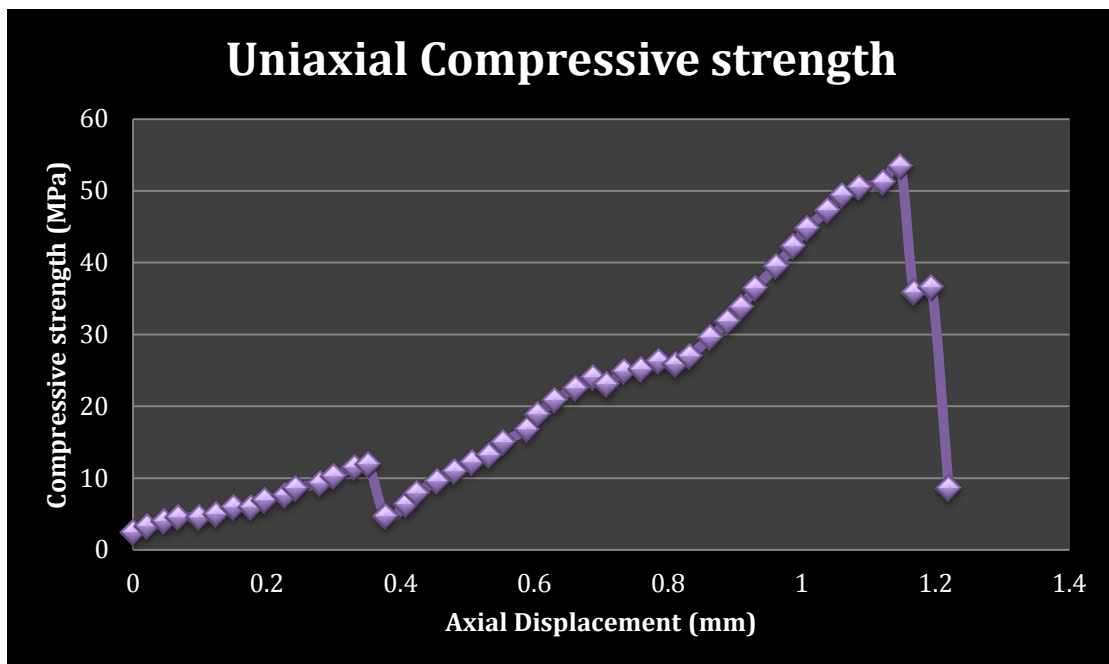
Lava core Number ° 5



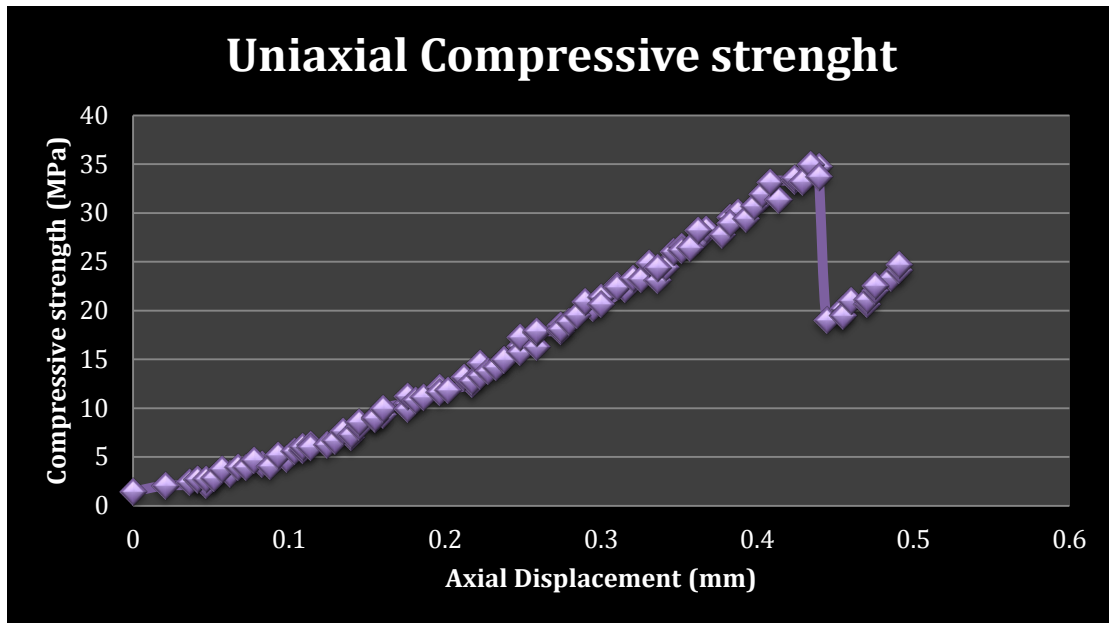
Lava core Number ° 6



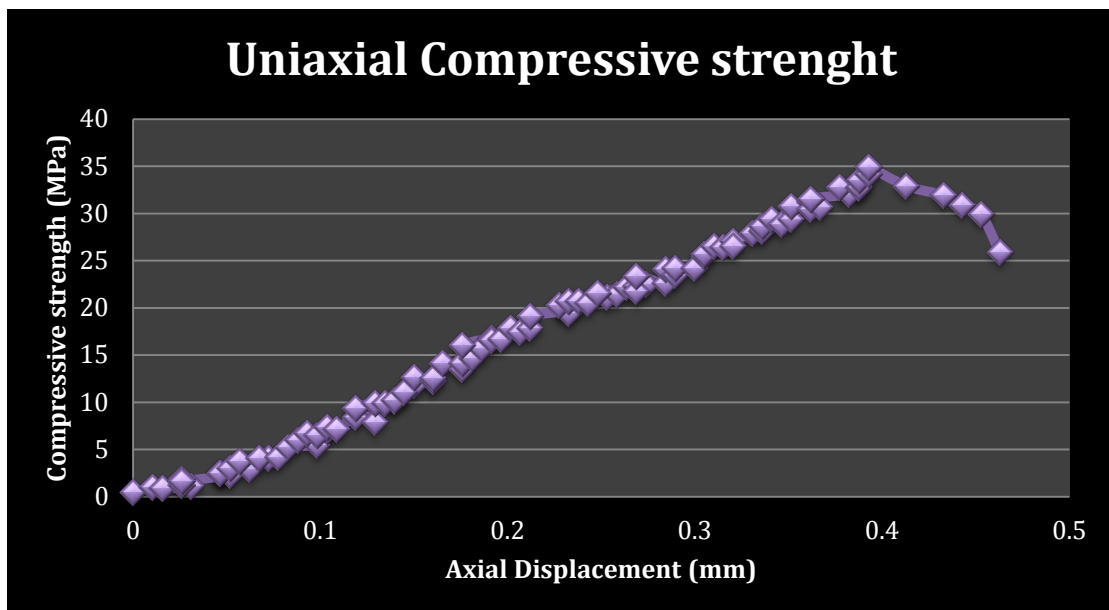
Lava core Number ° 7



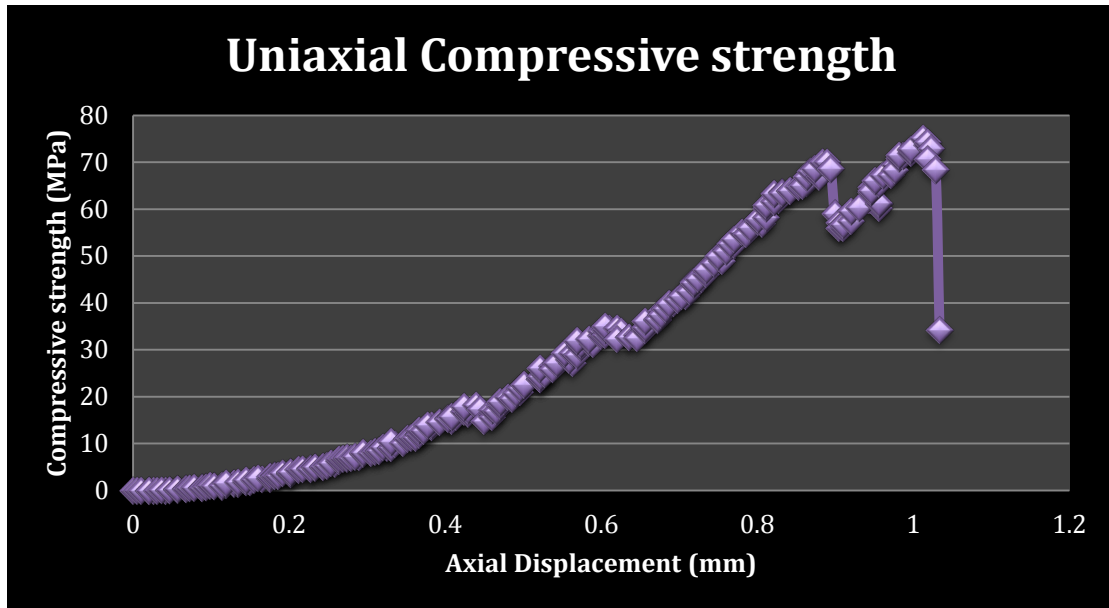
Lava core Number ° 8



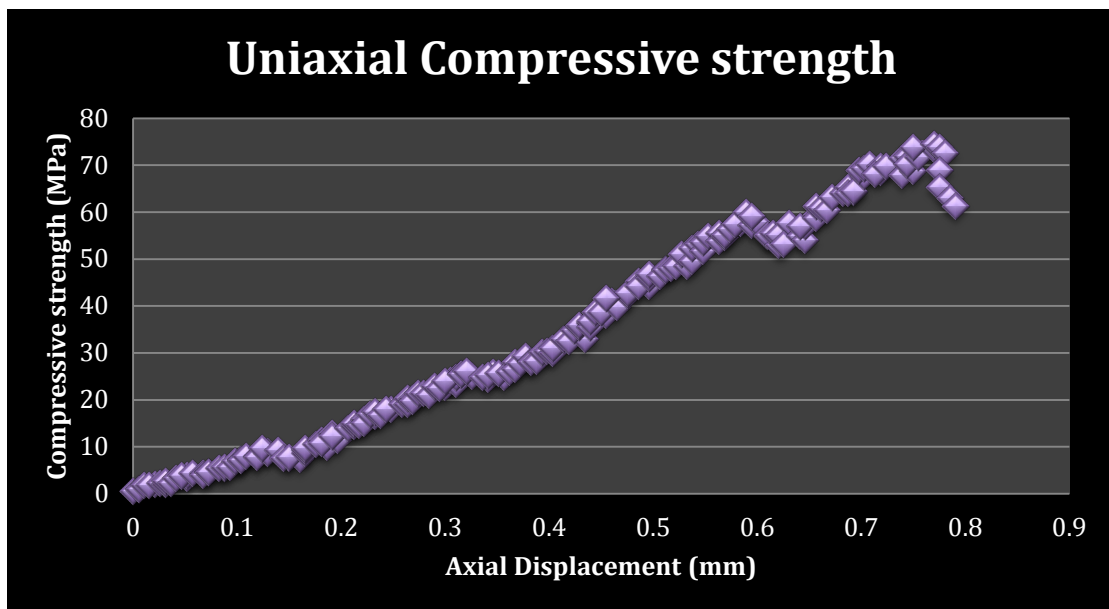
Lava core Number ° 9

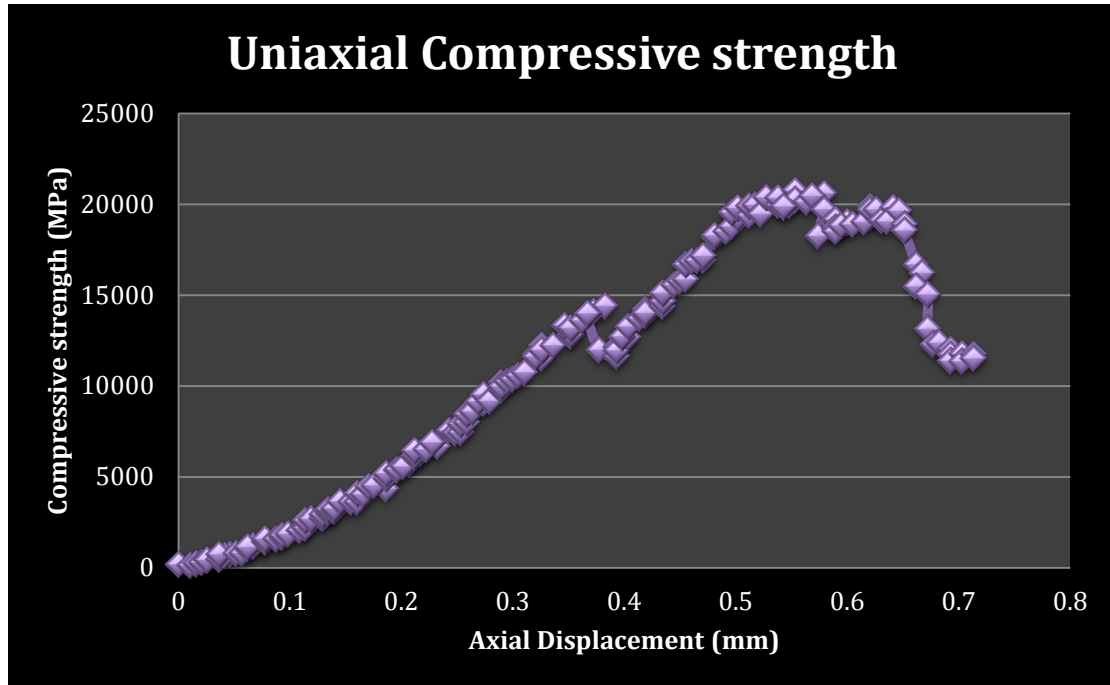


Lava core Number ° 10



Lava core Number ° 11





APPENDIX E: COPYRIGHT PERMISSIONS

E.1 License agreement for the use of Figure 2.1.

RightsLink - Your Account

8/17/12 5:15 PM

SPRINGER LICENSE TERMS AND CONDITIONS

Aug 17, 2012

This is a License Agreement between PATRICK MANZONI ("You") and Springer ("Springer") provided by Copyright Clearance Center ("CCC"). The license consists of your order details, the terms and conditions provided by Springer, and the payment terms and conditions.

All payments must be made in full to CCC. For payment instructions, please see information listed at the bottom of this form.

License Number	2961361388936
License date	Aug 03, 2012
Licensed content publisher	Springer
Licensed content publication	Bulletin of Volcanology
Licensed content title	Multiple sector collapses at stromboli volcano, Italy: how they work
Licensed content author	Alessandro Tibaldi
Licensed content date	Jan 1, 2001
Volume number	63
Issue number	2
Type of Use	Thesis/Dissertation
Portion	Figures
Author of this Springer article	No
Order reference number	None
Title of your thesis / dissertation	SLOPE STABILITY ANALYSIS OF THE PACAYA VOLCANO, GUATEMALA, USING LIMIT EQUILIBRIUM AND FINITE ELEMENT METHOD
Expected completion date	Aug 2012
Estimated size(pages)	150
Total	0.00 USD
Terms and Conditions	

E.2 This email dialogue establishes permission for the use of Figure 2.3 and 2.5.

Re-publishing material from Geological Society of London copyright

Using material from GSL publications

Extensive quotation (more than c. 100 words) and reproduction of previously published illustrations (even if redrawn) require permission from the copyright holder. In the UK, material remains in copyright until 70 years after the death of the author.

Material that can be used without permission

Authors may reuse their own material without permission subject to the exceptions listed below. They may include the whole article in a PhD or other thesis provided that it will not be published, and that the original source is fully acknowledged in the standard form. Authors may not republish their whole article, or a substantial part of it, without permission. Such permission will be granted only in exceptional circumstances.

Anyone may use up to three items (text extracts of 100 words or less, figures or tables) from GSL published material without permission or charge provided that a proper acknowledgement of source is used with the item. If you require written permission, please use the forms in the section below; note that payment will be required.

The abstracts of articles can be reproduced without permission or fees provided that a full reference and a link to the article abstract page are included.

Please check that GSL is the original copyright holder and that the material has not been taken from another source. In those cases, you must contact the original copyright holder. GSL is not usually the copyright holder for cover photographs, and permission must be sought from the copyright holder.

If your article forms part of a multi-author book, the publisher must ensure that the total number of items from GSL copyright does not exceed three (this does not apply to journal issues).

E.2, continued

COPYRIGHT PERMISSION

Angharad Hills <angharad.hills@geolsoc.org.uk>
To: Patrick Manzoni <pmanzoni@mtu.edu>

Thu, Aug 9, 2012 at 6:03 AM

Dear Patrick

Please see our website for what you can use without permission and how to obtain permission for other material: <http://www.geolsoc.org.uk/gsl/publications/permissions>

Best wishes

Angharad

From: Patrick Manzoni [mailto:pmanzoni@mtu.edu]
Sent: Wednesday, August 01, 2012 5:26 PM
To: Angharad Hills
Subject: Fwd: COPYRIGHT PERMISSION

COPYRIGHT PERMISSION

Patrick Manzoni <pmanzoni@mtu.edu>
To: angharad.hills@geolsoc.org.uk

Wed, Aug 1, 2012 at 6:26 PM

I'm completing my Master Research at Michigan Technology University and I'm requesting your permission to use Figure 2 and Figure 8 of the paper "McGuire WJ. 1996. Volcano Instability: a review of contemporary themes. Geological Society, London, Special Publications 1996, v. 110; p1-23. " to serve as description of factors affecting Pacaya volcano instability and features I encountered in the field in my thesis entitled " Slope Stability Analysis of the Pacaya volcano, Guatemala, using Limit Equilibrium and Finite Element Method".

The requested permission extend to any future revisions and editions of my dissertation, including non-exclusive world rights in all languages, and to the prospective publication of my dissertation by the UMI. This rights will in no way restrict republication of the material in any other forms by you or by others authorized by you. you signing in this letter will also confirm that you own [or your company owns] the copyrights to the above-described material.

Thank you very much,

Sincerely,

Patrick Manzoni

E.3 License agreement for the use of Figure 2.8.

RightsLink - Your Account

8/17/12 5:57 PM

SPRINGER LICENSE TERMS AND CONDITIONS

Aug 17, 2012

This is a License Agreement between PATRICK MANZONI ("You") and Springer ("Springer") provided by Copyright Clearance Center ("CCC"). The license consists of your order details, the terms and conditions provided by Springer, and the payment terms and conditions.

All payments must be made in full to CCC. For payment instructions, please see information listed at the bottom of this form.

License Number	2961370009390
License date	Aug 03, 2012
Licensed content publisher	Springer
Licensed content publication	Bulletin of Engineering Geology and the Environment
Licensed content title	Estimating the geotechnical properties of heterogeneous rock masses such as flysch
Licensed content author	Paul Marinos
Licensed content date	Jul 1, 2001
Volume number	60
Issue number	2
Type of Use	Thesis/Dissertation
Portion	Figures
Author of this Springer article	No
Order reference number	None
Title of your thesis / dissertation	SLOPE STABILITY ANALYSIS OF THE PACAYA VOLCANO, GUATEMALA, USING LIMIT EQUILIBRIUM AND FINITE ELEMENT METHOD
Expected completion date	Aug 2012
Estimated size(pages)	150
Total	0.00 USD
Terms and Conditions	

E.4 This email dialogue establishes permission for the use of Figure 3.2

COPYRIGHT PERMISSION

Rüdiger Escobar Wolf <rpesco@mtu.edu>
To: Patrick Manzoni <pmanzoni@mtu.edu>

Fri, Aug 3, 2012 at 11:45 PM

Mr. Patrick Manzoni

I grant you permission to use Figure 22 a, of the report "The eruption of Volcan Pacaya on May-June 2010" which I wrote in 2010. I own the copyrights to said figure, as I am the author of the figure, which I created using information from various sources as indicated on the figure and on this letter. You can use this figure in your thesis entitled "Slope Stability Analysis of the Pacaya volcano, Guatemala, using Limit Equilibrium and Finite Element Method". The requested permission extends to any future revisions and editions of your thesis, including non-exclusive world rights in all languages, and to the prospective publication of your thesis by the UMI. I retain the rights to further use and publish said figure, and to further grant usage and publishing rights to other parties.

It will be your responsibility to acknowledge and correctly cite the sources of the information indicated in the figure, which are as follows:

Carr, M., 1976, Underthrusting and Quaternary faulting in northern Central America. Geological Society of America Bulletin. V. 87, pp. 825 – 829.

IGN / Bonis, S., 1993, Mapa Geologico de Guatemala Escala 1:250,000. Hoja ND 15 – 8 – G , "Guatemala". First edition (map). Guatemala.

The background shaded relief map was derived from the SRTM DEM. The references for this data set is:

Jarvis A., H.I. Reuter, A. Nelson, E. Guevara, 2008, Hole-filled seamless SRTM data V4, International Centre for Tropical Agriculture (CIAT), available from <http://srtm.csi.cgiar.org>.

Sincerely,

Rüdiger Escobar Wolf

August 3, 2012

Houghton, Michigan USA.

E.4, continued

COPYRIGHT PERMISSION

Patrick Manzoni <pmanzoni@mtu.edu>
To: Rudiger Escobar Wolf <rpescoba@mtu.edu>

Fri, Aug 3, 2012 at 10:54 AM

I'm completing my Master Research at Michigan Technology University and I'm requesting your permission to use Figure 22.a of the report "Rudiger Escobar Wolf. 2010. The eruption of Volcan Pacaya on May-June 2010." to serve as description for tectonic setting at Pacaya volcano in my thesis entitled " Slope Stability Analysis of the Pacaya volcano, Guatemala, using Limit Equilibrium and Finite Element Method".

The requested permission extend to any future revisions and editions of my dissertation, including non-exclusive world rights in all languages, and to the prospective publication of my dissertation by the UMI.
This rights will in no way restrict republication of the material in any other forms by you or by others authorized by you. You signing in this letter will also confirm that you own [or your company owns] the copyrights to the above-described material.

Thank you very much,

Sincerely,

Patrick Manzoni

E.5 This email dialogue establishes permission for the use of Figure 4.9

Michigan Technological University Mail – COPYRIGHT PERMISSION

8/17/12 6:35 PM



Patrick Manzoni <pmanzoni@mtu.edu>

COPYRIGHT PERMISSION

Bavister, Rosemary <ROSEMARY.BAVISTER@contractor.cengage.com>
To: Patrick Manzoni <pmanzoni@mtu.edu>

Fri, Aug 17, 2012 at 5:16 PM

Dear Patrick

Re Figure 2.4 in 'Rock Slope Engineering, Civil and Mining 2004

Thank you for your email, I can confirm that permission has been granted as detailed below

Permission is granted for use of the above material in your forthcoming dissertation to be published by UMI, subject to the following conditions:

1. The material to be quoted/produced was published without credit to another source. If another source is acknowledged, please apply directly to that source for permission clearance.
2. Permission is for non-exclusive, English language rights, and covers use in your dissertation only. Any further use (including storage, transmission or reproduction by electronic means) shall be the subject of a separate application for permission.
3. Full acknowledgement must be given to the original source, with full details of figure/page numbers, title, author(s), publisher and year of publication.

Yours sincerely

Rosemary Bavister
Permissions Administrator
Taylor & Francis Books (UK)

Tel: +44 (0) 1264 342781

<https://mail.google.com/mail/u/0/?ui=2&ik=c505341e16&view=pt&search=inbox&msg=139352811728b22e>

Page 1 of 2

E.5, continued

Michigan Technological University Mail – COPYRIGHT PERMISSION

8/17/12 6:35 PM

Fax: +44 (0) 1264 342792

Rosemary.Bavister@contractor.cengage.com

Cengage Learning EMEA Ltd, Cheriton House, North Way, Andover, Hants, SP10 5BE, a Limited company registered in England and Wales under company number 929655.

This e-mail is confidential and may be privileged. Any opinions expressed in this communication are not necessarily those of the company. It may be read, copied and used only by the intended recipient. If you have received it in error please contact us immediately by return email. Please then delete the email and do not disclose the contents to any person. Although it is believed, but not warranted, that this email and any attachments are virus-free, it is your responsibility to check this.

Michigan Technological University Mail – COPYRIGHT PERMISSION

8/17/12 6:35 PM



Patrick Manzoni <pmanzoni@mtu.edu>

COPYRIGHT PERMISSION

Patrick Manzoni <pmanzoni@mtu.edu>
To: t&f.permissions@cengage.com
Cc: Christina.Taranto@taylorandfrancis.com

Thu, Aug 2, 2012 at 3:41 PM

I'm completing my Master Research at Michigan Technology University and I'm requesting your permission to use Figure 2.4 of the book "Rock Slope Engineering. Civil and Mining 2004. 4th edition. Duncan C. Wyllie & Christopher W Mah " to serve as description image of dip and dip-direction I found at Pacaya volcano in my thesis entitled " Slope Stability Analysis of the Pacaya volcano, Guatemala, using Limit Equilibrium and Finite Element Method".

The requested permission extend to any future revisions and editions of my dissertation, including non-exclusive world rights in all languages, and to the prospective publication of my dissertation by the UMI. This rights will in no way restrict republication of the material in any other forms by you or by others authorized by you. you signing in this letter will also confirm that you own [or your company owns] the copyrights to the above-described material.

Thank you very much,

Sincerely,

Patrick Manzoni

E.6 License agreement for the use of Figure 4.10

RightsLink - Your Account

8/17/12 6:45 PM

SPRINGER LICENSE TERMS AND CONDITIONS

Aug 17, 2012

This is a License Agreement between PATRICK MANZONI ("You") and Springer ("Springer") provided by Copyright Clearance Center ("CCC"). The license consists of your order details, the terms and conditions provided by Springer, and the payment terms and conditions.

All payments must be made in full to CCC. For payment instructions, please see information listed at the bottom of this form.

License Number	2961370541284
License date	Aug 03, 2012
Licensed content publisher	Springer
Licensed content publication	Rock Mechanics and Rock Engineering
Licensed content title	The shear strength of rock joints in theory and practice
Licensed content author	N. Barton
Licensed content date	Dec 1, 1977
Volume number	10
Issue number	1
Type of Use	Thesis/Dissertation
Portion	Figures
Author of this Springer article	No
Order reference number	None
Title of your thesis / dissertation	SLOPE STABILITY ANALYSIS OF THE PACAYA VOLCANO, GUATEMALA, USING LIMIT EQUILIBRIUM AND FINITE ELEMENT METHOD
Expected completion date	Aug 2012
Estimated size(pages)	150
Total	0.00 USD
Terms and Conditions	

E.7 This email dialogue establishes permission for the use of Figure 4.26 (Volume determination by the displacement of a dry medium).

COPYRIGHT PERMISSION

paul.webb@micromeritics.com <paul.webb@micromeritics.com>
To: Patrick Manzoni <pmanzoni@mtu.edu>

Tue, Aug 7, 2012 at 7:41 PM

Patrick,

You have my permission to use the referred-to illustration if accompanied by appropriate citation to its origin.

Good luck with your thesis.

Paul

From: Patrick Manzoni [pmanzoni@mtu.edu]
Sent: 08/07/2012 04:34 PM ZE2
To: Paul Webb
Subject: COPYRIGHT PERMISSION

[Quoted text hidden]

COPYRIGHT PERMISSION

Patrick Manzoni <pmanzoni@mtu.edu>
To: paul.webb@micromeritics.com

Tue, Aug 7, 2012 at 4:34 PM

I'm completing my Master Research at Michigan Technology University and I'm requesting your permission to use Figure 4 of the paper "P A Webb. 2001. Volume and Density Determinations for Particle Technologists" to serve as description image as device I used on computing the density envelope of Pacaya rock masses in my thesis entitled " Slope Stability Analysis of the Pacaya volcano, Guatemala, using Limit Equilibrium and Finite Element Method".

The requested permission extend to any future revisions and editions of my dissertation, including non-exclusive world rights in all languages, and to the prospective publication of my dissertation by the UMI.
This rights will in no way restrict republication of the material in any other forms by you or by others authorized by you. You signing in this letter will also confirm that you own [or your company owns] the copyrights to the above-described material.

Thank you very much,

Sincerely,

Patrick Manzoni